UNIVERSITY OF HAWAII
LIBRARY

ADVANCES IN PHYSICS

A QUARTERLY SUPPLEMENT of the PHILOSOPHICAL MAGAZINE

EDITOR
PROFESSOR B. H. FLOWERS, M.A., D.Sc.

CONSULTANT EDITOR
PROFESSOR N. F. MOTT, M.A., D.Sc., F.R.S.

EDITORIAL BOARD
SIR LAWRENCE BRAGG, O.B.E., M.C., M.A., D.Sc., F.R.S.
SIR GEORGE THOMSON, M.A., D.Sc., F.R.S.
PROFESSOR A. M. TYNDALL, C.B.E., D.Sc., F.R.S.

VOLUME 8 OCTOBER 1959 NUMBER 32

PRICE per part 20*s.*
PRICE per annum £3 15*s.* 0*d.* post free

PRINTED AND PUBLISHED BY TAYLOR & FRANCIS LTD
RED LION COURT, FLEET ST., LONDON E.C.4

QC1
A36

The Scientific Work of René Descartes (1596–1650)

By J. F. SCOTT, B.A., M.Sc., Ph.D.

This book puts the chief mathematical and physical discoveries of Descartes in an accessible form, and fills an outstanding gap upon the shelf devoted to the history of philosophy and science. The careful treatment that Dr. Scott has accorded to this work of Descartes is welcome, and will be an asset to all libraries. Publication is recommended and approved by the Publication Fund Committee of the University of London.

212 pages, 7 in. × 10 in. Price 20*s.* net plus postage

Correspondence and Papers of Edmond Halley

Arranged and edited by EUGENE FAIRFIELD MACPIKE

First published on behalf of The History of Science Society by Oxford University Press. Now re-issued by Taylor & Francis Ltd.

Price 21*s.* net plus postage
Limited stock still available

Memoirs of Sir Isaac Newton's Life

By WILLIAM STUKELEY, M.D., F.R.S. (1752)

This work is taken from an original manuscript now in the possession of the Royal Society, London. Price 5*s.* net plus postage

First Published 1936 *Limited stock still available*

Hevelius, Flamsteed and Halley

By EUGENE FAIRFIELD MACPIKE

This work contains an account of three contemporary astronomers and their mutual relations.

Published by arrangement with The History of Science Society

First Published 1937 Price 12*s.* 6*d.* net plus postage
Limited stock still available

Printed and Published by

TAYLOR & FRANCIS LTD

RED LION COURT, FLEET STREET, LONDON, E.C.4

CONTENTS

Threshold Effects in Nuclear Reactions. By A. I. Baz, Atomic Energy Institute, Moscow, U.S.S.R. 349

Intermetallic Reactions and Ageing Effects in Thin Films. By C. Weaver and R. M. Hill, Department of Natural Philosophy, The Royal College of Science and Technology, Glasgow . . 375

ADVANCES IN PHYSICS

A QUARTERLY SUPPLEMENT
of the
PHILOSOPHICAL MAGAZINE

VOLUME 8 OCTOBER 1959 NUMBER 32

Threshold Effects in Nuclear Reactions†

By A. I. BAZ
Atomic Energy Institute, Moscow, U.S.S.R.

ABSTRACT

We explore the idea that between the colliding particles or the reaction products of a nuclear reaction the interaction in the immediate neighbourhood of the nuclear surface may be represented by a static attractive potential. The Wigner–Eisenbud theory of nuclear reactions is readily reformulated to take this ' surface potential ' into account, whereupon quasi-bound states of the compound system are found to appear, with high probability, very close to the various thresholds for two-particle channels. Consequently, the cross section of a reaction close to any threshold should have a certain resonance-like behaviour. The relevant experimental data are reviewed and are found to support all the predictions of the theory.

§ 1. INTRODUCTION

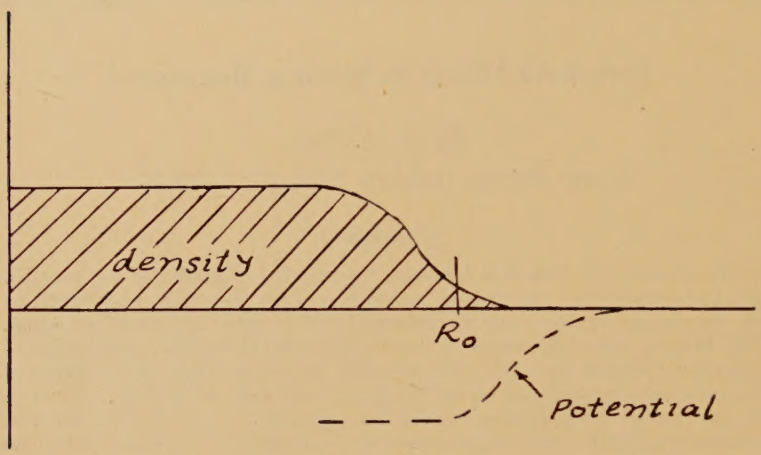
COMPARISON of the scattering of electrons and neutrons by complex nuclei suggests, as is well known, that the radius of nuclear interaction of a nucleus is larger than the radius of its charge distribution. One is therefore led to picture the nuclear surface as having a structure somewhat as shown in fig. 1: the neutron–nucleus interaction (here represented by a potential) falls to zero over a region which extends beyond the matter distribution of the nucleus. For charged particles there will also be at larger distances the Coulomb potential, of course.

In this paper we wish to examine certain effects of the surface region upon the mechanism of nuclear reactions. In particular, we shall suppose that the interaction of a nucleon with the nucleus in the region just outside the matter distribution can be described by a static and smoothly varying attractive potential, as shown in fig. 1. This being so, a collision process in which a nucleon interacts with the nucleus may be regarded as

† This work was completed in the Theoretical Physics Department, University of Manchester, during a year's study-leave in England.

proceeding in two stages. To avoid complications arising from the Coulomb potential we shall for the present consider only the case of a neutron. In the first stage the neutron enters the tail of the nuclear potential where we ignore the possibility of a reaction occurring : in this stage we have therefore only to solve the familiar two-body problem, the potential acting merely to distort the wave-function of the incoming particle. In the second stage the neutron enters the region of high nuclear density : here we have an essentially many-body problem in which a reaction may occur.

Fig. 1



Density and potential distribution in a nucleus.

This picture is naturally a very crude one. In the first place, the distinction between the two regions cannot be sharply defined ; and in any case it is not clear to what extent it is allowable to represent the interaction in the neighbourhood of the surface by a static two-body potential. Our only justification at the present time lies in the simplicity of the model and in the fact that the results appear to be supported by experiment.

We therefore assume that the nucleon–nucleus interaction is (*a*) very complicated if $r < R_0$, so that we shall describe it in terms of boundary conditions of the internal wave-function at $r = R_0$; and (*b*) is to be represented by a static, two-body potential $U(r)$ when $r \geqslant R_0$. With the optical model in mind we shall assume that

$$U(r) = -U_0 \exp\left[-\alpha(r-R_0)\right] \quad . \quad . \quad . \quad . \quad . \quad . \quad . \quad (1)$$

with $U_0 \approx 40$ Mev and $\alpha^{-1} \approx 10^{-13}$ cm. The value of R_0 cannot be chosen unambiguously with sufficient accuracy for our purpose and will be regarded as a free parameter of the theory. However, it is evident that it must be approximately equal to the radius of the charge distribution.

The most natural way to take the surface region into account is then to use the Wigner–Eisenbud formulation of the general theory of nuclear reactions : we merely have to insert for the external wave-functions of the

Wigner–Eisenbud formalism, functions appropriate to a particle moving in the potential $U(r)$. The interaction in the region $r < R_0$ will then be automatically accounted for in terms of the boundary conditions at $r = R_0$. In the usual treatment, the whole interaction (excepting the Coulomb field) is included in the boundary conditions. Such a treatment is appropriate when we wish to display our total ignorance of the details of the interaction. In the proposed modification we shall at least be able to take specific account of the simple interaction we have assumed to be effective in the nuclear surface.

Information regarding the interaction of incoming or outgoing particles when $r > R_0$ enters the general theory only through the quantities

$$\psi^{(\pm)}(R_0) \quad \text{and} \quad \tau^{(\pm)}(R_0) = \left.\frac{\psi^{(\pm)\prime}}{\psi^{(\pm)}}\right|_{r=R_0}$$

where $\psi^{(\pm)}$ are wave-functions of relative motion defined for $r \geqslant R_0$ and having the asymptotic property

$$\psi^{(\pm)}(r) \to \exp\left[\pm i\left(kr - \frac{l\pi}{2}\right)\right]$$

in the case of neutral particles. Here k is the wave number and l the angular momentum quantum number of relative motion. For charged particles this asymptotic property has to be modified in the usual manner.

When $U(r)$ is identically zero, ψ and τ assume their free particle values. For example, for neutral particles with $l = 0$,

$$\psi_{\text{free}}^{(\pm)}(R_0) = \exp(\pm ikR_0); \quad \tau_{\text{free}}^{(\pm)} = \pm ik.$$

We therefore have a simple criterion for determining whether the presence of a surface potential can produce a characteristic effect: we have to calculate ψ and τ for a finite potential $U(r)$ and compare them with their free particle values. Something new can emerge only if ψ and τ are considerably different from ψ_{free} and τ_{free}.

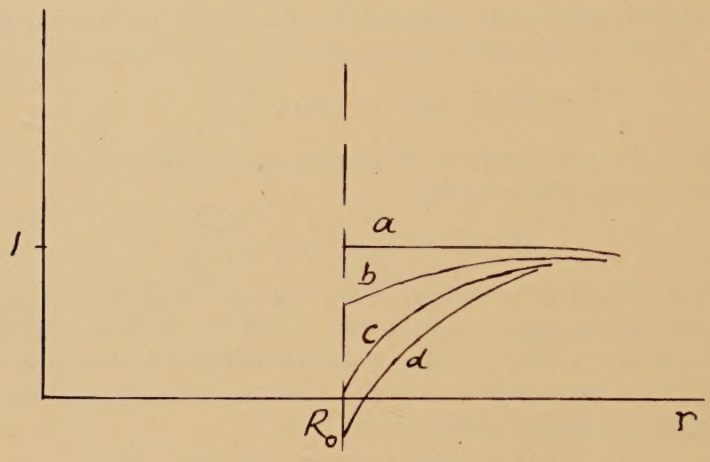
It is easy to see when this will happen. Let us consider how $\psi^{(+)}$ depends upon $U(r)$ and upon the energy E of relative motion, restricting ourselves to neutral s-waves. If E is very small and $U(r) \equiv 0$ we have

$$\psi^{(+)} = \psi_{\text{free}}^{(+)} = \exp(ikr) \sim 1 \quad \text{as} \quad k \to 0.$$

The out-going wave-function $\psi^{(+)}$ is almost real and constant for values of r which are sufficiently small (see curve a, fig. 2). Let us now gradually increase the value of U_0 in eqn. (1): this will lead to a gradually increasing curvature of the wave function (curve b). When U_0 reaches a certain value U_0^{crit} we shall find that $\psi^{(+)}(R_0) = 0$ (curve c). Further increases in U_0 will cause $\psi^{(+)}(R_0)$ to become negative (curve d), but eventually it will begin to increase again. Correspondingly, the logarithmic derivative $\tau^{(+)}(R_0)$ increases from $ik \approx 0$ when $U_0 = 0$ to infinity when $U_0 = U_0^{\text{crit}}$. For small E it is therefore apparent that both the wave-function and its logarithmic derivative are very sensitive functions of U_0. A similar argument shows that they also depend sensitively upon the range α^{-1} of the potential. For certain values of U_0 and α^{-1}, ψ and τ can be very different from their free

particle values. We can also show quite generally, using the WKB approximation, that at higher energies the existence of a short-range attractive potential $U(r)$ can change the wave-function only slightly, so that with increasing E the quantities ψ and τ will approach their free particle values. All these properties are illustrated in fig. 3, which depicts $\tau^{(+)}(R_0)$ as functions of energy for the simple case of a rectangular potential.

Fig. 2

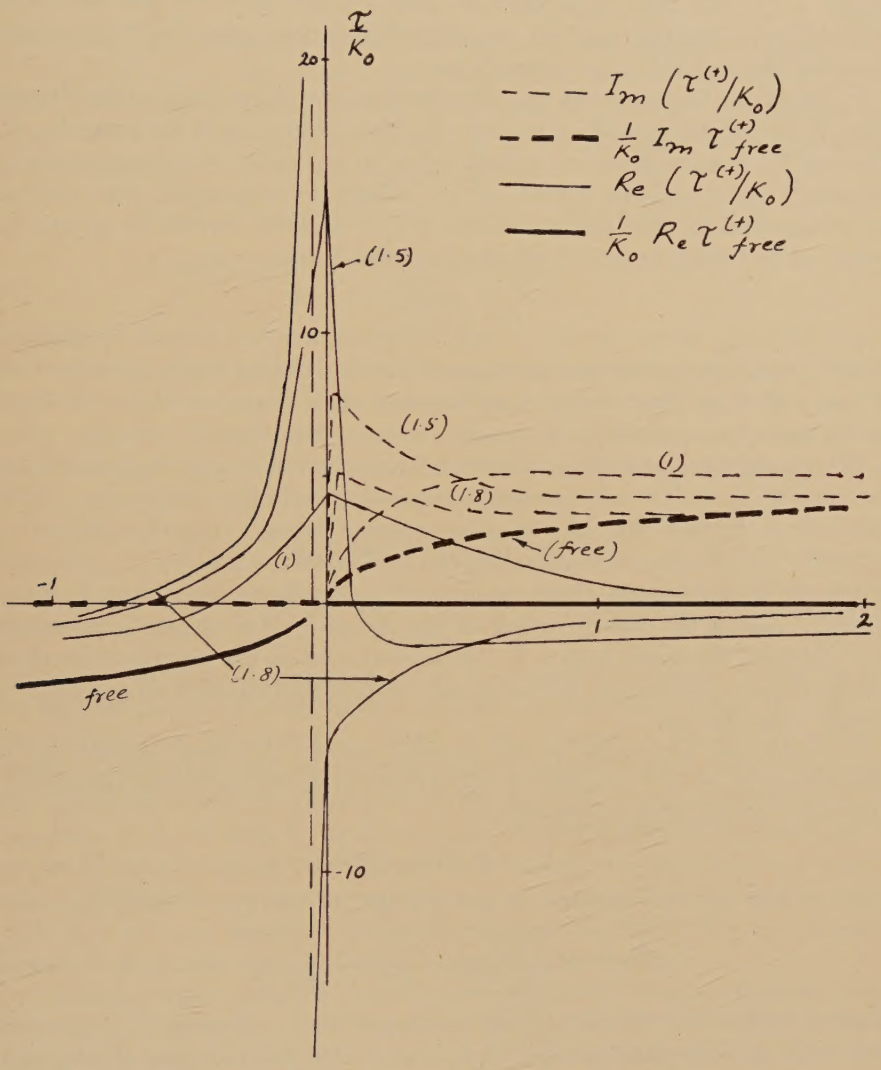


The above considerations indicate that new effects, connected with the possible existence of the surface potential, can be expected only if U_0 and α^{-1} are such as to make $\psi^{(+)}(R_0)$ close to zero, and this will happen (if at all) only for sufficiently small energies of ingoing or outgoing particles.

We must now consider what effects may be expected to arise from the existence of a surface potential satisfying the above conditions. Consider some intermediate state formed in the collision of two particles $a + X$. At certain energies quasi-stationary states will be formed which will give rise to resonances in all the cross sections. The condition for the existence of a quasi-stationary state is that the internal wave-function (defined for $r \leqslant R_0$) shall be matched at $r = R_0$ to an external wave function containing only outgoing waves $\psi^{(+)}$ of all possible pairs of particles into which our system may decay, or into which it could decay at higher energies. (We ignore the possibility of decay into more than two parts.) Usually this will happen only at some special energies at which the logarithmic derivatives of external and internal wave-functions happen to be equal at $r = R_0$, and we are then accustomed to speak of a resonance. However, if the energy of the system is close to the threshold for decay into another pair of particles $b + Y$, and if the potential $U(r)$ between these particles is sufficiently strongly attractive, then, as we have seen, the logarithmic derivative $\tau^{(+)}$ corresponding to the decay channel $b + Y$ is expected to vary widely due to a comparatively small variation of energy near to threshold. Consequently, the

probability that the equations of continuity of the logarithmic derivative, which determines the existence of quasi-bound states, shall have a solution close to threshold, is much greater than in a comparable energy interval far from threshold.

Fig. 3



Logarithmic derivative $\tau^{(+)}$ for a square well potential of a range ρ and a depth U_0; $K_0=(2\mu U_0/\hbar^2)^{1/2}$.

Hence, the existence of a surface potential increases the density of levels of a system in the neighbourhood of threshold energies. We shall show that this conclusion is confirmed by experimental data. The 'threshold states' have a number of predictable properties. For example, a threshold state

associated with the threshold for decay into $b+Y$ must have spin and parity equal to those for the system $b+Y$ with $l=0$. (All the above arguments are usually valid only for $l=0$.) If b and Y both have non-zero spins, so that the corresponding total spin can assume a number of values, then there may be several threshold states with spins equal to one or other of these values. In this case, experimental data on the spins of the threshold states could yield information regarding the surface potential $U(r)$ acting between the particles in the decay channel.

It may also be seen that the threshold states must have anomalously large radii and be composed mostly of a particular pair of particles $b+Y$. The complete wave-function of the system at an energy corresponding to a threshold state contains a part $\eta\psi^{(+)}(r)$, where $\psi^{(+)}$ represents the exterior wave-function for the decay particles $b+Y$, and the coefficient η may be obtained by fitting interior and exterior solutions at $r=R_0$: i.e.

$$\eta=\frac{\xi(R_0)}{\psi^{(+)}(R_0)}$$

where ξ is the interior wave-function of $b+Y$. Owing to the smallness of $\psi^{(+)}$ at threshold this factor may become very large, so that the term $\eta\psi^{(+)}(r)$ may be expected to dominate the wave-function.

The most important effect, however, concerns the energy dependence of the cross sections for various reactions near to one of the thresholds. This arises from the fact that all the cross sections depend upon the quantities $\psi^{(+)}$ and $\tau^{(+)}$ of all channels including the threshold channel $b+Y$. For the threshold channel itself these quantities, as we have seen, may become strongly energy dependent owing to the presence of a surface interaction $U(r)$ between the particles $b+Y$. It follows that in the neighbourhood of the threshold, *all* the cross sections may be expected to show an anomalous energy dependence.

For example, according to the general theory the cross section for a reaction $a+X\rightarrow b+Y$ near to its threshold is proportional to the imaginary part of $\tau^{(+)}$ for the decay particles:

$$\sigma=\zeta\,.\,\mathcal{I}m\,\tau_{bY}{}^{(+)}(R_0)$$

where in first approximation ζ is independent of energy. We have

$$\mathcal{I}m\,\tau^{(+)}\equiv\frac{1}{2i}\left[\frac{\psi^{(+)\prime}}{\psi^{(+)}}-\frac{\psi^{(-)\prime}}{\psi^{(-)}}\right]=\frac{k}{|\psi^{(+)}|^2}$$

where k is the wave-number of the decay particles. Hence, if $U\equiv 0$ then $\mathcal{I}m\,\tau^{(+)}=k$, and the usual result $\sigma\sim k$ follows. But if $U\neq 0$, then $\psi^{(+)}(R_0)$ can be very small near to threshold, increasing rapidly with increasing energy. Thus we would expect σ/k to be a rapidly *decreasing* function of energy just above the threshold. This behaviour has been observed experimentally, and will be described in detail in § 3.

Before presenting a more quantitative treatment we must first obtain, in the next section, analytical formulae for the exterior wave function $\psi^{(+)}$ and its logarithmic derivative $\tau^{(+)}$.

§ 2. FORMULAE FOR $\psi^{(+)}$ and $\tau^{(+)}$ (S-STATES, NEUTRAL PARTICLES)

To understand the features of $\psi^{(+)}$ and $\tau^{(+)}$ which are of physical interest let us first consider the simple case where $U(r)$ is a rectangular well:

$$\begin{aligned} U(r) &= -U_0 \quad \text{for} \quad R_0 \leqslant r \leqslant R_0+\rho \\ &= \quad 0 \quad \text{for} \quad r > R_0+\rho. \end{aligned}$$

Evidently ρ represents the thickness of the surface region. Let $k=(2\mu E/\hbar^2)^{1/2}$ be the exterior wave-number, and let $K_0=(2\mu U_0/\hbar^2)^{1/2}$. Then the wave-number in the surface region is given by $K=K_0\sqrt{(1+\epsilon)}$, where $\epsilon=E/U_0$ is a convenient dimensionless measure of the energy of the decay particles $b+Y$ whose reduced mass is μ. We find

$$\left.\begin{aligned} \psi^{(+)}(R_0) &= \exp\left[ik(R_0+\rho)\right]\left[\cos K\rho - i(k/K)\sin K\rho\right], \\ \tau^{(+)}(R_0) &= K\,\frac{\sin K\rho + i(k/K)\cos K\rho}{\cos K\rho - i(k/K)\sin K\rho}. \end{aligned}\right\} \quad . \; . \quad (2)$$

Graphs of the real and imaginary parts of $\tau^{(+)}$ are shown in fig. 3 for various values of $K_0\rho$ together with the corresponding free particle values. It may be seen that $\tau^{(+)}$ approaches its free particle value when $|\epsilon| \geqslant 1$, but may be very different for smaller values of $|\epsilon|$. The difference is particularly marked when $K_0\rho \approx \pi/2$ and $|\cos K\rho| \ll 1$. In this case it is easy to expand (2) in powers of ϵ: we find to lowest order that

$$\left.\begin{aligned} \psi^{(+)}(R_0) &= \exp(ikr_0)\,\Lambda\,(\delta - i\epsilon^{1/2}), \\ \tau^{(+)}(R_0) &= \frac{1}{R}\,\frac{1}{\delta - i\epsilon^{1/2}}, \end{aligned}\right\} \quad . \; . \; . \quad (3)$$

where $\Lambda=\sin K_0\rho \sim 1$, $\delta=\cot K_0\rho$, $r_0=R_0+\rho$ and $R=\Lambda^2/K_0$. Consideration of the derivation of these expressions shows that they should be valid for $|\epsilon| \ll |\delta| \ll 1$, i.e. say for $|E| \lesssim 2$ MEV if $U_0=40$ MEV. These approximate formulae (3), although derived above for a square well potential, appear to be generally valid for small $|\epsilon|$, except for the numerical values of the constants† r_0, Λ and δ, for potentials of reasonable shape such as the exponential and triangular potentials for which the calculations are again straightforward.

If Λ and δ are regarded as slowly varying functions of ϵ, the range of validity of (3) is almost certainly increased considerably.

Let us consider the approximate expressions for $\psi^{(+)}$ and $\tau^{(+)}$ in more detail. For the energy region below threshold (negative ϵ) $\psi^{(+)}(r)$ decays exponentially at large distances, $\psi^{(+)} \to \exp(-\kappa r)$, where $\kappa=K_0\sqrt{(-\epsilon)}$. Its value at $r=R_0$ is

$$\psi^{(+)}(R_0) = \exp(-\kappa r_0)\,\Lambda\,(\delta + \sqrt{(-\epsilon)}) \quad . \; . \; . \; . \; . \quad (4)$$

† Because of an exact relation $\mathcal{I}m\,\tau^{(+)}=k/|\psi^{(+)}|^2$, we find for any potential that

$$R \simeq \Lambda^2/K_0$$

where r_0 is determined so as to give $\epsilon^{1/2}=k/K_0$.

which vanishes if δ is negative when $\epsilon = -\delta^2$. This means that the potential $V(r)$ given by

$$V(r) = U(r) \quad \text{if} \quad r > R_0$$
$$= \infty \quad \text{if} \quad r \leqslant R_0 \qquad \ldots\ldots\ldots \quad (5)$$

has a bound state whose binding energy is $E_{\text{bind}} = \delta^2 U_0$. At the energy corresponding to the bound state the logarithmic derivative $\tau^{(+)}$ has a discontinuity. In fig. 3 this is shown in the curve for $K_0\rho = 1{\cdot}8$ when the value $\delta = -0{\cdot}23$ gives for the position of the discontinuity $\epsilon_{\text{disc}} = -0{\cdot}05$.

If the potential $U(r)$ is not deep enough there can be no bound state of the potential $V(r)$, and no discontinuity occurs in $\tau^{(+)}$. This is the case of positive δ. Nevertheless, $\tau^{(+)}$ can become quite large, reaching a maximum value

$$\tau^{(+)}(R_0) \simeq 1/R\delta$$

when $\epsilon = 0$.

In the region above threshold ($\epsilon > 0$), $\tau^{(+)}$ is complex. The real part goes to zero fairly rapidly with increasing ϵ; but the imaginary part has a more complicated behaviour:

$$\mathcal{I}m\,\tau^{(+)} \simeq \frac{1}{R} \cdot \frac{\epsilon^{1/2}}{\delta^2 + \epsilon} = \frac{1}{K_0 R} \cdot \frac{k}{\delta^2 + \epsilon} \qquad \ldots\ldots \quad (6)$$

Thus, for δ not very small, the denominator is constant at small energies and $\mathcal{I}m\,\tau^{(+)}$ will differ from its free particle value only by an approximately constant factor $(K_0 R\,\delta^2)^{-1}$. This is the case $K_0\rho = 1$ of fig. 3 for which $\delta \simeq 1$. If δ is small, however, the denominator is a sensitive function of ϵ and $\mathcal{I}m\,\tau^{(+)}$ attains a maximum at $\epsilon = \delta^2$ corresponding to $E = U_0\delta^2$. At higher energies, where (3) is no longer valid, $\mathcal{I}m\,\tau^{(+)}$ must increase again to attain its asymptotic value.

From these considerations it follows that $\psi^{(+)}$ and $\tau^{(+)}$ will differ very strongly from their free particle values, and consequently we can expect marked threshold effects, if δ is sufficiently small. In the case of negative small δ we saw that the potential $V(r)$, defined by (5), has a bound state of small binding energy; and if δ is small and positive $V(r)$ has a virtual state of small energy. Hence we conclude that threshold effects will be important if $V(r)$ has a bound or virtual state near to the threshold energy. Only this case will interest us in this paper.

The exponential form (1) of $U(r)$ is especially interesting for applications. For the corresponding wave function we find

$$\psi^{(\pm)}(R_0) = \left(\frac{\alpha}{2K_0}\right)^{\mp ip} J_{\mp ip}(y) \qquad \ldots\ldots \quad (7)$$

where J is a Bessel function,

$$p = \frac{2k}{\alpha}, \quad y = \frac{2K_0}{\alpha}, \quad K_0 = (2\mu U_0/\hbar^2)^{1/2},$$

while α and U_0 have the same meaning as in (1). Formulae (3) follow immediately for small $\epsilon \equiv E/U_0$, where now $r_0 = R_0$. In terms of the dimensionless parameter y we obtain the values of the quantities Λ and δ shown in the following table.

Value of the Parameters δ and Λ of Eqn. (3) for the Exponential Potential (1). Here $r_0 = R_0$

y	1·7	2·1	2·7	2·7
δ	0·430	0·112	0	−0·062
Λ	1·59	1·76	1·92	2·28

From the optical model we may expect $U_0 \simeq 40$ Mev and $\alpha^{-1} \simeq 0{\cdot}65 \times 10^{-13}$cm, from which we obtain $y \simeq 2$, so that δ is expected to be quite small and strong threshold effects therefore seem inevitable.

§ 3. The Behaviour of Cross Sections Near Threshold (Neutral Particles, $l = 0$)

In terms of the results obtained in the previous section we shall now develop a semi-quantitative theory of the behaviour of cross sections in the neighbourhood of a threshold assuming the existence of a surface potential of the kind we have described. We start by considering the simplest case in which there are only two channels to be considered. If the energy E of the colliding particles $a + X$ is less than the threshold energy E_{th} only elastic scattering $X(a,a)X$ is possible; the reaction channel $X(a,b)Y$ is also open if $E > E_{\text{th}}$. We shall study the effect of a surface potential $U(r)$ between the particles $b + Y$.

In a state of definite angular momentum the radial wave-function in the external region ($r > R_0$) can be written

$$\Psi = \frac{1}{v_a^{1/2}}(\psi_a^{(-)} - U_{aa}\psi_a^{(+)})\,\Phi(a, X) - \frac{1}{v_b^{1/2}}\,U_{ab}\psi_b^{(+)}\,\Phi(b, Y). \quad . \quad (8)$$

where $\Phi(a, X)$ and $\Phi(b, Y)$ are internal wave-functions for the reacting particles, $\psi_a^{(\pm)}$ and $\psi_b^{(\pm)}$ are corresponding radial wave-functions of relative motion, while v_a and v_b are the relative velocities. Asymptotically, $\psi^{(\pm)}(r) \to \exp(\pm ikr)$. The coefficients U_{ik} are elements of the scattering matrix and are given, according to the general theory of Wigner and Eisenbud, by (Lane and Thomas 1958):

$$\left.\begin{aligned} U_{aa} &= \frac{\psi_a^{(-)}}{\psi_a^{(+)}}\,\frac{(1 - R_{aa}\tau_a^{(-)})(1 - R_{bb}\tau_b^{(+)}) - \tau_a^{(-)}\tau_b^{(+)}R_{ab}^{\,2}}{(1 - R_{aa}\tau_a^{(+)})(1 - R_{bb}\tau_b^{(+)}) - \tau_a^{(+)}\tau_b^{(+)}R_{ab}^{\,2}}, \\ U_{ab} &= \frac{2iR_0(k_a k_b)^{1/2}}{\psi_a^{(+)}\psi_b^{(+)}}\,\frac{R_{ab}}{(1 - R_{aa}\tau_a^{(+)})(1 - R_{bb}\tau_b^{(+)}) - \tau_a^{(+)}\tau_b^{(+)}R_{ab}^{\,2}}. \end{aligned}\right\} \quad . \quad (9)$$

The elements R_{ik} of the R-matrix which enter these expressions depend only upon the wave-functions in the interior region ($r < R_0$). The quantities $\psi^{(+)}$, $\tau^{(+)}$ are here to be evaluated at $r = R_0$.

As we have seen, the existence of a surface potential $U(r)$ will produce characteristic effects only at small energies. The surface potential can act differently between the ingoing pair and between the outgoing pair since it can depend upon their spins, angular momenta, and other properties. However, we expect surface effects of two kinds: firstly, when the energy of the ingoing pair $a+X$ is small (when ψ_a and τ_a are very different from their free-particle values), and secondly when their energy is close to the threshold of the reaction $X(a,b)Y$ where ψ_b and τ_b may behave anomalously.

Let us consider the threshold region first; the result for the other region will appear as a by-product. In the threshold region only k_b(or v_b), ψ_b and τ_b will be sensitive functions of energy near to threshold, depending in fact upon $(E-E_{\text{th}})$ rather than on E itself. On the other hand, k_a, ψ_a and τ_a depend upon E and may be regarded as slowly varying functions of E provided that E_{th} is not very small. The elements of the R-matrix are also expected to be slowly varying with energy since they refer to the interior region.

With this in mind we re-write (9) in the form

$$\left.\begin{aligned} U_{aa} &= \exp(2i\phi)\,\frac{1-\tau_b^{(-)}/\Delta^*}{1-\tau_b^{(+)}/\Delta}, \\ U_{ab} &= \frac{k_b^{1/2}}{\psi_b^{(+)}}\cdot\frac{C}{\Delta-\tau_b^{(+)}}, \end{aligned}\right\} \quad . \quad . \quad . \quad . \quad . \quad (10)$$

where we have clearly shown the dependence of U_{ik} upon k_b, ψ_b and τ_b. All other quantities in (9) which are slowly varying functions of E near threshold have here been absorbed into the parameters ϕ, Δ and C. It can be seen that ϕ is real and Δ is complex: we have seen further that $\mathcal{I}m\,\Delta = -\frac{1}{4}|C|^2 < 0$. Since we are interested only in the behaviour of cross sections in a narrow energy range about threshold we shall in all that follows disregard the energy dependence of ϕ, Δ and C.

3.1. *Elastic Scattering*: $X(a,a)X$

Using (3) and (10) we find for the element of the scattering matrix corresponding to elastic scattering the following expression:

$$U_{aa} = \exp(2i\phi)\left\{1+\frac{2iy_2/(y_1^2+y_2^2)}{[\delta-y_1/(y_1^2+y_2^2)]-i[\epsilon^{1\,2}+y_2/(y_1^2+y_2^2)]}\right\} \quad (11)$$

where $y_1 = R\,\mathcal{R}e\,\Delta$ and $y_2 = -R\,\mathcal{I}m\,\Delta$. For the partial cross section we then obtain the usual resonance formula

$$\begin{aligned} \sigma_{aa} &= \frac{\pi}{k_a^{\,2}}|U_{aa}-1|^2 \\ &= \frac{4\pi}{k_a^{\,2}}\left\{\sin^2\phi+\frac{\Gamma_a^{\,2}}{(E_0+S)^2+(\Gamma_a+\Gamma_b)^2}\right. \\ &\qquad \left.+2\,\mathcal{R}e\left[\exp(-i\phi)\sin\phi\,\frac{\Gamma_a}{(E_0+S)-i(\Gamma_a+\Gamma_b)}\right]\right\} \quad . \quad . \quad (12) \end{aligned}$$

where

$$\begin{aligned} E_0 &= U_0\,[\delta - y_1/(y_1^2+y_2^2)], \\ \Gamma_a &= U_0 y_2/(y_1^2+y_2^2), \\ \Gamma_b &= U_0\sqrt{(E_b/U_0)} \quad \text{if} \quad E_b \equiv E - E_{\text{th}} > 0 \\ &= 0 \qquad\qquad\quad \text{if} \quad E_b < 0, \\ S &= 0 \qquad\qquad\quad \text{if} \quad E_b > 0 \\ &= U_0\sqrt{(|E_b|/U_0)} \quad \text{if} \quad E_b < 0. \end{aligned}$$

If particles $a + X$ were both charged, eqn. (12) would have to be modified to include Coulomb scattering. The differential cross section would then become

$$\sigma(\theta) = \left| f_{\text{Coul}}(\theta) + \frac{1}{2ik_a}\sum_l (2l+1)\exp(2i\sigma_l)\,(U_{aa}{}^l - 1)\,P_l(\cos\theta)\right|^2 \qquad (13)$$

where $f_{\text{Coul}}(\theta)$ is the usual Coulomb scattering amplitude, σ_l the Coulomb phase shift for l-waves, and $U_{aa}{}^l$ the element of the scattering matrix for orbital angular momentum l as calculated above.

It is necessary to stress very strongly that the resonance-like appearance of eqns. (11) and (12) is due entirely to the assumed presence of a surface potential $U(r)$ of strength U_0 between b and Y. If $U_0 = 0$, the quantity

$$\frac{\tau_b^{(+)}}{\Delta} \approx \frac{k_b}{K'},$$

where K' is an effective wave number for particles inside the nucleus, is very small and can be neglected near threshold. In this case we would obtain only the first term in (12), which resembles potential scattering in that its energy dependence *close to threshold* is small. The term $E_0{}^2$ which replaces the more usual $(E - E_0)^2$ arises from the assumption that $\epsilon = (E - E_{\text{th}})/U_0 \ll 1$.

3.2. *Reaction*: $X(a,b)Y$

In a similar fashion to that employed to derive the partial cross section for elastic scattering we may obtain for the reaction cross section near threshold

$$\sigma_{ab} = \frac{\pi}{k_a{}^2}|U_{ab}|^2 = \frac{4\pi}{k_a{}^2}\frac{\Gamma_a\Gamma_b}{E_0{}^2 + (\Gamma_a+\Gamma_b)^2} \quad . \quad . \quad . \quad . \quad (14)$$

where all quantities have the same meaning as before. The cross section for the inverse reaction $Y(b,a)X$ is obtained in the usual manner by means of detailed balance.

3.3. *Elastic Scattering*: $Y(b,b)Y$

We may represent the matrix element U_{bb} for elastic scattering of $b + Y$ in terms of the energy sensitive quantities as follows (Lane and Thomas 1958):

$$U_{bb} = \frac{\psi_b^{(-)}}{\psi_b^{(+)}}\frac{\Delta - \tau_b^{(-)}}{\Delta - \tau_b^{(+)}} = \exp(-2ik_b r_0)\frac{E_0 - i(\Gamma_a - \Gamma_b)}{E_0 - i(\Gamma_a + \Gamma_b)} \quad . \quad . \quad (15)$$

so that the scattering cross section becomes

$$\sigma_{bb} = \frac{4\pi}{k_b^2}\left\{\frac{\Gamma_b^2}{E_0^2+(\Gamma_a+\Gamma_b)^2} + \sin^2 k_b r + 2\,\mathcal{R}e\left[\exp(ik_b r_0)\sin k_b r_0 \frac{\Gamma_b}{E_0 - i(\Gamma_a+\Gamma_b)}\right]\right\}. \quad . \quad . \quad . \quad (16)$$

All the cross sections (12), (14) and (16) are very similar to the usual resonance formulae. The essential difference is that, apart from the trivial factors k_a^2 and k_b^2, the energy dependence in our case is contained only in S and Γ_b as defined following eqn. (12).

The inelastic width is seen to be

$$\Gamma_b = U_0\left(\frac{E-E_{\text{th}}}{U_0}\right)^{1/2} = U_0\frac{k_b}{K_0} = \frac{\hbar^2 K_0^2}{2\mu\Lambda^2}Rk_b = \frac{\hbar^2}{2\mu R^2}\Lambda^2 Rk_b \approx \frac{\hbar^2}{2\mu R^2}(Rk_b) \quad . \quad . \quad . \quad (17)$$

where we have used the relations which follow eqns. (3). Thus Γ_b is anomalously large: in fact the reduced width $\gamma_b^2 \equiv \Gamma_b/Rk_b$ is roughly equal to the Wigner limit $\hbar^2/2\mu R^2$. This clearly demonstrates that we are dealing with a resonance level having a predominantly single particle flavour. It is not possible to derive estimates for Γ_a and E_0, however, since they depend upon the internal quantity Δ. In § 7 we shall see that experiment would suggest that they are several Mev in order of magnitude.

In view of the differences between (12), (14) and (16) from the conventional resonance formulae, it is worth examining a little more the energy dependence of these cross sections.

In the cross sections (14) and (16) the resonance denominator rapidly grows with increasing energy, and the quantity

$$\frac{\sigma_{ab}}{\sqrt{(E-E_{\text{th}})}} = \frac{4\pi}{k_a^2}\frac{\Gamma_a\sqrt{(U_0)}}{E_0^2+(\Gamma_a+\Gamma_b)^2} \quad . \quad . \quad . \quad . \quad . \quad (18)$$

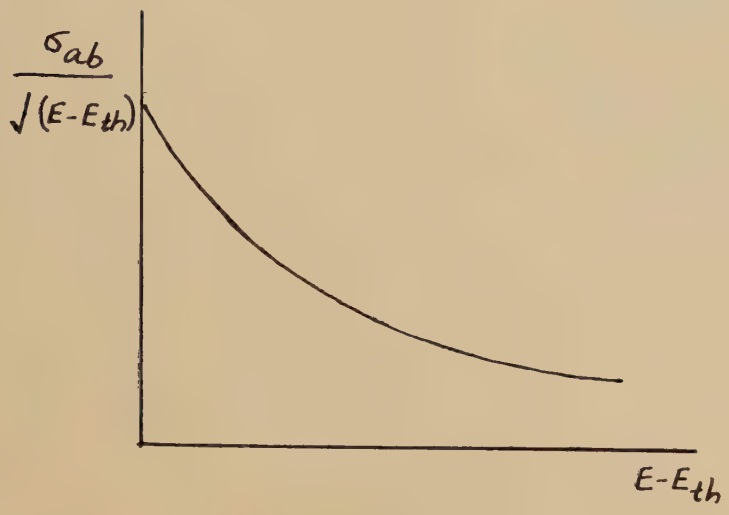
correspondingly decreases, since $\Gamma_b = U_0\sqrt{[(E-E_{\text{th}})/U_0]}$. This is shown in fig. 4. In the conventional Wigner (1948) theory of threshold reactions, however, the quantity $\sigma_{ab}/\sqrt{(E-E_{\text{th}})}$ is a *constant* near threshold. The behaviour of σ_{ab} itself, according to (14), is shown in fig. 5: the cross section rises rapidly from threshold to a maximum near $E = E_{\text{th}} + (E_0^2+\Gamma_a^2)/U_0$ after which it decreases.

The cross sections for the inverse reaction $Y(b,a)X$ and of the scattering process $Y(b,b)Y$ differ from the conventional threshold prescriptions (Wigner 1948) also. For the latter we find, neglecting the second and third terms in (16),

$$\sigma_{bb} = \frac{k_a^2}{k_b^2}\frac{\Gamma_b}{\Gamma_a}\sigma_{ab} = \frac{\mu_a}{\mu_b}\frac{E}{\Gamma_a}\frac{\sigma_{ab}}{\sqrt{(E-E_{\text{th}})}}$$

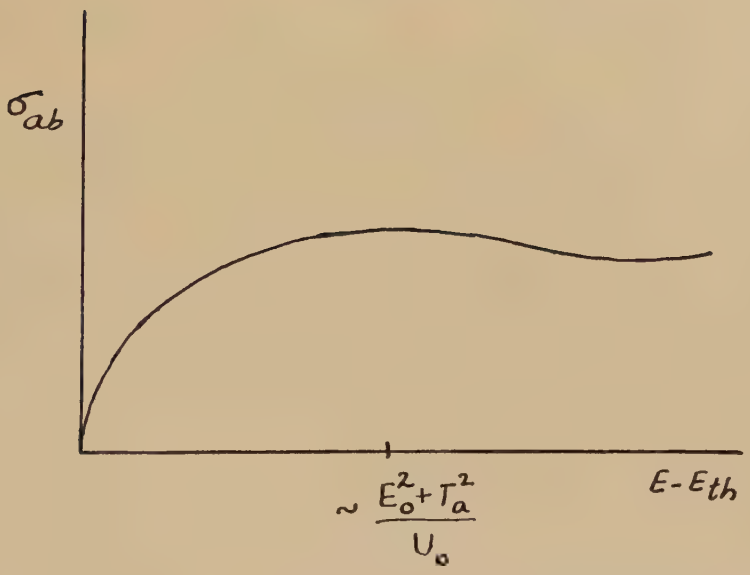
so that σ_{bb} has near to threshold the same energy dependence as the quantity shown in fig. 4. It is usually supposed that σ_{ba} follows a

Fig. 4



Energy dependence of reaction cross section near threshold ($l=0$, neutral particles).

Fig. 5



Energy dependence of reaction cross section near threshold ($l=0$, neutral particles).

$1/v$-law, (Wigner 1958), but we now find a more rapid decrease with energy. In fact the quantity

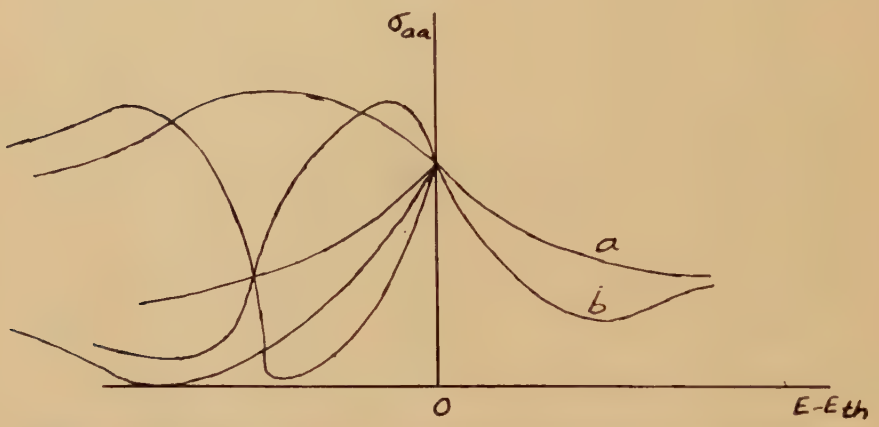
$$\sigma_{ba}\sqrt{(E-E_{\rm th})} = \frac{k_a^{\,2}}{k_b^{\,2}}\sqrt{(E-E_{\rm th})}\,\sigma_{ab},$$

instead of being constant as for the $1/v$-law, has the same energy dependence as $\sigma_{ab}/(E-E_{\rm th})$ shown in fig. 4.

The energy dependence of the elastic scattering $X(a,a)X$ is much more complicated because of an interference term in the cross section (12). In the region above threshold we may write

$$\sigma_{aa} = \frac{4\pi}{k_a^{\,2}}\frac{(E_0\sin\phi+\Gamma_a\cos\phi)^2+\Gamma_b{}^2\sin^2\phi}{E_0{}^2+(\Gamma_a+\Gamma_b)^2}, \quad (E>E_{\rm th}) \tag{19}$$

Fig. 6



Different types of behaviour of a scattering cross section near threshold.

for which there are essentially two types of behaviour, depicted as curves a and b on the right-hand side of fig. 6. Below threshold there are many more varieties. In this region we may write

$$\sigma_{aa} = \frac{4\pi}{k_a^{\,2}}\frac{[(E_0+S)\sin\phi+\Gamma_a\cos\phi]^2}{(E_0+S)^2+\Gamma_a{}^2} \quad . \ . \ . \ . \tag{19a}$$

and the form assumed by σ_{aa} depends upon the values of ϕ, Γ_a and E_0. Several possibilities are shown on the left-hand side of fig. 6. It is important to notice that, depending upon the values of E_0, Γ_a and ϕ, σ_{aa} may attain a value almost equal to the maximum possible value of $4\pi/k_a{}^2$ somewhere just below threshold.

§ 4. The Nature of the 'Threshold State'

All the cross sections obtained in § 3 have a resonance-like structure. We must therefore ask what is the nature of the state which gives rise to this behaviour. We know nothing about the internal region, but in the simple picture we have adopted we do at least know everything that happens

in the external region $r < R_0$ which includes the surface. In this region the radial wave function (eqn. (8)) consists of two parts. The first describes ingoing and outgoing waves of the particles $a + X$; the last term $U_{ab}\psi_b^{(+)}$ describes the particles $b + Y$. Above threshold $\psi_b^{(+)}$ describes an outgoing wave of particles formed in the reaction $X(a, b)Y$. Below threshold k_b is imaginary and $\psi_b^{(+)}$, decaying exponentially with distance, describes the 'leakage' of the particles $b + Y$ from the internal region, where conservation of energy does not prohibit their formation, to the external region. When E is far below E_{th}, $\psi_b^{(+)}$ decays very rapidly, as $\exp(-|k_b|r)$, and the leakage does not play an important rôle. But as E approaches E_{th}, $\psi_b^{(+)}(r)$ extends to great distances. As a result, the intermediate state formed in the collision $a + X$ may be regarded, near threshold, as being composed almost entirely of particles $b + Y$ moving at large distances from each other.

To see this we may compare the probabilities for finding $b + Y$ outside and inside the sphere $r = R_0$ respectively. We have

$$\frac{\rho_{\text{out}}}{\rho_{\text{in}}} = \frac{|U_{ab}|^2 \int_{R_0}^{\infty} |\psi_b^{(+)}(r)|^2 dr}{\int_0^{R_0} |\Psi|^2 dr}$$

where Ψ is a wave function for $b + Y$ in the internal region. We should expect that Ψ can be replaced by unity within $r < R_0$, whereas

$$\int_{R_0}^{\infty} |\psi_b^{(+)}|^2 dr \simeq \int_{R_0}^{\infty} \exp(-2\kappa r) dr \simeq \frac{1}{2\kappa}$$

where $\kappa = |k_b| = K_0\sqrt{(-E_b/U_0)}$. Using (3) and (10) we therefore obtain as a crude estimate of the ratio

$$\frac{\rho_{\text{out}}}{\rho_{\text{in}}} \simeq \frac{|U_{ab}|^2}{\kappa R_0} \simeq \frac{U_0\Gamma_a}{(E_0 + S)^2 + \Gamma_a^2}. \quad \ldots\ldots \quad (20)$$

Now all our considerations refer to the case when Γ_a and E_0 are much smaller than U_0, so that this ratio is quite large, having a maximum value of U_0/Γ_a when $S = -E_0$.

Thus the threshold resonance refers to a peculiar state in which the system is largely decomposed into particles $b + Y$ moving at a large distance from each other. To this extent the threshold state resembles the normal state of the deuteron in which neutron and proton spend most of their time outside the range of the interaction between them. This is a result which is at least consistent with our starting assumption that the surface interaction could be represented by a potential. If it were not for the fact that the threshold state consists of two such well separated particles the whole concept of a static surface potential would be open to serious objection. From the picture of the threshold state given above it is also clear that such a state cannot be effective above threshold since it would immediately disintegrate into $b + Y$.

The spin and parity of the threshold state can of course be compounded from those of b and Y in the usual way.

§ 5. Charged Particles and Higher Angular Momenta

If the particles b and Y are both charged, or if they are in a state of motion with $l \neq 0$, there is a long range repulsive potential $U_1(r)$ representing Coulomb and centrifugal forces in addition to the short range attractive potential $U(r)$. To study the effect of the long-range potential in the simplest manner we shall assume that $U(r)$ is a square well and that $U_1(r)$ may be neglected in the region occupied by $U(r)$. This should be sufficient to show the qualitative effect of a repulsive long range interaction on the threshold phenomena.

Using the same notation as in (2) we find for this case

$$\left.\begin{aligned} \psi_b^{(+)}(R_0) &= \phi_b^{(+)}(R_1)\left\{\cos K\rho - \left(\frac{\gamma}{K}\right)\sin K\rho\right\} \\ \tau_b^{(+)}(R_0) &= K\frac{\sin K\rho + (\gamma/K)\cos K\rho}{\cos K\rho - (\gamma/K)\sin K\rho} \end{aligned}\right\} \quad . \quad . \quad . \quad (21)$$

where $R_1 = R_0 + \rho$ is the outer boundary of the surface potential $U(r)$. Here, now, $\phi_b^{(+)}(r)$ is an out-going radial wave function in the potential $U_1(r)$, normalized in such a way that $|\phi_b^{(+)}(r=\infty)| = 1$, while γ is its logarithmic derivative at R_1:

$$R_1\gamma = R_1\frac{\phi_b^{(+)\prime}}{\phi_b^{(+)}}\bigg|_{r=R_1} \equiv -S + iP.$$

The quantities S and P are usually referred to as the shift function and the penetrability factor, respectively. In the case $l = 1$, and neutral particles we have

$$U_1(r) = \frac{\hbar^2}{\mu r^2},$$

so that

$$\phi_b^{(+)}(R_1) = j_1(kR_1) + in_1(kR_1)$$

where j_1 and n_1 are the usual spherical Bessel functions (Schiff 1949), so that S and P are given by

$$-S + iP = -\frac{1}{1+(kR_1)^2} + i\frac{(kR_1)^3}{1+(kR_1)^2}.$$

Their energy dependence is shown in fig. 7. Although calculated for a special case, this behaviour is typical for any angular momentum and for charged particles. Writing $U_1(R_1) = U_1$ we find, as is well known, that:

(*a*) P is zero for $\epsilon < 0$, very small if $\epsilon \ll U_1/U_0$, rising to $P \approx 1$ at $\epsilon = U_1/U_0$, and approaching the free particle s-wave value $P = kR_1$ for $\epsilon \gg U_1/U_0$;

(*b*) S is close to its free particle s-wave value $|kR_1|$ for $\epsilon < -U_1/U_0$, attains a finite value $S(0)$ at $\epsilon = 0$, and gradually tends to zero for large ϵ, becoming small for $\epsilon > U_1/U_0$. For an uncharged pair, of orbital angular momentum l, we find

$$S(0) = l; \qquad \text{(uncharged)}$$

while for the corresponding charged case (Prosser and Biedenharn 1958)

$$S(0) = l + (2\eta kR_1)^{1/2}\frac{K_{2l}((8\eta kR_1)^{1/2})}{K_{2l+1}((8\eta kR_1)^{1/2})} \qquad \text{(charged)}$$

where $\eta = e^2/\hbar v$ and K_n is the modified Hankel function. The essential conclusion, therefore, is that $\gamma R_1 = -S + iP$ differs appreciably from its free particle s-wave values only within the energy range $|\epsilon| < U_1/U_0$.

Referring to eqns. (21) we see that the effects of the repulsion U_1 may be neglected if $|\epsilon| > U_1/U_0$. In that case, the theory of the preceding sections remains valid.

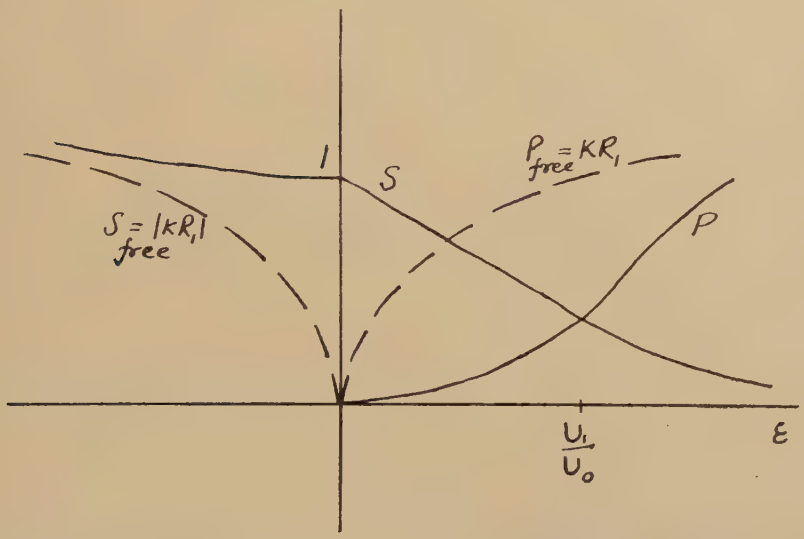
In the immediate neighbourhood of threshold, however, where $|\epsilon| < U_1/U_0$, the formulae require further examination. In this region the penetration factor P is small, and if the quantity

$$\zeta(\epsilon) = \cos K\rho + (S/KR_1)\sin K\rho$$

should be small, $\tau_b^{(+)}$ may become very large. This will be the case if the attractive surface potential $U(r)$ is such that

$$\frac{\pi}{2} < K_0\rho = \rho(2\mu U_0/\hbar^2)^{1/2} < \pi.$$

Fig. 7



Energy dependence of the shift function S and the penetrability factor P for a long range repulsive potential $U_1(r)$.

In the neighbourhood of a zero of $\zeta(\epsilon)$ it is then possible to neglect the energy dependence of all quantities in (21) except $\zeta(\epsilon)$ and $\phi_b^{(+)}$, so that we obtain instead

$$\left.\begin{aligned} \psi_b^{(+)}(R_0) &= \Lambda'\phi_b^{(+)}(R_1)[(\Lambda')^{-1}\zeta(\epsilon) - iP], \\ \tau_b^{(+)}(R_0) &= \frac{1}{R'}\,\frac{1}{(\Delta')^{-1}\zeta(\epsilon) - iP}, \end{aligned}\right\} \quad . \ . \ . \quad (22)$$

where $\Lambda' = \sin K_1R_1/K_1R_1$ and $R' = R_1/(K_1{}^2R_1{}^2 + S^2)$ are to be regarded as constants in this approximation. If $\epsilon = \epsilon_1$ is a zero of $\zeta(\epsilon)$, then K_1 is the corresponding value of K. Approximately, $K_1 \approx K_0$.

For values of ϵ near the zero ϵ_1 we may write

$$\zeta(\epsilon)=(\epsilon-\epsilon_1)\eta+\ldots$$

where $|\eta|\approx(U_1/U_0)S(0)$. In the notation of §§ 2 and 3 we then obtain for the cross sections

$$\left.\begin{aligned}\sigma_{aa}&=\frac{4\pi}{k_a^2}(2l+1)\left\{\sin^2\phi+\frac{\Gamma_a^2}{(E-E_r)^2+(\Gamma_a+\Gamma_b)^2}\right.\\&\qquad\left.+2\,\mathcal{R}e\left[\frac{\exp(i\phi)\,\Gamma_a\sin\phi}{(E-E_r)-i(\Gamma_a+\Gamma_b)}\right]\right\},\\\sigma_{ab}&=\frac{4\pi}{k_a^2}(2l+1)\,\frac{\Gamma_a\Gamma_b}{(E-E_r)^2+(\Gamma_a+\Gamma_b)^2},\\\sigma_{bb}&=\frac{4\pi}{k_b^2}(2l+1)\,\frac{\Gamma_b^2}{(E-E_r)^2+(\Gamma_a+\Gamma_b)^2}\end{aligned}\right\}\quad\ldots\quad(23)$$

except that, in the case of charged particles, it is necessary to add in the usual way the Coulomb scattering and interference terms. In these formulae

$$\begin{aligned}\Gamma_a&=U_0y_2\Lambda'/R'\eta,\\\Gamma_b&=U_0P\Lambda'/\eta\\E_r&=U_0(\epsilon_1+y_1\Lambda'/R_1\eta)\end{aligned}$$

where the y_i are defined in § 3.

Once again, therefore, we obtain resonance-like formulae for the cross sections, which shows that the basic nature of the threshold behaviour is unchanged by the inclusion of the long range repulsive potential U_1 representing Coulomb and centrifugal forces. There are some important qualitative differences, however:

(*a*) A 'threshold resonance' can now be situated above the threshold. In fact, if a threshold state exists at all it is much more likely to occur above threshold than below. This is because S changes more rapidly in the interval $0<\epsilon<U_1/U_0$ than in the interval $-(U_1/U_0)<\epsilon<0$ (see fig. 7) and it is therefore more probable that $\zeta(\epsilon)$ should have a zero in the former interval. This is contrary to the situation of § 3 where the threshold state could occur (if at all) only below threshold. The physical reason for the difference is that particles $b+Y$ cannot easily escape from each other at low positive energy because of the potential barrier $U_1(r)$.

(*b*) The threshold state is no longer the almost pure one-particle state found in section 3. This is seen from the fact that the reduced width of the $b+Y$ channel is now expected to be small, for

$$\frac{\Gamma_b}{P}=\frac{U_0\Lambda'}{\eta}\simeq\frac{U_1}{S(0)}\ll U_0.$$

(*c*) If there is a threshold state it no longer need have the large effective radius, of order $|k_b|^{-1}$, that we found in § 3. The external wave function $\phi_b^{(+)}(r)$ is now peaked at quite small radii, giving an effective radius of order R_1. However, we cannot dismiss the possibility that R_1 itself

may be quite large particularly for light nuclei. For example, if $U(r)$ were an exponential potential, $U(r)=50\exp(-0{\cdot}65(r-R_0))$ MeV, and $U_1(r)=1{\cdot}44Z_1Z_2/r$ MeV is the usual Coulomb potential, where r and R_0 are measured in fermis, then the following values may be obtained for R_1 in the case $R_0=2$ fermis:

Z_1Z_2	3	5	10
R_1	10 f	8·5 f	7 f

All the results of this section have been derived for the case of a square well potential $U(r)$. However, our conclusions regarding the nature of threshold states do not depend upon this assumption: only the exact shapes of the cross sections depend upon the form of $U(r)$ through the relatively weak energy dependence of the factors Λ', R' and ζ.

§ 6. Discussion

In previous sections only two-channel systems were considered and a very simple form for the surface potential $U(r)$ was assumed. The latter assumption we found to be unimportant because it is the energy dependence of $\psi_b^{(+)}(R_0)$ and $\tau_b^{(+)}(R_0)$ which matters, and the formulae we used for these quantities are fairly general. All that is required is that $U(r)$ should have a bound or virtual state at an energy small compared with the depth U_0 of $U(r)$, and that we confine ourselves to an energy region in the neighbourhood of the threshold state.

The restriction to two-channel systems is more serious. In a many-channel system the scattering matrix depends upon $\psi_b^{(+)}$ and $\tau_b^{(+)}$ in a more complicated manner than we assumed, so that the energy dependence of the resulting cross sections can be quite complex. In fact it will be shown in a forthcoming paper that the behaviour of the cross sections cannot in general be described by formulae of the Breit–Wigner type with real widths, if more than two channels are involved. In spite of this complication, however, the physical nature of the threshold phenomena remains unchanged. This is because the properties of the threshold state, and even its existence, depend almost entirely on the potential $U(r)$ acting between $b+Y$ (the threshold channel) and only indirectly on all the other properties of the system provided that two or more thresholds do not occur close together in energy. This should be the case at least for uncharged particles with $l=0$: for higher angular momenta and for charged particles the threshold state may not be so extended in space so that the behaviour of the internal wave function may play a more important rôle.

We conclude the theoretical part of this paper by remarking that the above formulae include all the usual results of the theory of theshold cusps (Breit 1957, Baz 1958). Let us take, for example, the cross section for elastic scattering $X(a,a)X$. Near the $b+Y$ threshold, where Γ_b is

small just above threshold, or S is small just below, we can expand (11) and obtain

$$U_{aa}=\exp(2i\phi)\frac{E_0+i\Gamma_a}{E_0-i\Gamma_a}(1-\xi\sqrt{E})\equiv U_{aa}{}^0(1-\xi\sqrt{E}) \quad . \quad . \quad (24)$$

where E is the energy of $b+Y$ at infinity ($E=E_a-E_{\text{th}}$) and

$$\xi=\lim_{E\to 0}\frac{k_a{}^2}{2\pi}\frac{\sigma_{ab}}{\sqrt{E}}.$$

This result coincides with that obtained by Breit (1957) and Baz (1958). However, we are now in the position to estimate the range of validity of the usual cusp theory. From the above derivation, it follows that (24) is valid provided Γ_b (or S) $\ll|E_0|$ or Γ_a (whichever is the larger) so that in order to apply (24) the energy must be quite close to threshold:

$$|E|\ll\frac{\alpha^2}{U_0}, \quad . \quad . \quad . \quad . \quad . \quad . \quad . \quad . \quad . \quad (25)$$

where α is the larger of $|E_0|$ and Γ_a. If, for example, $\alpha=1$ Mev and $U_0=40$ Mev, we require that $|E|\ll 25$ kev. At energies further distant from the threshold the more complete formula (11) must be used.

§ 7. Comparison with Experiment

In this section we confine ourselves to the region of light nuclei with atomic weight $A<16$ where the most extensive and precise data are available†. Our aim is to show, using some examples, that the theory of the preceding sections seems to agree quite well with what is known of the reactions involving these nuclei.

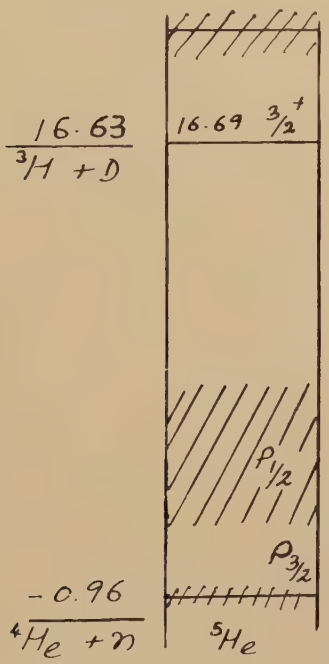
One of the main results of the theory was that there should be a concentration of levels near to the thresholds of two-body channels $b+Y$. The reason was that if there is a strongly attractive surface potential $U(r)$ acting between b and Y the corresponding logarithmic derivative $\tau_b{}^{(+)}(R_0)$ varies very rapidly near to the threshold.

The case of the mirror nuclei ^{5}He and ^{5}Li is one of the simplest examples. Each of the two nuclei possesses only two well-established levels although others are suspected (fig. 8). Both levels occur slightly above the two relevant thresholds, the $3/2-$ level close to the $^4\text{He}+\text{n}$ threshold, and the $3/2+$ levels close to the $^3\text{H}+^2\text{H}$ threshold at 16·6 Mev (in the case of ^{5}He). Just as the $3/2-$ level can be thought of as the consequence of an attractive surface interaction between neutron and alpha particles, so the $3/2+$ level can be regarded as the result of a surface interaction between triton and deuteron. This picture is in accord with the current interpretation of these levels as $^2\text{P}^-_{3/2}$ and $^2\text{D}^+_{3/2}$ respectively.

† All the experimental data in this section are taken from Ajzenberg-Selove and Lauritsen (1959) except where it is stated otherwise, and will not be referred to.

As our next example we consider the nucleus ^{8}Be. The ground state is clearly a 'threshold' state, composed of two α-particles in a state with $l=0$. Experimental value of the α-particle reduced width is about 0·15 of Wigner limit. The radius of this state must be extremely large ($\gtrsim 10$ f, see table in § 5). The 16·67 Mev-level also seems to have 'threshold' properties, corresponding to a structure ^{7}Li + p in a p-state: it is close to the ^{7}Li + p threshold, has reasonable spin and parity and (as follows from the very large ^{7}Li(dn) cross-section to this level) is composed mostly of ^{7}Li in the ground state together with a proton.

Fig. 8



Level structure and positions of two-body thresholds of ^{5}He.

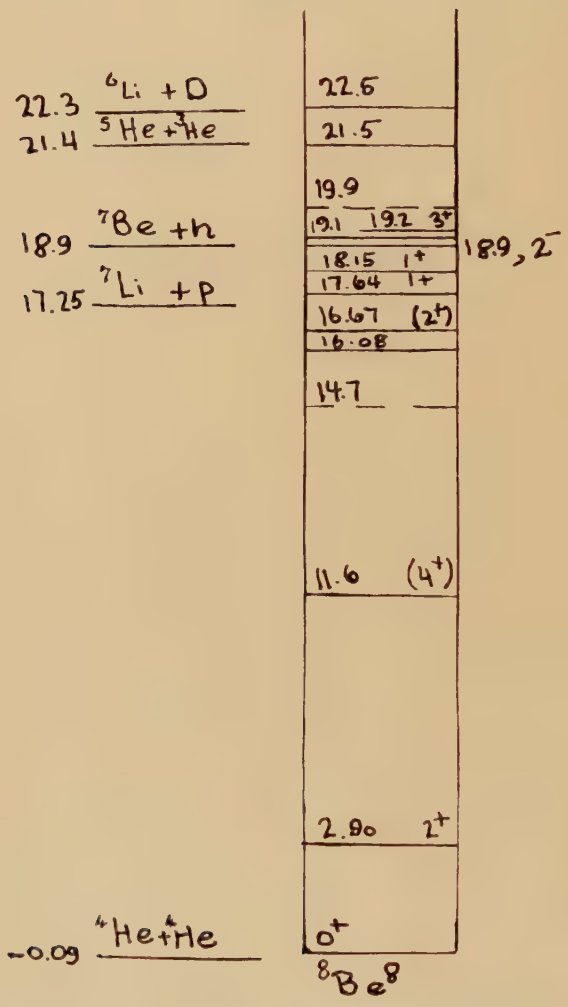
At higher energy there is a very interesting region near the (^{8}Be + n)-threshold (levels 18·9, 19·1 and 19·2 Mev) which we consider in some detail. The only indication on the 18·9 level comes from a study of the ^{7}Li (pn)^7Be-reaction (Bergman *et al.* 1958, Maclin and Gibbons 1958). The behaviour of the cross section at small energy is shown on fig. 12. The authors of the above paper fitted the data having assumed the existence of the 18·9 Mev level of ^{8}Be. The neutron reduced width of the level was found to be very large—about five times larger than the corresponding proton reduced width—contrary to all the predictions of charge independence. From the point of view of the above theory, however, the picture

looks quite natural. The cross-section is very well described by eqn. (18) with

$$\frac{E_0}{\Gamma_a} = \pm 0{\cdot}7\,; \quad \frac{\Gamma_b}{\sqrt{[E(\text{kev})]}} \simeq 6\Gamma_a \quad . \quad . \quad . \quad . \quad . \quad (26)$$

and, therefore, its energy dependence may be interpreted as an indication of a strong attractive interaction between ^{7}Be and n in an s-state. The large neutron width and the lack of the charge independence† strongly

Fig. 9

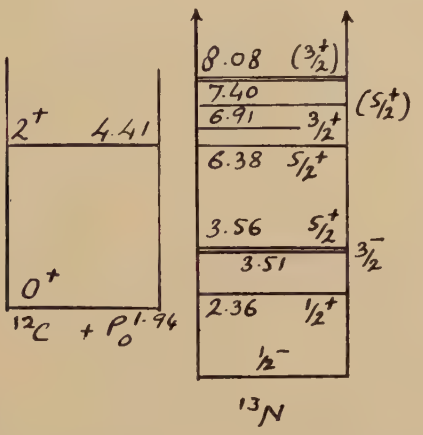


Level structure and positions of two-body thresholds for ^{8}Be.

† Charge independence holds of course in the interior region $r < R_0$. At $r > R_0$, however, where most of the wave function of a ' threshold state ' is concentrated, there is no charge independence whatsoever, In this exterior region wave functions are very sensitive to energy and the small mass difference between n and p is important.

support this interpretation. From (26) and the results of §3 it follows further, that the ^{7}Li(pp) scattering cross section must have a sharp resonance just below the (^{7}Be + n)-threshold if E_0 is negative. Experiment shows no resonance, however. We conclude, therefore, that $E_0 > 0$, and referring again to the results of §§3–4 we see that in the strict sense there is no well defined threshold state at all (the phase shift does not go through $\pi/2$), although the reaction cross section has a Breit–Wigner shape. All the effects are due to the fact, that the radius (and, correspondingly, life-time) of the intermediate system, formed in a (^{7}Li + p)-collision, grows indefinitely when the energy of the protons approaches the (^{7}Be + n)-threshold from below.

Fig. 10



Level structure and positions of two-body thresholds for ^{13}N.

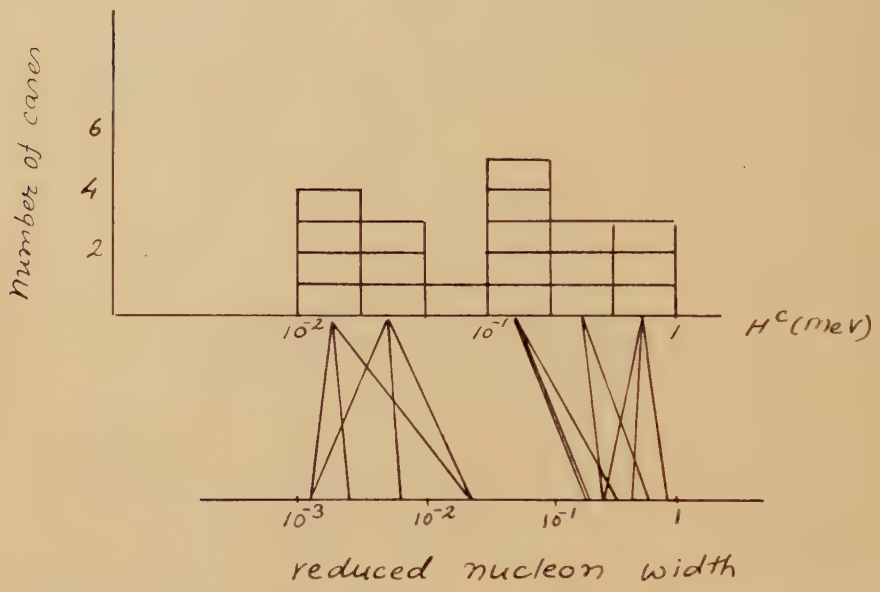
The 19·2 Mev level of ^{8}Be is also most naturally interpreted as a 'threshold' state, corresponding to ^{7}Be + n in a $^5P_3$-state. A strong indication (besides spin, parity and location) is its large neutron reduced width which is again much larger than that for protons. This level must appear also in a ^{7}Li (pp)-scattering at a slightly different energy (the shift is due to interference with the usual potential scattering). It is very probable then that a maximum in the ^{7}Li(pp) cross section at 2·1 Mev (which is usually accounted for by postulating a 19·1 Mev level of ^{8}Be) is a result of this 19·2 Mev 'threshold' state. If this is true (there is no evidence to the contrary at present), all the phenomena near the ^{7}Be + n threshold can be completely explained in terms of the two 'threshold' states at 18·9 and 19·2 Mev.

In exactly the same way we can find 'threshold' states in other light nuclei. Some of the examples are shown in a table on p. 372.

The case of ^{13}N is worth mentioning. The level structure is shown on fig. 10. Spins, parities and locations of levels suggest that the first three excited levels are (^{12}C + p)-threshold states, while the next few levels

(around 7 MeV) are (^{12}C + p)-threshold states associated with the 2+ state of ^{12}C at 4·43 MeV. Very large reduced widths of the levels in question strongly support this suggestion.

Fig. 11



Distributions of isotopic spin impurities (in terms of Coulomb matrix elements H_c). For those states for which the reduced nucleon width γ^2 in units of $\hbar^2/\mu R$ for emission to the ground state of A−1 nucleons is known, a line connects the appropriate H_c box to the appropriate range of reduced width to show a correlation between H_c and γ^2 (after D. H. Wilkinson).

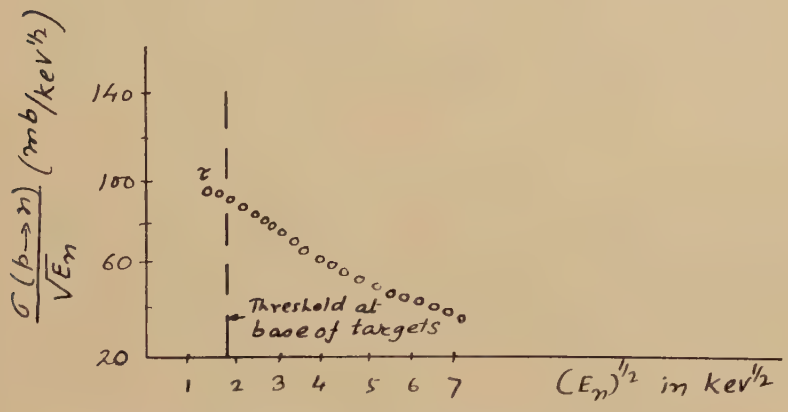
Nucleus	Energy of threshold	Angular momentum	Composition of the state	Specification of the state	Reduced width in units $\frac{3}{2}\hbar^2/MR_0^2$
^{7}Li	6·54	(1/2+, 3/2+)	^{6}Li + n	$S_{1/2,\ 3/2}$	large
	7·47	5/2−	^{6}Li + n	$^{4}P_{5/2}$	$\gamma_n^2 = 0{\cdot}42$
^{9}Be	1·75	1/2+	^{8}Be + n	$^{2}S_{1/2}$	$\gamma_n^2 \approx 1$
^{9}B	0	>1/2−	^{8}Be + p	$P_{1/2,\ 3/2}$	
^{12}C	7·656	0+	^{8}Be + d	$^{1}S_0$	

As we have mentioned (see footnote on p. 370), the 'threshold' effects destroy isobaric-spin invariance of 'threshold' states. On the other hand, a particular property of the 'threshold' states is a large reduced width for

slow particles. Hence there must be a correlation between large reduced width and non-conservation of isobaric spin. The existence of such a correlation was shown in a paper by D. H. Wilkinson (1957) and we reproduce in fig. 11 a relevant picture from his paper.

It may happen that the attractive potential interaction is not strong enough to create a 'threshold' state. If it is not very weak, however, it will always manifest itself by changing the energy dependence of all the cross sections in the fashion shown in §§3, 5. For example, the cross section for elastic scattering of slow neutral particles $b + Y$ must decrease monotonically as the energy increases (fig. 4).

Fig. 12



Cross section for the ^{7}Li(pn) reaction near threshold.

Reliable data on neutron scattering at small energies in the region of light nuclei exist for ^{4}He, ^{7}Li, ^{9}Be, ^{11}B and ^{12}C. The cross section is constant for ^{4}He and ^{7}Li and this shows that there is no strong attractive interaction in an s-state between the neutron and these nuclei. For the last three nuclei, however, cross sections behave in the predicted way.

For (pn)-reactions near the threshold the theory predicts deviations from a $1/v$-law (§3). These are two nuclei for which the (pn) reaction was carefully measured near the threshold (^{3}T and ^{7}Li) (Bergman *et al.* 1958, Maclin and Gibbons 1958). In both cases the cross sections have the prescribed behaviour and were fitted with an s-wave resonance formula (the case of ^{7}Li is shown in fig. 12, but the case of ^{3}T is very similar).

Brief and incomplete though this survey of experimental data may be, it does seem to indicate the relevance of the theory of the first part of this paper to threshold phenomena in light nuclei. This is especially satisfying because we might expect these effects to exist from what we know about the nuclear potential already (see §2).

In order to be completely sure of a widespread existence of the threshold effects, however, it will be necessary to have more extensive experimental

data, which will confirm or deny the following most significant predictions of the theory:

(1) A specific energy dependence of cross sections near two-body thresholds (§§ 3, 5).

(2) The existence of 'threshold' states with reasonable spin and parity (reasonable in the sense of a shell model: in p-shell nuclei there should be a strong interaction in p-states, in d-shell nuclei in d-states, and so on) and with large one-particle reduced widths.

(3) The large radius of a 'threshold' state permits a quantitative check of the theory: a large radius means that the 'threshold' particles $b + Y$ are well outside the region of strong interaction and that we consequently know the wave function of the system. This makes it possible to calculate the energy dependence of many different processes such as radiative capture and stripping. Comparison with experiment will provide a quantitative check of the theory.

Acknowledgments

The author would like to express his gratitude to Professors Wilkinson and Flowers for their kind invitation to work in their departments, and for the hospitality enjoyed during his stay in Oxford and Manchester. He is most thankful to both for their helpful discussions and criticism of his work, and to Professor Flowers in particular, for all his help in the preparation of this paper. Finally, the author wishes to express his thanks to Dr. G. R. Satchler and Dr. A. M. Lane for stimulating discussions of the subject.

References

Ajzenberg-Selove, F., and Lauritsen, T., 1959, *Nuclear Phys.*, **11**, 1.
Baz, A. I., 1958, *J. exp. theor. Phys.*, **6**, 709.
Bergman, A. A., Isakov, A. I., Popov, I. P., and Shapiro, F. L., 1958, *J. exp. theor. Phys.*, **6**, 6.
Breit, G., 1957, *Phys. Rev.*, **107**, 1612.
Lane, A. M., and Thomas, R. G., 1958, *Rev. mod. Phys.*, **30**, 257.
Maclin, R. L., and Gibbons, J. H., 1958, *Phys. Rev.*, **109**, 105.
Prosser, Jr., F. W., and Biedenharn, L. C., 1958, *Phys. Rev.*, **109**, 413.
Schiff, L., 1949, *Quantum Mechanics* (McGraw-Hill).
Wigner, E. P., 1948, *Phys. Rev.*, **73**, 1002.
Wilkinson, D. H., 1957, Proc. Rehovoth Conference on Nuclear Structure.

Intermetallic Reactions and Ageing Effects in Thin Films

By C. Weaver and R. M. Hill
Department of Natural Philosophy
The Royal College of Science and Technology, Glasgow

CONTENTS

§ 1. Introduction. 375

§ 2. Preparation of Alloy Films. 377
2.1. Evaporation of Alloys. 377
2.2. Simultaneous Evaporation. 378
2.3. Successive Evaporation. 379
2.4. Alternate Evaporation. 380

§ 3. Diffusion in Thin Films. 380
3.1. Theory of Diffusion. 380
3.2. Application of Theory. 385
3.3. Effects of Film Structure on Diffusion. 386

§ 4. Electron Diffraction. 387
4.1. General. 387
4.2. Gold–Copper. 389
4.3. Aluminium–Copper. 391
4.4. Aluminium–Silver. 393
4.5. Indium–Antimony. 396

§ 5. X-ray Methods. 397

§ 6. Electrical Resistivity. 399

§ 7. Age-hardening in Thin Films. 409
7.1. Introduction. 409
7.2. Theories of Age-hardening. 410
7.3. Experimental Results. 412

§ 8. Diffusion Measurements. 423
8.1. General. 423
8.2. Diffusion Through Films. 423
8.3. Diffusion Along Films. 425

§ 9. Conclusions. 427

§ 10. Summary. 429
10.1. Binary Systems. 429
10.2. Other Systems. 434

References. 434

§ 1. Introduction

Techniques for producing thin films by vacuum deposition have been known for a considerable time. Sputtering was discovered in 1852 and used to produce thin metallic films but it was regarded mainly as a scientific

† Now with Commonwealth Scientific and Industrial Research Organization, Metrology Division, Sydney, N.S.W., Australia.

curiosity. It has only recently been used to produce non-metallic films by what is termed ' reactive sputtering ' (Holland 1956). The technique of evaporation appears to have been known from about 1912 (Pringsheim and Pohl 1912), although it has been attributed to Edison (1890), and it was used only for metallic films to start with. The method really came into its own with the introduction of oil diffusion pumps, following the development of suitable pumping fluids (Burch 1928). It rapidly ousted sputtering for most applications but the major developments came only during the early 1930's with the increasing use of reflecting films and the introduction of transparent films as anti-reflection coatings (Bauer 1934, Strong 1936).

The applications of transparent films developed rapidly during the war years with the increasing use of anti-reflection coatings and the introduction of interference filters, multi-layer reflectors and beam-splitters, and the theory of interference effects in multi-layer films developed rapidly. Metal films were introduced much earlier but have not been subject to the same development. Except in very thin films, the absorbing properties of metals make interference effects comparatively unimportant and the metals used for thin films have been chosen generally for their optical or electrical properties and there has been little demand for films consisting of more than a single metal. Where two or more metals have been used, this has generally been in the form of an alloy because the properties for a specific purpose were better than those of the individual metals. The only well-known application of metal films formed of more than a single layer was the use of a chromium underlayer to improve the adhesion and durability of an evaporated aluminium reflecting film (Strong 1935).

In these applications the films have generally been regarded as uniform, continuous and homogeneous even though extensive investigations have shown that the properties of the films differ from those of bulk material (Holland 1956). The refractive indices and densities of dielectric films are generally lower than corresponding bulk properties, suggesting the existence of voids, and it has been shown that most metallic films condense as aggregated structures (Appleyard 1937, Levinstein 1949) and only in a few cases do metals condense as continuous layers. A variety of methods have been used to investigate structure, the most direct evidence being obtained by electron diffraction and electron microscopy although optical properties have been extensively studied and used to give structural information.

Even though the structure is not necessarily as continuous and uniform as has been assumed, the individual layers of dielectric multilayer films do appear to remain separate and distinct layers, as far as can be ascertained. This is, however, not true for the case of metals. At the interface between two metallic films there is always a tendency for diffusion to occur, and for layers of an intermetallic compound or solid solutions to form at the interface. When such layers form between two thin metal films they can be detected much more readily than corresponding layers in diffusion

couples produced from bulk material. In bulk material the intermediate layers must be thick enough to be detected by sectioning, i.e. greater than 1 micron. In thin films the individual layers may only be of the order of 100Å thick and the intermediate layer or layers may consist of only a few atomic layers when detected, using the techniques which have already been used so effectively to study film structures. There has therefore been an increasing tendency to study alloy formation and age-hardening processes in thin films. The early investigations all relied upon what was then the comparatively new technique of electron diffraction and it is only during the last decade that significant advances have been made using other methods. Even as yet, most of the information which has been obtained is essentially of a qualitative nature and few attempts have been made to measure rates of diffusion in thin films.

§ 2. Preparation of Alloy Films

2.1. *Evaporation of Alloys*

When an alloy is vaporized the composition of the vapour phase is seldom the same as the composition of the original alloy. This is particularly true when the melting points of the pure components are widely separated. When the vapour is allowed to condense on a suitable surface, the film which is produced will therefore in general have a different composition from the original alloy. The phenomenon is, of course, analogous to the fractional separation of a mixture of two liquids by distillation. There is no exact relationship between the partial vapour pressures of the alloy components and the vapour pressures of the pure components and consequently it is difficult to predict the composition of the vapour phase and any films which may be produced from a knowledge of the original alloy composition. In the case of binary alloys, approximate calculations can be made by treating the alloy as a pure solution and assuming that Raoull's law can be applied. Reasonably accurate results are obtained when one component is much more volatile and present in much larger proportion, but otherwise considerable discrepancies can occur. This has been discussed by Dushman (1949) and by Holland (1956) who used the method to predict a number of " constant evaporation rate alloys " which would vaporize more or less unchanged.

In general the composition of the vapour phase changes during the course of the evaporation of an alloy, being initially richer in the more volatile component just as in the fractional distillation of a mixture of two liquids. Consequently there is some separation of components in the films which are produced. This was observed by Germer *et al.* (1942) who evaporated an alloy of Au–Cu on to a lucite substrate and then dissolved the substrate in ethylene dichloride. On examination of the film, copper could be seen on the substrate side and gold on the other side, showing that the copper tended to vaporize before the gold. Electron diffraction photographs obtained with the film in this state showed broad

bands with sharp edges. The rings were typical of a face-centred cubic structure and the inner and outer edges of the rings corresponded to gold and copper patterns respectively. The broad bands indicated the presence of alloys of other compositions as well as gold and copper. Heating to 450° and then quenching produced a new ring system corresponding to $AuCu_3$, showing that the gold and copper had interdiffused. In further experiments, films were heated for 16 hours to temperatures of 127°c, 148°c and 160°c and upon examination it could be seen that complete mixing had occurred at 148°c and 160°c, but mixing was still incomplete for the specimen at 127°c.

Much earlier a 50% Au–Cu alloy was evaporated on to a mica substrate by Eisenhutt and Kaup (1931) and the films were then annealed at various temperatures from 225°c to 400°c. In all cases, a few minutes at these temperatures resulted in electron diffraction patterns corresponding to $AuCu_3$ and superstructure lines were observed. They found that ordering of the atoms had begun after only one minute but that 10–20 min were required to produce a complete phase. These effects are not confined to Au–Cu alloys and Trillat and Takahashi (1952) carried out similar experiments with an alloy $CuAl_2$. They obtained diffuse haloes by electron diffraction with freshly prepared films and the compound $CuAl_2$ was only formed after 30 min at 300°c or 1 month at 18°c. Deposition on a hot substrate at 200°c resulted in immediate formation of the compound.

The difficulties of component separation in the evaporation of alloys were eliminated by Harris and Siegel (1948) using a ' flash technique '. The powdered alloy was dropped, a few grains at a time, into a molybdenum boat maintained at a high temperature so that the grains vaporized almost instantaneously. Alloys of Au–Cd and Cu–Zn were used and homogeneous films were formed immediately.

2.2. *Simultaneous Evaporation*

The uncertainties and difficulties involved in evaporating an alloy can be eliminated by having two sources and evaporating the two components of the alloy separately but simultaneously to produce homogeneous films. The two sources are adjusted in preliminary experiments so that the rates of evaporation are approximately equal. This method was used by Michel (1952) who obtained a number of specimens of different compositions from the one evaporation by arranging his specimen grids at different relative spacings from the two heaters which were spaced apart and screened from one another to prevent direct contamination of one source by material from the other. He thus obtained the pure components at either extreme and a range of intermediate compositions. The method is extremely convenient and flexible, producing homogeneous films without the necessity for annealing. It is eminently suitable for a general investigation of any alloy system but it has not so far been possible to use this method to prepare alloys of desired, known compositions. Kurov and Pinsker (1958) used the same technique as Michel for investigation of the

indium–antimony system and the method has also been used by Trillat and Takahashi (1953) for aluminium–gold alloys.

2.3. *Successive Evaporation*

The aim of the first two methods is to obtain intimate mixing of the alloy components so that a homogeneous alloy film is produced. Alternatively, it is possible to evaporate the pure components consecutively and rely upon diffusion to produce the required alloy. When a two-layer film is produced by successive evaporation of two pure metals, the metals are in intimate contact at the interface but form separate distinct layers. A film of alloy is only produced as the two metals diffuse into one another. There is therefore an ageing process and information on the nature and speed of this process can be obtained from any measurements which are affected by the formation of the intermediate alloy layer or which can detect the migration of the metal atoms. The process of diffusion is obviously temperature dependent and, in many cases, higher temperatures have been used to accelerate the ageing. In a few cases attention has been concentrated on the temperature relationship and the specimens have been subjected to temperature cycles, the time factor being neglected. Since both time and temperature are involved, it would appear that, in general, observation of ageing at two or more temperatures is desirable if a reasonably complete picture is to be obtained.

Electron diffraction is not usually a very satisfactory method of following the ageing process since the patterns of the pure metals tend to obscure the weaker lines of the alloy in the early stages and there is usually a time lapse before these lines become sufficiently distinct for observation. This method has, however, been used by Michel (1956), who used the same range of metals as for his experiments on simultaneous evaporation. He calculated the mean distance of diffusion in each case and used these figures to explain the differences between the results. Electron diffraction had been used much earlier to follow ageing by Eisenhutt and Kaupp (1931) who evaporated a layer of copper on to a mica substrate and covered it with a layer of gold, the total film thickness being about 300 Å of which 70% was copper. Ageing was observed at a number of temperatures up to 300°C and a relationship

$$Z = 10^{15} \exp(-T/16{\cdot}0)$$

between the time Z taken for formation of homogeneous mixed crystals and the temperature T, was obtained.

More recently, measurements of the electrical and mechanical properties of the films during ageing (Boettcher 1950, Belser 1954, Weaver and Hill 1958, 1959a, b) have been used to throw further light upon the nature of the processes at the interface. Significant changes occur as soon as alloying starts and allow the early and intermediate stages of ageing to be followed. It is possible to detect the effect of intermediate alloy layers which would be far too thin to affect the electron diffraction patterns appreciably and these methods seem to offer most scope for future development.

Optical methods present another method of attack and have been used not only to check deductions from other measurements but also to detect migration of the atoms of one metal through the other, and hence, for determination of diffusion coefficients.

2.4. *Alternate Evaporation*

In two cases at least multi-layer films have been formed by alternate evaporation of two metals. DuMond and Youtz (1940) deposited copper on glass at a uniform rate whilst gold was deposited in one hundred stratified layers by alternately raising and lowering the temperature of the molybdenum heater. The resultant film was about 10 000 Å thick and was formed of alternate layers of pure copper and gold–copper alloy. They did not attain their original objective of obtaining sufficient uniformity of layer spacing for an accurate determination of the absolute wavelength of x-rays by Bragg reflection, but they did observe the effects of diffusion of one component into the other. The x-ray diffraction maxima produced by selective interference within the films decreased in intensity as the films tended to become more uniform and homogeneous. From the rate of fall, the diffusion coefficient of gold through copper at room temperature was calculated.

Multi-layer films of nickel and aluminium were used by Weaver and Hill (1959 a) but in this case the object was to obtain a greater thickness of alloy relative to the pure components than could be obtained in a simple two-layer film. Earlier work with two-layer films of aluminium and chromium (Weaver and Hill 1958) had shown that the intermediate alloy layer formed on ageing at room temperature could only be detected when the films of the pure components were made very thin so that the pure metal patterns did not obscure the alloy pattern. The use of a multi-layer film gave an effective increase in sensitivity of the electron diffraction method so that alloy formation was detected more readily.

§ 3. Diffusion in Thin Films

3.1. *Theory of Diffusion*

When a two-layer film is produced by successive evaporation of two metals the interface region will be perfect, i.e. there will be atomic contact between two superimposed metal deposits. The presence of this close bonding has been shown by the results of investigations of oriented overgrowths. Overgrowths of this type require intimate contact for the high degree of structural continuity that exists. This gives to the system one of the most sought-after conditions for perfect diffusion. Diffusion occurs in one direction only and the limiting boundaries of the system are perpendicular to the direction of the highest concentration gradient. The concentration/displacement conditions for the system, immediately after preparation are illustrated by the graph ($t = 0$) shown in fig. 1. Assuming that the metals alloy to give a perfect miscible solution the concentration/displacement graph at a time $t'(t' > 0)$ will follow the form of the second

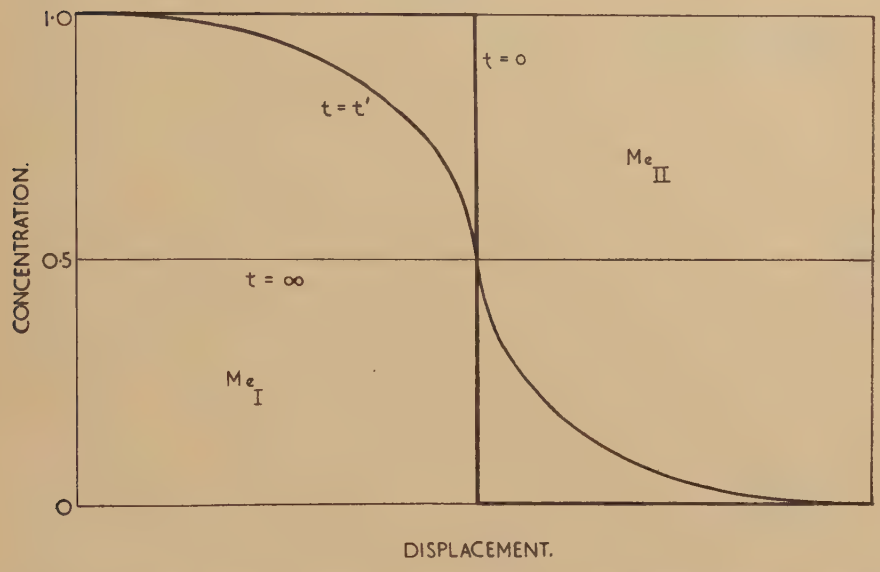
curve in the diagram. After an infinite time the relative concentrations will everywhere be the same and for an alloy of equal proportions the displacement curve will be a straight line parallel to zero concentration at the value of $c = 0{\cdot}5$.

If the metals are Me_I and Me_{II}, and the corresponding diffusion constants are D_I and D_{II}, then for the case illustrated,

$$D_I = D_{II} = \text{a constant},$$

where $D_I \neq D_{II}$ conditions similar to those shown in fig. 2 will prevail.

Fig. 1



Diffusion of two metals across a boundary. Single phase system $D_I = D_{II}$.

For a system such as this the diffusion equation

$$\frac{\partial c}{\partial t} = \frac{\partial}{\partial x}\left(D\frac{\partial c}{\partial x}\right)$$

where c = concentration,

x = displacement relative to the plane of diffusion,

t = time of diffusion,

cannot be replaced by the simpler, and more familiar form,

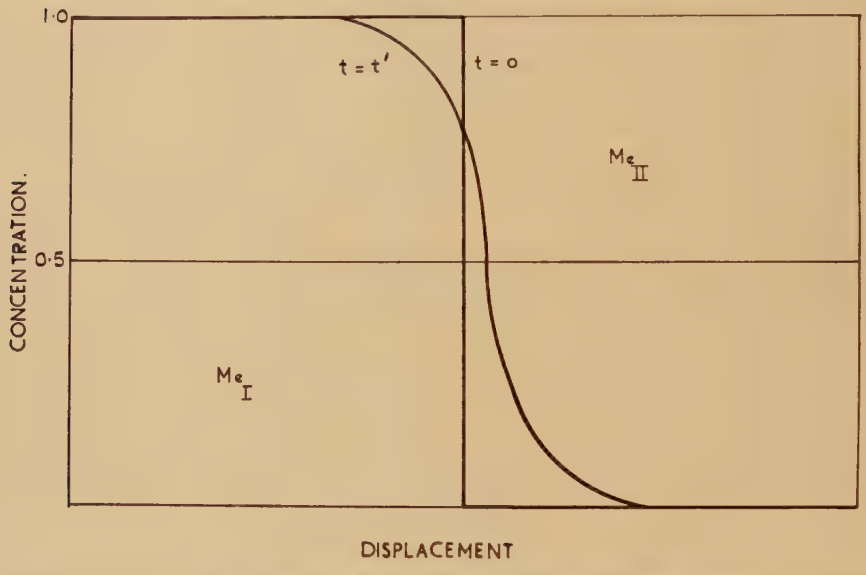
$$\frac{\partial c}{\partial t} = D\frac{\partial^2 c_2}{\partial x}$$

as the 'diffusion constant' is concentration dependent.

In the simple systems in which the diffusion constant is not concentration dependent we would obtain, in a finite time, a perfect gradation of structure and concentration from one perfect metal region to the other. Such a transition is only obtained when the two parent metals possess very

similar structures and lattice spacings. In this case the elimination of an atom of one metal and subsequent replacement by an atom of the other does not affect, to any degree, the energy state of the structure. Where the parent metals show differing characteristics the energy state changes greatly for a substitution of this type and only a limited number of 'foreign' atoms can be contained in the parent structure. Once the limit has been passed the structure is distorted to such an extent that it shows the properties of a mixture of two phases, one the parent structure, which has become saturated, and the other a new phase richer in the 'foreign' atoms than the saturated solid solution.

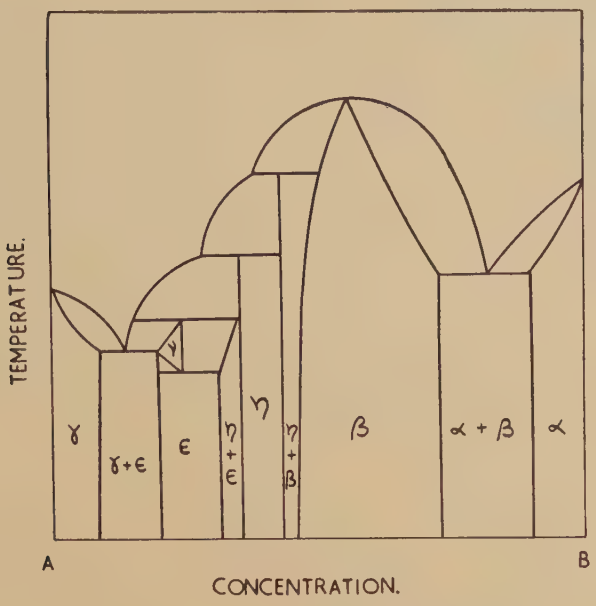
Fig. 2



Diffusion of two metals across a boundary. Single phase system $D_{\mathrm{I}} \neq D_{\mathrm{II}}$.

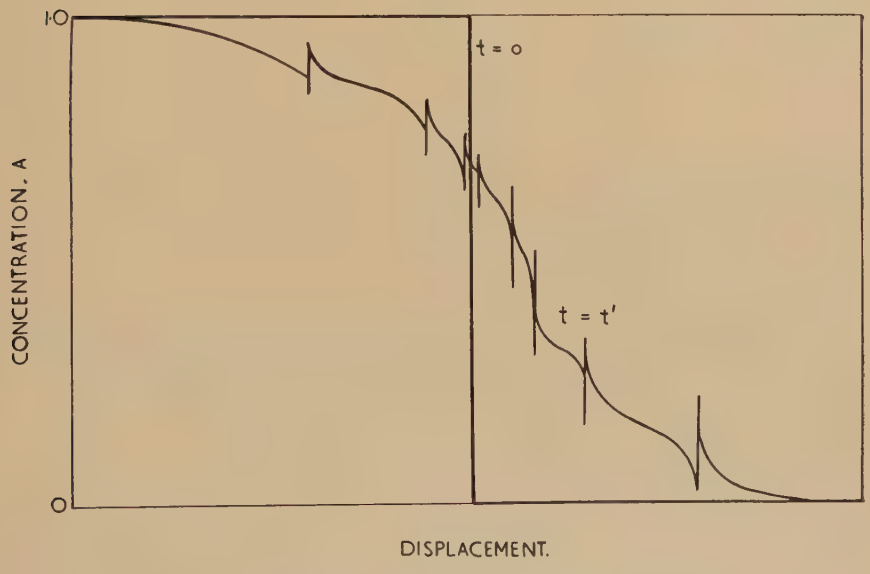
This can be seen clearly when we consider a system of two metals which alloy to form a number of distinct phase regions at low temperatures. We will take as an example of this system the phase equilibrium diagram shown in fig. 3. Here we have five distinct phases present at temperature t_0. The majority of these are bounded by regions of mixed phase structures. The higher temperature region of the diagram which has only been sketched in, shows that there is a preferential compound, AB, of high energy of formation, the β phase. The concentration/displacement curve across the boundary between the two metals at time zero will be given by a graph of the form of the first curve ($t = 0$) in fig. 4. However, after the metals have been allowed to diffuse the form of the curve might well be as shown for $t = t'$, but this curve cannot be determined with any accuracy as it is totally dependent on a knowledge of the diffusion constants and concentration gradients in each region of the phase system. In order to

Fig. 3



Phase equilibrium diagram for two metals A and B. Multi-phase system.

Fig. 4

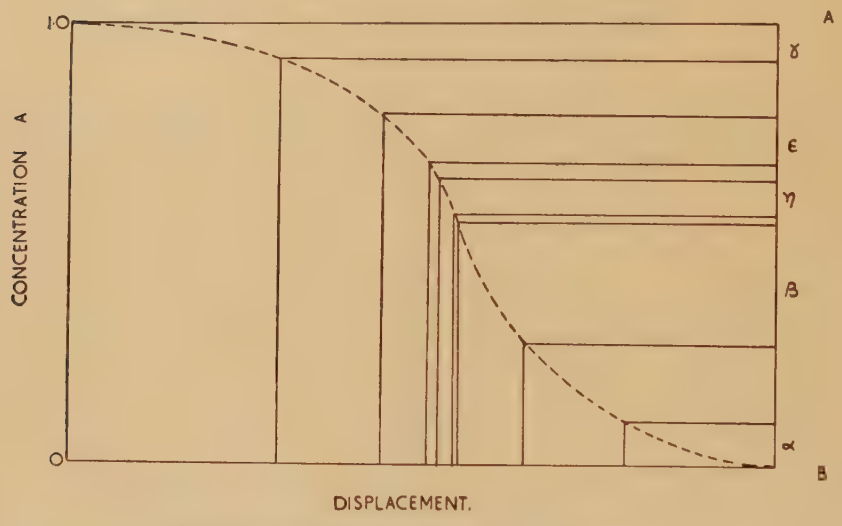


Diffusion in multi-phase system.

discuss the system further it is necessary to replace this curve with the simpler form shown by the dashed line in fig. 5.

The validity of this step is questionable but it will be seen that both forms of the curve give similar results, i.e. both show that there will exist between the parent structures a transition region containing the alloy phase structures. The relative amounts of each of these have been altered by the substitution of the simpler concentration/displacement curve, but as the data required for an accurate estimate of the relative widths are not obtainable, and as we will only be considering qualitative results, the step appears fully justified. It is, however, possible that the case might arise in which we are masking out or over-emphasizing a particular phase region. For example, the preferential compound might well show in excess, a result that could be obtained by energy considerations, whereas using the method outlined here it will only show excessive prominence if the concentration region, over which it is stable, is large.

Fig. 5



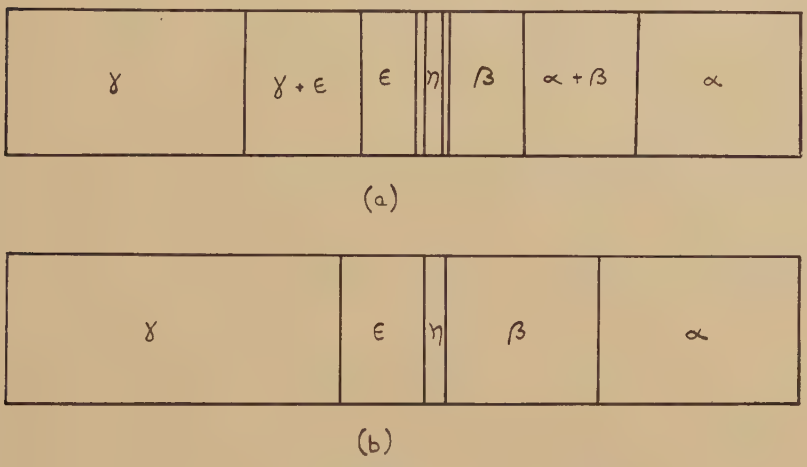
Simplified diffusion in multi-phase system.

The diagram given in fig. 5 shows the effect of the formation of the transition structure. Each phase region, and mixed phase region, are present in order. Applying Wagner's results (Jost 1952) to this region we would expect the pure phase regions to grow at the expense of the mixed regions. The final result is shown diagrammatically in fig. 6.

It can thus be said that at the interface between two metals which are miscible, there will be formed a transition region. It is also possible to say that in the transition region there will be deposited all or most of the thermally stable metal phases formed by alloying of the parent metals. As ageing continues the width of the transition region, and of each phase

region, will grow, and there will be a constant precipitation and reprecipitation as the boundaries of the phase regions move outwards. As we have shown, the actual or relative widths of the phase regions cannot be determined at present; nevertheless the maximum number of stable phases can be determined from the phase diagram and this will given an estimate of the complexity to be expected. In suitable materials the movement of the phase boundaries will produce age-hardening effects. These will not, however, be as sharply seen as in a perfectly homogeneous body of metal where the reaction will be occurring in every elemental volume, for in the system we are considering it will only be occurring in one layer.

Fig. 6



Transition region between two metals.
(*a*) From fig. 5, (*b*) after applying Wagner's results.

3.2. *Application of Theory*

The results of the previous section are directly applicable to the case of successive evaporation of metal films. Using this technique perfect surface contact will be obtained, as has been shown by the contouring ability of thin films (Tolansky 1955), and a sharp initial boundary, with no trace of surface impurities, is possible. With no other method of investigation of diffusion are these conditions so easily obtained.

In the practical case one-dimensional diffusion conditions prevail but the thickness of the films limits the displacement that can be given to any one atom. It is, however, possible to measure the actual time taken for the atoms of one metal to diffuse through the complete film of the other, and diffusion data from this type of experiment have been recorded. The presence, or absence, of the complete range of alloy phases is difficult to show experimentally but electron diffraction experiments have given some details. Reflection electron diffraction, in conjunction with the ion stripping technique (Trillat *et al.* 1956) should be useful. In this an ionic

bombardment is used to strip the specimen. This gives a series of diffraction exposures of the surfaces as they are exposed right through the specimen. Care would have to be taken that one of the metals did not sputter preferentially and there is a danger that the ionic bombardment itself could affect the results and lead to confusion.

It is also possible to prepare mixed films by vacuum evaporation. These films are prepared by evaporating both the materials at the same time. With this type of film the metallic interactions giving phase precipitation will occur throughout the film at the same rate. However, a perfectly randomly mixed film would be required for this to be the case. In effect the film will contain clusters of similar atoms and interdiffusion will be required before the precipitation process can continue. Should there be a localized region of composition varying from the average of the whole film, then the phase equivalent to that concentration will be deposited, and will require to be broken up and reprecipitated as the long-range order increases.

The process of precipitation will be directly affected by the initial state of the mixed film and it will be impossible to estimate diffusion data from the results obtained. However, qualitative data on the type of phase structure for a given alloy concentration can be obtained simply. Many investigations have been carried out on films of this type.

3.3. *Effect of Film Structure on Diffusion*

The structures of thin metallic films have been investigated extensively by electron microscopy and other methods (Holland 1956). It has been shown (Pickard and Duffendack 1943, Levinstein 1949, McLauchlan *et al.* 1950) that evaporated films are rarely deposited as uniform monolayers but instead, the incident atoms gather in clusters or aggregates which vary in size from a few atoms to fractions of a millimetre in diameter. The degree of aggregation is dependent upon the mobility of the atoms on the surface and the energy of the metal-substrate interface (Barrer 1951, Appleyard 1937). The deposition of more material causes the aggregates to grow and extend laterally until eventually they meet and perhaps coalesce. This gives a uniform appearance to the films as viewed optically. The aggregates in these thicker films can be considered as crystallites of very small size and electron diffraction results show that usually the crystallites are randomly arranged, bearing no direct relationship to each other.

A thin film may thus be considered as a polycrystalline material with numerous voids within the structure, some caused by the initial aggregates not merging together completely and some formed within the quasi-continuous structure of the aggregates themselves during growth. These voids will tend to hinder atom movements, particularly between crystallites. It is also known (Hoffman and Storey 1956) that vacuum-deposited films are frequently highly stressed, partly due to cooling effects and partly as

a result of lattice defects produced during deposition. These structural defects on both the atomic and crystalline scale are likely to affect the diffusion constants of the material. The films can be annealed and a more homogeneous structure can be obtained but there is always the possibility that, while the initial layer of a two-layer film is being annealed, its surface will become contaminated and the intimate contact between the two layers will be lost.

It has also been suggested that grain boundaries in metals can act as highly conducting channels for diffusing atoms (Cottrell 1955). At elevated temperatures normal lattice diffusion takes place so rapidly that this effect is unimportant but at lower temperatures grain boundary diffusion becomes increasingly important and can become the main factor. On this basis it would appear that higher diffusion constants would be obtained from measurements on thin films than from the bulk materials since thin film measurements are normally made at relatively low temperatures and the high proportion of grain boundaries would favour this form of diffusion. Whether this effect would be lessened by the presence of voids and internal stresses already mentioned, it is at present impossible to say. The results obtained so far, which are described later, show no definite higher or lower bias. More experimental evidence will be required before it is possible to draw any conclusions on the variation of rates of diffusion with relative concentrations of structural defects.

Metallic films were evaporated on to polished or etched metal surfaces by Finch *et al.* (1934) and they showed by electron diffraction that at room temperature the evaporated metal rapidly disappeared into a polished surface but not into an etched surface. This suggested a rapid diffusion into the disturbed structure of the Beilby layer. The results for copper surfaces were, however, not confirmed by Cramer (1939) who attributed the earlier findings to contamination of the surface by hydrocarbon films.

§ 4. Electron Diffraction

4.1. *General*

Electron diffraction methods have been used extensively for investigation of alloying in thin films. The most extensive results are due to Michel (1956) in France, Boettcher and Raether and his colleagues in Germany and, more recently, Pinsker and others in Russia. There have, however, been a large number of other investigations where the field has been more restricted or where electron diffraction has been ancillary to the main objective.

Michel (1956) examined the binary systems Ag–Mg, Ag–Zn, Ag–Sn, Al–Cu and Au–Cu using both simultaneous evaporation and successive evaporation to produce his specimens. In each case simultaneous evaporation of two constituents produced alloy films containing only simple phases of the system. In the case of Ag–Mg all phases except γ appeared immediately after evaporation. Furthermore, β and δ phases appeared

together in several specimens, suggesting that these phases had a common boundary with a region where they could co-exist. In the case of Ag–Zn the γ phase appeared only after ageing for several days at room temperature. The results are summarized in table 1. Successive evaporation produced alloy films immediately in the case of Ag–Zn and Ag–Sn but no alloy formation could be detected in the other cases even after ageing for several weeks at room temperature. Michel attributed this to differences in rates of diffusion and showed that the calculated rates of diffusion for Ag–Zn, Ag–Sn were considerably higher than for the other systems (see table 2). In view of his failure to detect alloy formation in these other

Table 1

Metals	Phases observed after simultaneous evaporation
Ag–Mg	α β δ
Ag–Sn	α ϵ'
Ag–Zn	β' γ† δ
Cu–Al	β', β† γ†
Cu–Au	continuous solid solution

† Observed after ageing.

Table 2

Metals	D_0	E	D (at 27°C)	Depth of penetration in 1 day at 27°C
	(cm_2/sec)	(kcal)	(cm_2/sec)	(Å)
Ag–Zn	$2{\cdot}1 \times 10^{-4}$	14·1	$1{\cdot}31 \times 10^{-14}$	$4{\cdot}75 \times 10^{3}$
Ag–Sn	$7{\cdot}82 \times 10^{-5}$	21·4	$2{\cdot}5 \times 10^{-20}$	6·6
Cu–Au	$5{\cdot}8 \times 10^{-4}$	27·4	$8{\cdot}4 \times 10^{-24}$	$1{\cdot}2 \times 10^{-1}$
Cu–Al	2·3	34·9	$1{\cdot}45 \times 10^{-25}$	$1{\cdot}47 \times 10^{-2}$
Ag–Mg	No data available.			

systems he suggested that there was a lower limit for the coefficient of diffusion below which diffusion would not occur at room temperature. It seems more probable, however, that an intermediate layer of alloy was formed but was too thin to be detected by electron diffraction particularly against the background of the patterns due to the pure metals.

Raether and his colleagues in Germany have been mainly concerned with age-hardening in Al–Ag alloys and this is discussed later. Some work has also been done on other alloys including Au–Cu and Al–Cu. Recent work in Russia has tended to deal with semi-conducting materials, In–Sb

being a typical example. An interesting development in examination of alloy formation by electron diffraction has been the introduction of a moving-film technique by Trillat and Takahashi (1953), by Boettcher (1953) and by Boettcher and Thun (1952, 1954). The photographic plate normally used to record the electron diffraction patterns was replaced by a film moving continuously behind a transverse slit. The diffraction pattern was thus screened off except for a narrow diametral strip, and movement of the film past the slit caused the diffraction pattern to be recorded as straight lines parallel to the direction of motion of the film. Any structural changes in the specimen caused corresponding changes in the spacings of these lines and were recorded continuously. This continuous recording arrangement was used to follow changes in specimens as they were slowly heated and cooled, markers being put on the film at suitable temperature intervals by a momentary illumination of the slit. It was used for the Al–Cu system by Trillat and for Ag–Al and Cu–Al and Cu–Sb by Boettcher and Thun (1954). This gave information on structural changes in films of known composition. The method was also modified by Boettcher and Thun (1954) to investigate phase diagrams over the full composition range by depositing wedge-shaped films of the two components one on top of the other but with the wedges in opposite sense so that the relative proportions of the two components varied continuously along the line of maximum slope. Annealing these specimens gave alloys over the full range of compositions and by traversing the specimen across the electron beam in synchronism with the film a continuous record of variations in diffraction pattern with concentration could be obtained. The method was applied to the Au–Sn system and its application to three-component systems was discussed.

An examination of the work which has been done shows that certain alloys have been particularly popular and have been the subject of several investigations. These are covered here, whilst individual or less detailed investigations are given in the final summary.

4.2. *Gold–Copper*

This alloy system has been the subject of repeated investigations, both theoretical and experimental, using bulk material and thin films. The earliest application of electron diffraction to alloy formation (Eisenhutt and Kaupp 1931) used successive evaporation of copper and gold in the proportions 3 : 1. The films were deposited on mica substrates and annealed in vacuum at a series of different temperatures. The diffusion process was followed by measuring the diameter of the 111 ring as the lattice spacing changed from 4·07 Å for pure gold to 3·92 Å for the alloy and a relationship was obtained between the temperature of annealing and the time taken for complete mixing. The same workers also evaporated a 50/50 gold–copper alloy and annealed at temperatures between 225°C and 400°C. A tetragonal structure was obtained within a few minutes

and superstructure lines were observed. At higher temperatures a cubic diamond or zinc blonde type structure was observed but this has never been confirmed. Order–disorder transitions in this alloy were considered theoretically (Bragg and Williams 1934, Bethe 1935, Peierls 1936, Kirkwood 1938) and were followed by experimental investigations of thermal effects and electrical resistivity using bulk material (Sykes and Evans 1936, Sykes and Jones 1936, and Jones and Sykes 1938). The results tended to show that the theory of Bethe and Peierls was more nearly correct and this was confirmed by Buinow and Komar (1939). The theory of Bethe and Peierls took account of short-range order whereas the previous theory of Bragg and Williams considered only the long-range order of the alloy. The face-centred cubic lattice of $AuCu_3$ may be considered in terms of four interpenetrating simple cubic lattices to which it is equivalent. When perfectly ordered, one of these lattices is formed of gold atoms only while the other three contain copper only but on cooling through the critical temperature, gold atoms may segregate on any of the four lattices and ordering starts at a number of nucleating centres which are not normally in phase with one another. As a result ordered aggregates are formed which remain distinct, one from another.

Examination of thin films by electron diffraction was again used by Germer *et al.* (1942) to investigate the ordering of the $AuCu_3$ alloy. They produced films about 400 Å thick by evaporating the alloy and found a partial separation of components (see § 2.1). They did, however, obtain direct proof by diffraction and observation of superstructure lines that the ordering process went on at temperatures as low as 169°C and that perfect order could be obtained in 16 hours at 270°C, whereas ordering had previously been detected by X-rays only above 320°C (Sykes and Jones 1936). The results were also used to calculate diffusion rates and agreement was obtained with the earlier observations of Eisenhutt and Kaupp (see § 2.3). Agreement was also obtained with rates calculated from the results of Jost (1932, 1933) who investigated diffusion in bulk metal specimens over a temperature range 301–616°C, obtaining for gold in copper 27 400 cal/mole for the activation energy and a value of $1{\cdot}05 \times 10^{-3}$ cm^2/sec for D_0. For copper diffusing into a copper–gold alloy containing 10% copper by weight, the same value of activation energy was obtained and a value of D_0 just over half the above value.

The ordering of this alloy was again investigated by Raether (1950, 1951) who emphasized the importance of using single crystal specimens. He prepared single-crystal films by evaporating the alloy and depositing on rock-salt cleavage faces maintained at 380–400°C. Homogeneity of the resultant films was ensured by heating them to 600°C for about 30 min. The composition was checked by measuring the lattice spacing. The films were then annealed at various temperatures between 200°C and 370°C and examined by electron diffraction. An hour at 370°C gave single crystal patterns with superlattice spots almost equal in intensity to the fundamental spots. On heating the films, the superlattice spots

disappeared between 386°C and 388°C which agreed with results obtained by X-rays on bulk metal specimens.

The experiments of Germer *et al.* (1942) were repeated by Ogawa and Watanabe (1952) who extended their experiments to cover also the Au_3Cu alloy, this superstructure having been detected a year earlier by Hirabayashi (1951) using X-rays. The films were prepared by successive evaporation of two films of the required thicknesses on to a rock salt cleavage face, and this was followed by annealing at 400°C to allow the metals to interdiffuse and produce a homogeneous structure. The specimens were then enclosed in silica tubes and maintained at 200°C for a long period, finally quenching in cold water. Superstructure lines of the ordered Au_3Cu lattice were obtained, thus confirming the work of Hirabayashi. Heating above 200°C produced gradually increasing disorder in accordance with the theoretical work of Cowley (1950) who predicted a critical temperature of about 190°C. The $AuCu_3$ and AuCu structures were also obtained in the corresponding alloys.

The critical temperature for the order–disorder transition in the Au–Cu_3 structure is so clearly marked that it has been used (Winkelmann 1956 a) to determine experimentally the heating effect of the electron beam. This was found to be of the order of 10°C. Similar results were obtained by using the melting point of paraffin crystals as a reference temperature (Yamaguchi 1956).

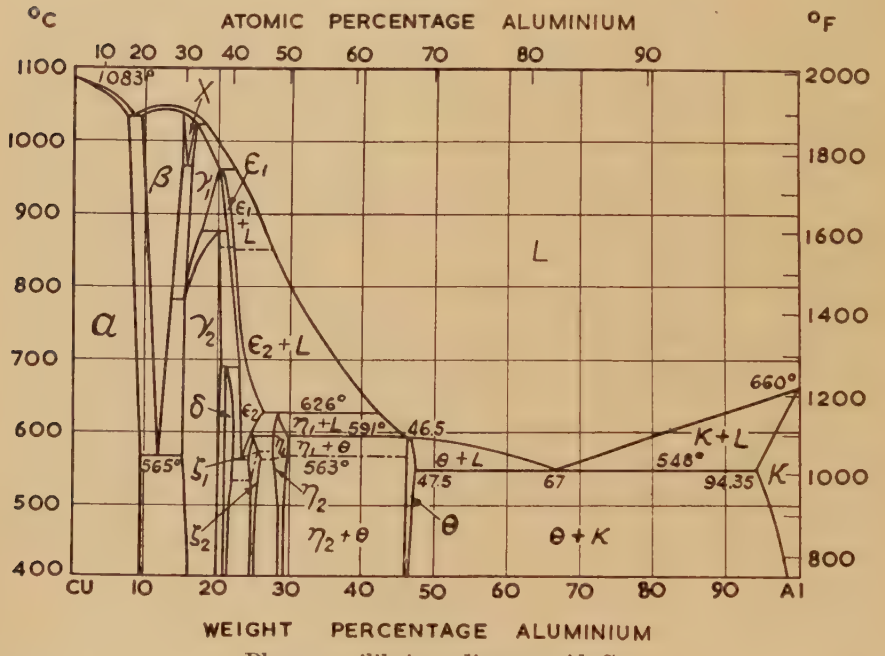
The results obtained on this system indicate that electron diffraction with thin films not only gives all the information which can be obtained by X-rays but is also more sensitive and can be used to follow processes at lower temperatures or lower concentrations. Observations have been made on polycrystalline and single crystal specimens and all known phases and transitions have been observed. Where diffusion has been involved, the rates have shown reasonable agreement with figures for bulk material and the distance of diffusion has been so small that equilibrium has been attained more rapidly.

4.3. *Aluminium–Copper*

Gold and copper are miscible in all proportions but do not form definite compounds. The next popular systems for investigation, aluminium–copper and aluminium–silver, both form several intermetallic compounds and have been the subject of extensive age-hardening investigations. The age-hardening of aluminium–copper alloys has been fully described (Smith 1949) and it has been shown how the ageing properties are related to the physical structures as shown by the phase diagram. The diagram itself (fig. 7) is extremely complex and shows that at room temperature there are five pure phases apart from the terminal solid solutions. Aluminium and copper were evaporated simultaneously on to glass slides (Trillat 1954) but the resultant films showed only the pure metals and did not show any of these structures when the condensing surface was at room temperature. However, deposition on surfaces at 300°C gave various

phases according to the relative proportions of the two metals, $CuAl_2$ being particularly prominent. It was suggested that the failure to alloy at room temperature was due to the low mobility of the condensing atoms at that temperature. Using a single source and evaporating either a mixture of the two pure metals or an alloy gave extremely diffuse patterns indicating that the films had a microcrystalline heterogeneous structure without any regularity (Takahashi and Fert 1953). Ageing of these films (1 month at 18°C or 30 min at 300°C) gave rise to various phases according to their composition. Condensation on a hot substrate gave the various alloy phases immediately, indicating again the strong dependence upon temperature.

Fig. 7



Phase equilibrium diagram Al–Cu.

Michel (1956) also studied the aluminium-copper system, preparing specimens by simultaneous evaporation and by successive evaporation. He did not obtain any alloy formation by successive evaporation, even after ageing for several weeks at room temperature but obtained alloys immediately by simultaneous evaporation, the main component being the β phase Cu_3Al. After ageing he also obtained the γ phase Cu_9Al_4. This is in marked contrast to the results of Trillat who repeatedly observed the θ phase $CuAl_2$. It suggests that Trillat worked mainly on aluminium-rich specimens while Michel may have observed more copper-rich alloys. This could be due to the difference in ease of evaporation of aluminium and copper. Michel mentioned preliminary experiments to obtain equal

evaporation rates by adjusting the heater currents. In the absence of such adjustment the aluminium would vaporize much faster, and Michel actually studied the evaporation of $CuAl_2$ alloy showing that the rate of evaporation of aluminium would be 500 times greater than that of copper at the same temperature (996°C). He also showed experimentally that a higher source temperature gave an increasing proportion of copper. The mixture and alloys which were evaporated by Trillat would certainly be affected in this way and would give aluminium-rich specimens unless he completely vaporized the charge and this is not stated.

The structural changes with temperature for one composition of the alloy were examined continuously by Trillat and Takahashi (1953) using the method described in §4.1. They showed the separation of $CuAl_2$ from a mixture of the two metals between 350°C and 375°C. For another specimen of different composition, the precipitation of CuAl occurred in the range of 350–400°C. The diffraction patterns could be seen clearly and there was no indication of other phases.

These experiments did not give information on age-hardening but served to indicate the possibilities and difficulties of thin film methods. Winkelmann (1956b) tried to use thin film specimens to investigate age-hardening. His attempts to produce single-crystal films of Al–4% Cu alloy were unsuccessful and he finally used polycrystalline films which were condensed at room temperature. Initially these gave the pattern of pure aluminium only and only on heating to 300°C were the first signs of θ phase observed. The film compositions were determined by measuring the saturation temperatures and the films were then tempered at 550°C and finally quenched and examined by electron diffraction. There was an interval of 20 min between quenching and examination and in each case the θ phase had already separated. This is in marked contrast to results obtained on bulk material using x-rays. Bulk specimens show the formation of Guinier–Preston zones but no separation of a stable end-phase. Further experiments showed that the rate of separation of θ phase was a function of film thickness being slower for thicker films, and that the rate decreased with increasing grain size. This was in agreement with results obtained for aluminium–silver alloys (Winkelmann 1956a).

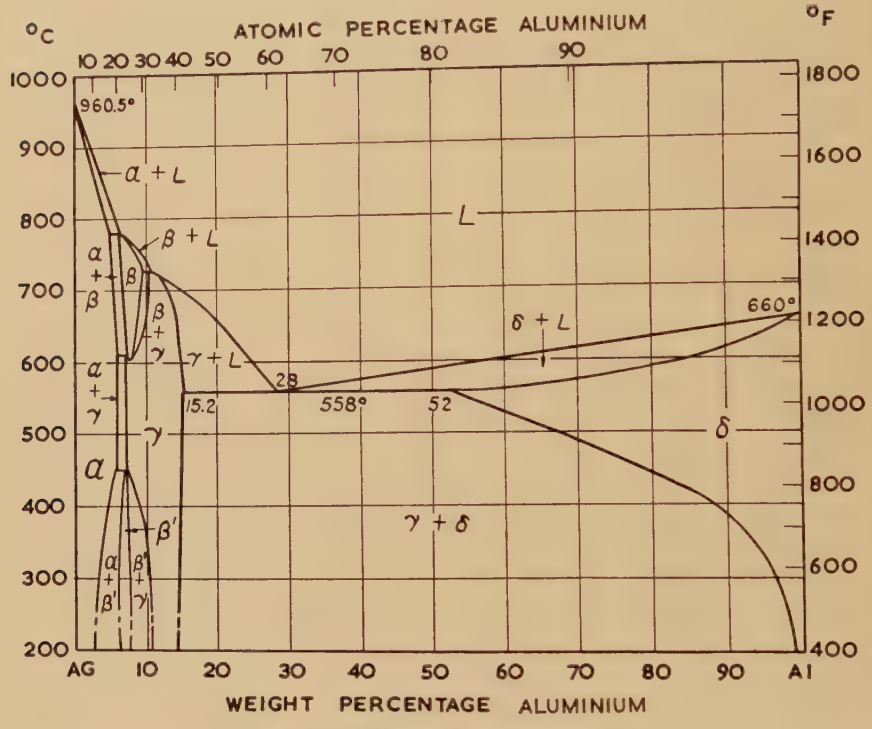
The initial formation of θ phase only above 300°C is in agreement with the observations of Trillat and tends to confirm our suggestion that his specimens were rich in aluminium. Winkelmann mentioned that he had to evaporate alloys of relatively high copper content in order to obtain films containing about 4% copper.

4.4. *Aluminium–Silver*

The alloys of aluminium and silver also show age-hardening properties in bulk form (Hansen 1928, Agew and Shoyket 1933, Hirano 1953, Hirano *et al.* 1955a, b). The phase diagram shown in fig. 8 is complex and shows the existence of two intermetallic compounds which are stable at room temperature and one stable in a higher temperature range. It has been

suggested that the ageing properties are due to the precipitation of the γ phase Ag_2Al and x-ray studies (Walker and Guinier 1953, Belbeoch and Guinier 1954) have shown that Guinier–Preston zones are formed by segregation of silver atoms on the (111) planes of the matrix lattice, followed by precipitation of Ag_2Al in the form of lamellae parallel to the (111) planes.

Fig. 8



Phase equilibrium diagram Ag–Al.

Electron diffraction was used by Göttsche (1953) to investigate the structure of thin single-crystal films prepared by evaporating a silver–aluminium alloy containing 30% silver by weight onto heated rock-salt surfaces. He showed that preferential evaporation of silver led to a partial separation of components and formation of a three-layer structure. A thin layer of silver-rich, cubic α phase containing up to 20% aluminium was deposited first, followed by γ phase with a close-packed hexagonal structure and, finally, a layer of the terminal solid solution or δ phase. This agreed with earlier work (Boettcher 1950). By stopping the evaporation whilst a portion of the charge remained in the heater, films containing only α phase and γ phase were produced. At a substrate temperature of 350°C the films were not oriented and gave Debye ring patterns showing a superposition of the cubic and hexagonal structures. Films deposited on rock-salt at 450°C were, however, oriented and gave single-crystal

patterns. These patterns showed a strong orientation of the γ phase with the (0001) plane parallel to the (111) plane of the cubic α phase. Extra points which were observed were attributed to lattice defects and a detailed mechanism of orientation was described.

Similar films were used by Winkelmann (1955 a, b) and Winkelmann and Raether (1953) to investigate age-hardening processes in this alloy. They used the same original alloy containing 30% silver by weight but tried to avoid separation of components by using the 'flash' technique of Harris and Siegel (1948). In order to ensure homogeneity the films were then annealed at about 500°C. Winkelmann wished to compare his results with the results obtained from bulk specimens by X-ray diffraction and emphasized that this was only possible by using single-crystal or oriented polycrystalline films which he produced by deposition on heated rock-salt faces in the same way as Göttsche. The films were dissolved off the rock-salt and picked up on nickel grids for examination by electron diffraction. The composition of each film was determined accurately by measuring the saturation temperature. In order to do this, the films were heated slowly and examined continuously. At the saturation temperature all the diffraction spots due to the hexagonal structure and lattice defects vanished, only to reappear after quenching. This quenching was carried out in the original evaporation chamber by heating the specimens to 530°C for one hour and then quenching to less than -10°C immediately. There was a time lapse of about 20 min in transferring the specimens back to the electron diffraction camera for examination but the pattern showed complete precipitation of the hexagonal γ phase. This was in complete contrast to the results of X-ray examination using bulk material where complete segregation of γ phase took over a month at a temperature of 150°C. It was argued that of the two main factors determining the rate of precipitation, namely, nucleation and diffusion, diffusion would be more important at low temperatures and nucleation would be more important at higher temperatures with a smaller degree of supercooling. Consequently, with quenched specimens which were cooled far below the saturation temperature, diffusion would be the main factor. The work of Göttsche made it appear that the separation of γ phase was due to a glide along the (111) planes and it was at first suggested that the glide process was obstructed in bulk specimens by the internal stresses and could take place relatively freely in thin films. It is, however, well known (Hoffman and Storey 1956) that evaporated films frequently condense in a highly stressed state containing a large proportion of vacant atomic sites and voids. Furthermore, later work on aluminium–copper films (Winkelmann 1956 c) showed similar differences in rates of segregation between films and bulk material, where glide is not involved and the same explanation is not tenable. It was concluded that the rate of precipitation was a function of crystallite size, being most rapid with smaller crystallites such as were found in the thinnest films. Other explanations were discussed (Winkelmann 1956 b) but shown to be untenable. The dependence upon

crystallite size suggests that the high rate of precipitation in thin films is due to the relatively high proportion of grain boundaries or lattice defects and recent investigations have used electron microscopy (Thomas and Nutting 1956, Thomas and Whelan 1958) to follow the positioning and growth of precipitate particles.

The aluminium–silver system was also investigated by Boettcher and Thun (1954) using a moving-film method and recording continuously as the specimen temperature varied (see § 4.1). Their attention was concentrated on an alloy containing 88% silver which was examined over a temperature range 20°C to 360°C and down again to 200°C. They showed that there was a phase transition at about 300°C with formation of a cubic β phase and that the high temperature structure persisted on cooling.

Alloy phases for the whole system were investigated by Watanabe (1956) by evaporating the two metals simultaneously onto rock-salt cleavage planes. The close-packed hexagonal phase was formed with an axial ratio of 1·63 : 1, indicating stacking faults. This was particularly noticeable at high temperatures. The β phase was found to be difficult to form directly by evaporation but could be obtained after ageing at a suitable temperature to ensure equilibrium conditions.

4.5. *Indium–Antimony*

A study of the alloys produced by interaction of the metals indium and antimony has been made by a number of workers in Russia using electron diffraction methods. Antimony films condense in a manner which is particularly dependent on film thickness (Richter 1943). Götzberger (1955) has also shown that the films remain amorphous up to a thickness of about 200 Å but above this value the films tend to crystallize, the growth proceeding outwards from active centres. The rate of crystallization increases with film thickness and can occur at an explosive rate in films about 2000 Å thick. This tends to remove the antimony deposit from the substrate and renders the films useless for further investigation. For these reasons most of the work on antimony films has used thicknesses between 200 and 2000 Å.

Kurov and Pinsker (1958) deposited films on glass microscope slides using separate heaters at opposite ends of the slides for the two metals. Wedge-shaped films of the two metals were thus produced with the wedges in opposite sense. The films were annealed at 100–120°C under vacuum to produce an alloy film with a continuous variation of composition along the length of the slide. In addition to examining the specimens by electron diffraction, they measured the electrical conductivity and thermo-e.m.f. by probes at various points to show the existence of a definite InSb compound.

Indium has a tetragonal structure while metallic antimony has a rhombohedral structure and the compound InSb generally has a cubic zinc blend structure but there is a hexagonal modification. Electron diffraction

examination showed that the antimony gave an amorphous pattern while the indium had a tetragonal structure. Between these extremes both the hexagonal and cubic forms of the intermetallic compounds were identified. Presnov and Synorov (1957) had already measured the electrical properties of similar films and shown the existence of peaks in the curves of resistivity and thermo-e.m.f. against concentration, the peaks corresponding to a 1 : 1 atomic concentration. The small hole mobility which was obtained was attributed to the microcrystalline structure of the films. Similar results were obtained by Semiltov and Rozsival (1957) who used both collodion and rock-salt surfaces for condensation. The compound InSb was examined in more detail and the lattice parameter was measured by Konozenko and Mikhnovsky (1956) who found the cubic unit cell had a parameter of 6·463 Å, in close agreement with the tabulated value of 6·46 Å obtained by x-rays (Smithells 1949).

§ 5. X-ray Methods

There is no doubt that x-rays have been the mainstay of metallurgists for identification of alloy phases in bulk specimens. However, x-ray diffraction does not have the sensitivity of electron diffraction and a much greater bulk of material must be exposed to the x-ray beam to obtain effective diffraction patterns. Consequently, the use of x-rays for work on thin films has not been very profitable. Evaporated films are generally too thin and contain too little material, but there are a few recorded instances were x-rays have been used.

Multi-layer films of gold and copper were produced by DuMond and Youtz (1940), evaporating copper continuously from one source whilst gold was evaporated periodically from a second source. They obtained films having a total thickness of 10 000 Å with layers of gold alloy every 100 Å. Theoretically, their method should give a square wave distribution of the gold but they showed that the distribution would rapidly become sinusoidal and this was confirmed experimentally when they used the multi-layer as a diffraction grating for x-rays and showed that only the first order diffracted image was obtainable. Assuming a sinusoidal distribution they were able to calculate the diffusion coefficient from the rate of decay of the ordered structure as the films tended to become homogeneous. A value of 5×10^{-20} cm^2/sec was obtained for diffusion at room temperature, which is in good agreement with values obtained for bulk material (Jost 1932, 1933). The original objective of the experiments was not achieved but the modified experiments represent an ingenious way of using thin film methods in conjunction with x-rays. The multi-layers give a sufficient bulk of material for x-ray diffraction and yet the distance of diffusion remains comparatively short. However, the method does not appear to have been developed further.

X-rays were used in a more orthodox manner by Burr *et al.* (1944) to nvestigate the alloying of copper and zinc. They deposited these metals

on glass by successive evaporation producing films 6000 Å thick. An automatic X-ray spectrometer which had been developed earlier (Harding *et al.* 1942) was used to measure relative intensities of diffraction maxima during ageing from films *in situ* on the glass substrates. This could not be done with powder photographs because of the high background level. Ageing was carried out at 198°C and the diffraction records showed a gradual formation of β brass with a strong orientation of the (110) plane parallel to the substrate. Corresponding records for the pure metals were compared with results obtained using metal filings scattered on glass and showed that copper films on glass were oriented with the (111) or (100) plane parallel to the substrate while zinc films on glass were oriented with the (001) or (101) planes parallel to the substrate.

From these results they were able to suggest a mechanism whereby the gradual addition of zinc to a copper film oriented with its (111) plane parallel to the substrate could produce a series of transitions from pure copper to α brass and thence to β and γ brass and further through the ϵ and η phases to pure zinc without drastic lattice disturbances and always preserving orientation relative to the substrate. This work on orientation in thin films supplemented X-ray powder photographs which were obtained by scraping films off slides into cellophane specimen holders. They claimed that all stable alloy phases were present 30 sec after commencement of diffusion. This is probably an underestimate since the powder photographs each required an exposure of 90 min and there is a possibility that some reaction continued in the powdered state during the exposure, but certainly all phases were produced in a remarkably short time and the spectrometer results showed a complete disorganization of the zinc lattice within 2 min. Further diffusion and complete homogenization favoured the β phase, possibly due in part to the equal thicknesses of copper and zinc which were used. The early formation of all alloy phases is an interesting confirmation of the diffusion theory outlined earlier (§ 3) and the growth of one region at the expense of the others is to be expected.

Their work shows the difficulty of obtaining results from undisturbed films. They had some trouble with background level using films 6000 Å thick and this is probably close to the sensitivity limit even for the special spectrometer which was used and yet a 6000 Å film is comparatively thick. Results can be obtained by scraping films off but the small quantity of material means long exposures and there is an implicit assumption that the disturbance and the long exposure have no effect. Thinner films would be even more difficult. The technique of scraping films off the substrate and using the powdered material for X-ray measurements has also been used by Belser (1954) to obtain evidence of alloying for a number of metal pairs and the results were used to supplement his work on resistivity of bi-metallic films (see § 6). The films used were about 2000–3000 Å thick and he comments that somewhat thicker films would be desirable for best results by this method. In some cases there was difficulty in identifying phases. Attempts at using a recording spectrometer for films

in situ were unsatisfactory because of high background levels due to scattering by the glass substrate.

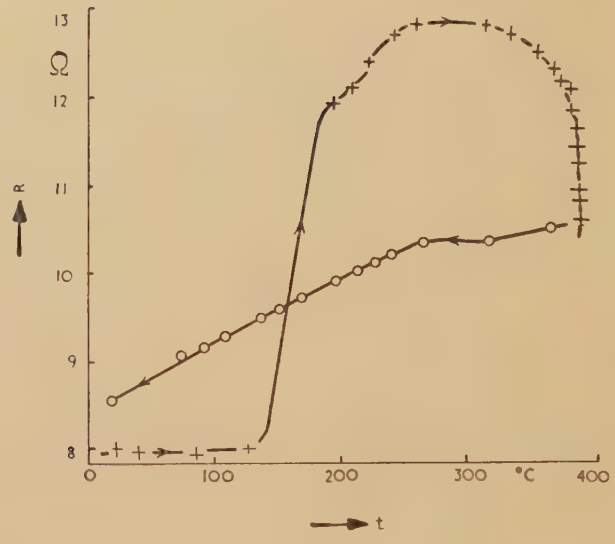
§ 6. Electrical Resistivity

Resistivity changes in thin metallic films have been studied extensively (Blanc-Lapierre and Perrot 1954, Mostovetch and Vodar 1951) but these investigations have, in the main, been confined to single-layer films of pure metals. Ageing effects in two-layer and alloy films have, however, been considered by Boettcher (1950) and Belser (1954, 1957) and used to obtain information on the intermetallic reactions which occur in such films. Boettcher demonstrated the possibilities of this method of investigation with his work on AgAl and AlMg films. The films which he used were prepared by evaporation of alloys of known composition and in each case the charge was completely vaporized. Naturally, separation of the alloy components occurred and approximate calculations were made of the variation of composition through the resultant films assuming Raoult's law to hold over the full concentration range. The films were then put through a temperature cycle, the temperature rising to 400°C and falling again over a period of about an hour. The apparatus was arranged so that the films could be prepared and all measurements made continuously under vacuum.

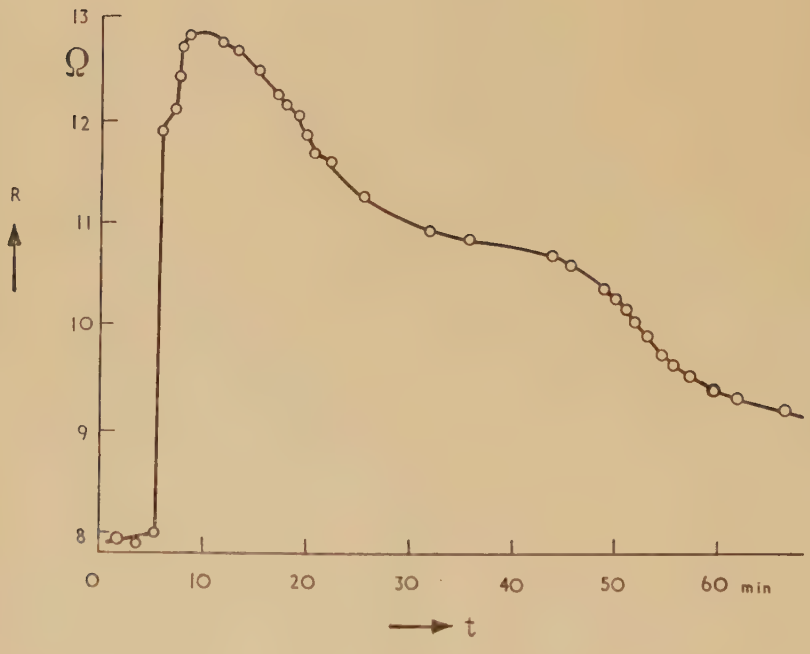
Fig. 9 shows the changes in resistance for a film produced by evaporating an alloy containing 6% aluminium by weight. In equilibrium such a film would consist only of α phase and β' phase, the latter forming about 30% of the total. Calculations showed that due to separation of components during evaporation, the film as deposited would consist mainly of α phase with an upper layer of β' phase, itself covered by successive thin layers of γ phase and δ phase. Electron diffraction examination of the film by transmission immediately after deposition showed mainly unsaturated α phase containing less than 1% aluminium and diffuse reflections from β' and γ phases suggesting that these were in the form of minute crystallites. Heating to 215°C produced an extension of the β' phase while the α phase reflections became more diffuse and the γ phase disappeared. The diffuse rings from the α phase were attributed to lack of homogeneity as aluminium diffused into the lattice. At 295°C the α phase reflections became stronger, due apparently to a progressive establishment of equilibrium, which at the higher temperature favours the α phase, together with a partial transformation of β' phase into saturated α phase. Heating further and cooling gave α, β' phases in equilibrium. Diffraction photographs obtained by reflection showed the upper layers only. Both hexagonal γ phase and cubic δ phase were present immediately after deposition but on heating, the δ phase rapidly disappeared and was followed by the γ phase. Above 200°C only β' phase could be seen, and this remained during further heating and cooling.

These changes are reflected in the electrical resistance measurements. The resistivities of the different phases had already been measured for bulk

Fig. 9



(*a*)



(*b*)

Resistance changes in Ag-Al alloy containing 6% Al (after Boettcher). (*a*) Resistance/temperature, (*b*) resistance/time.

material (Broniewski 1912) and it had been shown that the terminal solid solutions had much higher resistivities than the pure metals while the β' and γ phases had even higher resistivities, the β' phase having a resistivity about 1·4 times greater than the γ phase. Figure 9 (*a*) shows the film resistance plotted against the temperature as it rises and falls again while fig. 9 (*b*) shows the same results on a time scale. Absolute resistivities could not be calculated since film thickness was not measured, but it may be assumed that the films were greater than 1000 Å thick, since the same specimens were used for reflectivity measurements, assuming opaque films. The rapid rise of resistance at about 150°C was attributed to formation of the high resistance β' phase at the expense of α phase. The kink at the upper end was not explained but might be due to the disappearance of γ and δ phases almost simultaneously. Further heating caused a decrease in resistance. It was assumed that up to this point equilibrium was not established and the α phase remained unsaturated. The electron diffraction results showed the α phase growing stronger at higher temperatures and the drop in resistance was therefore explained as a transformation of β' phase back into saturated α phase as equilibrium was progressively established. This tendency continued more slowly as the temperature was reduced again. As shown in fig. 10, similar results were obtained with an alloy containing 7% aluminium by weight, except that the resistances were everywhere higher even though the same weight of alloy was evaporated and the film should therefore have been about the same thickness. This higher resistance would, of course, be due to the greater proportion of β' phase. The slight rise in resistivity on cooling which had already appeared in less marked form in fig. 9 (*b*) was attributed to the lower solubility of aluminium in the α phase at lower temperatures as shown by the equilibrium diagram, fig. 8. This lower solubility would cause a slight partial transformation of α phase back again into β' phase on cooling and a resulting increase of resistance.

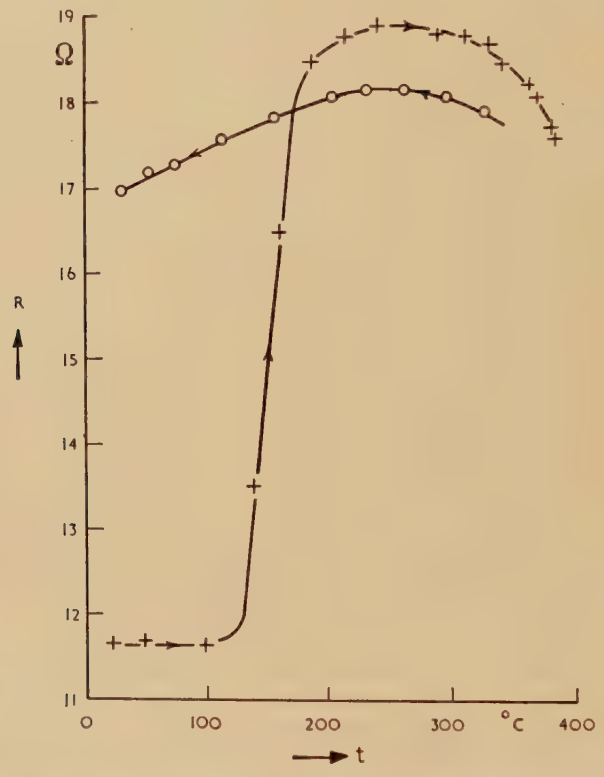
According to the phase diagram, these effects should not persist beyond about 10% aluminium when the β' phase is unstable and fig. 11 shows results obtained by Boettcher for an alloy containing 19% aluminium by weight. At equilibrium this should contain only γ and δ phases but separation of components during evaporation produced an underlayer of β' phase. On heating, the β' phase was progressively transformed to γ phase with a consequent, rapid fall in resistance and the β' phase was never re-formed, even on cooling.

The results in general suggested that there must be a very high coefficient of diffusion of at least one component in the β' phase to account for the rapid extension of the β' phase region. This is particularly remarkable since the β' phase has a very narrow range over which it is homogeneous and this suggests low diffusion velocities of either component in it. There is so far no explanation of this point or of the rapid changes around 100–150°C.

The corresponding record of Boettcher's work on AlMg films is relatively incomplete, only a descriptive account of the results having been given.

As a result of the great difference in vapour pressures there was almost complete separation of the basic components during evaporation. During diffusion the α, β, δ and ϵ phases were formed but there was no trace of the γ phase found by Kawakami (1933). In general the hexagonal β phase formed slowly while the δ phase formed much more rapidly. During heating a broad zone of δ phase would form and either remain or decay slowly in favour of β phase according to the overall composition of the film, but a thin film of β phase was always present between the α phase

Fig. 10 (*a*)



Resistance changes in Ag–Al alloy containing 7% Al (after Boettcher).

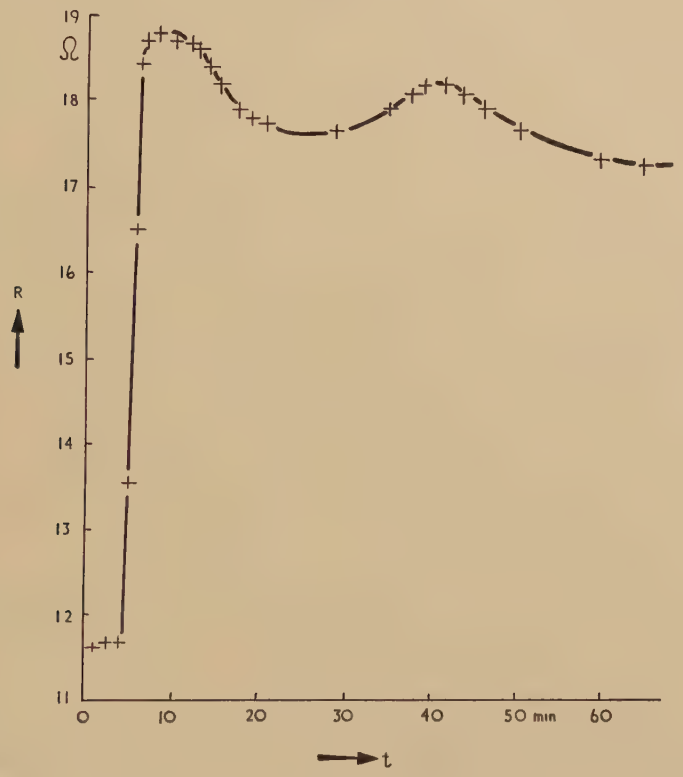
Resistance/temperature.

and the δ phase. The results generally agreed with results on bulk material (Bungardt 1937) except that the β phase seemed to be favoured more in bulk specimens. No resistance curves were given for this work.

There is always difficulty with alloy films prepared by evaporation of alloys since it is almost impossible to predict accurately the distribution of the various components in the final film and most of the work of Belser (1954) on alloys has dealt with two-layer films prepared by successive evaporation of the pure metals. He investigated the ageing of single metal

films before extending his activities to consider double-layer films. For single films he found that ageing generally resulted in a decreased resistance (Belser 1957) (Belser and Hicklin 1957) provided that a critical aggregation temperature characteristic of each metal was not exceeded. These results were obtained by ageing films in an infra-red vacuum oven and putting the specimens through repeated temperature cycles from 25°C to 600°C until the resistances became stable. Excessive temperatures, particularly with very thin films, tended to cause agglomeration and a

Fig. 10 (*b*)



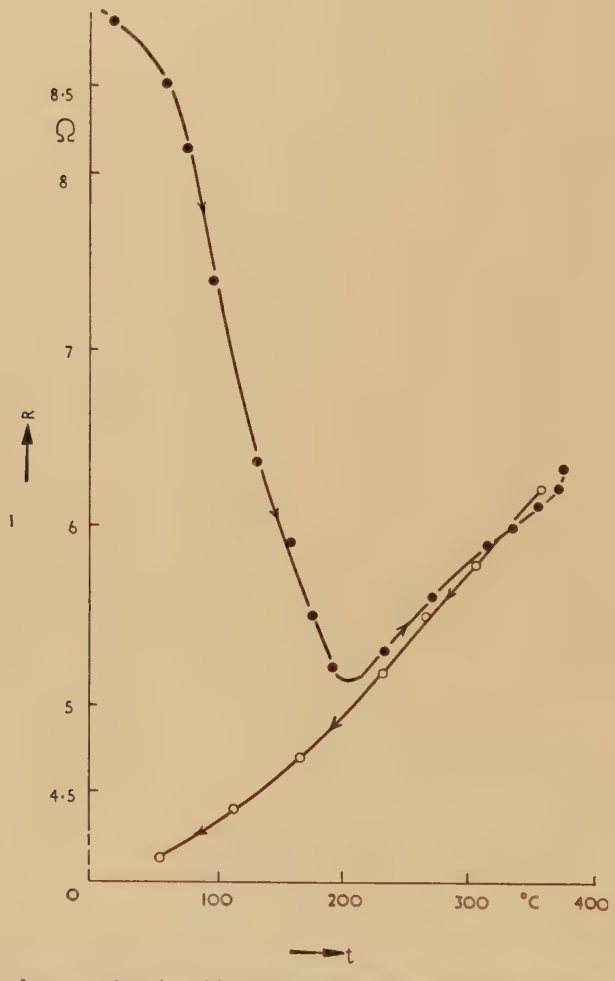
Resistance changes in Ag–Al alloy containing 7% Al (after Boettcher).
Resistance/time.

very rapid resistance rise. The temperature at which this occurred varied from one metal to another.

In considering bimetallic films, Belser suggested that, in the absence of any alloying effects the two layers of a bimetallic film should behave independently and, since they form two conducting paths in parallel, it should be possible to predict the ageing behaviour of a two-layer film from the behaviour of the individual single metal films. This is not strictly correct since the structure of the upper layer will depend upon the energy of the interface between itself and the lower layer and will not necessarily be the

same as for the same metal on glass. There may therefore be structural effects but this assumption does form a useful approximation. Diffusion or alloying will result in the formation of an intermediate layer or layers which grow at the expense of the original films. A different type of behaviour is therefore to be expected. The effects of the first temperature cycle are in general different from the succeeding cycles as shown by the

Fig. 11

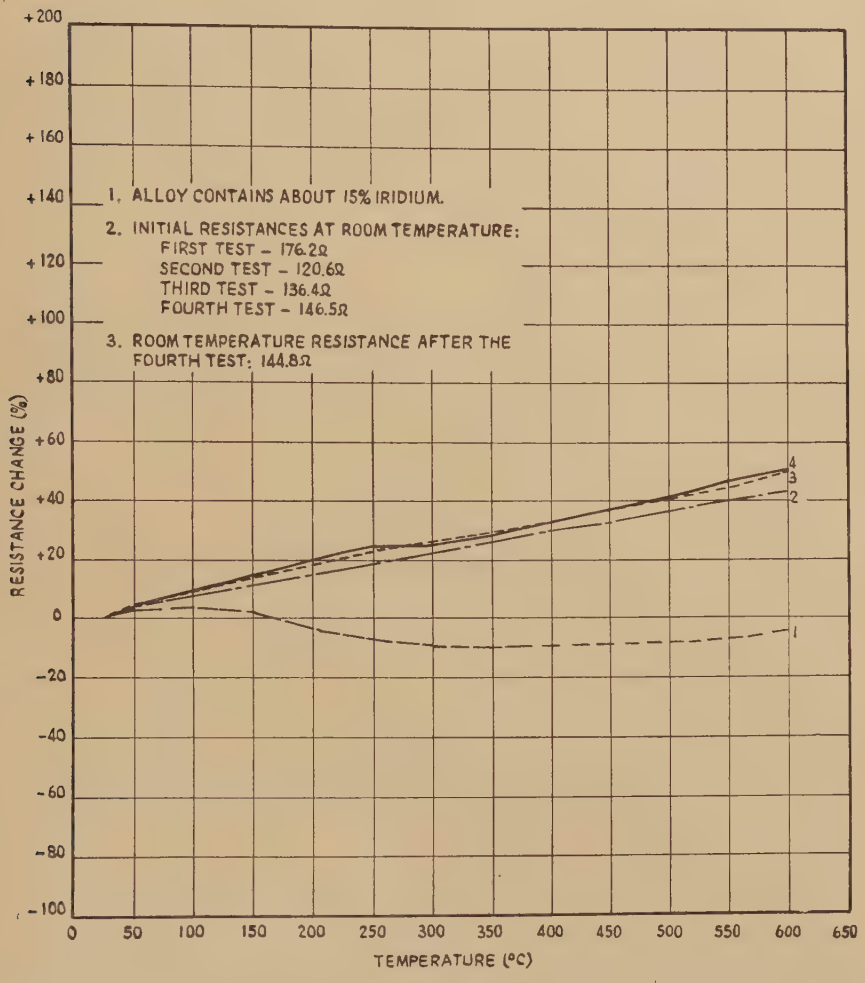


Resistance changes in Ag–Al alloy containing 19% Al (after Boettcher).

results for platinum-iridium and platinum–gold given in figs. 12, 13 (Belser 1957). Platinum was deposited first by sputtering and the results for platinum–iridium show that, during the first temperature cycle there was an annealing effect of the type observed with single metal films and thereafter the temperature coefficient of resistance remained more or less

constant while the resistance rose steadily in successive cycles as alloying occurred. The metals were both of high melting point and similar, so that relatively slow diffusion was to be expected. The annealing effect was less obvious in the case of platinum–gold and evidence of alloying

Fig. 12

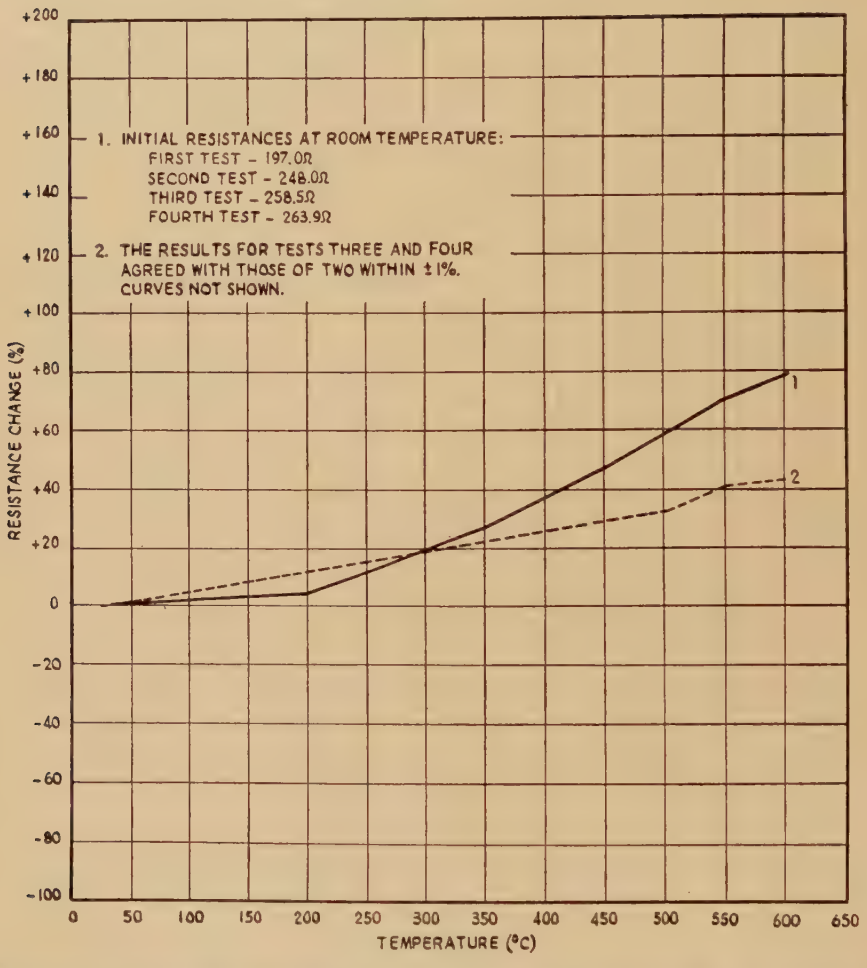


Resistance versus temperature characteristics of a film composed of successively deposited layers of sputtered platinum and sputtered iridium. Note that alloying increased the film resistivity and decreased the temperature coefficient of resistance (after Belser).

appeared at 200°c in the first cycle. This temperature was close to the recrystallization temperature for the gold. The resistance rose in successive cycles as indicated, due to progressive diffusion, while the temperature coefficient of resistance remained constant. In neither of these cases are strongly marked alloying effects to be expected since there

are wide ranges of solid solution in both cases and no intermediate compound formation. The general nature of the results which have been obtained may conveniently be illustrated by reference to the silver–aluminium system.

Fig. 13

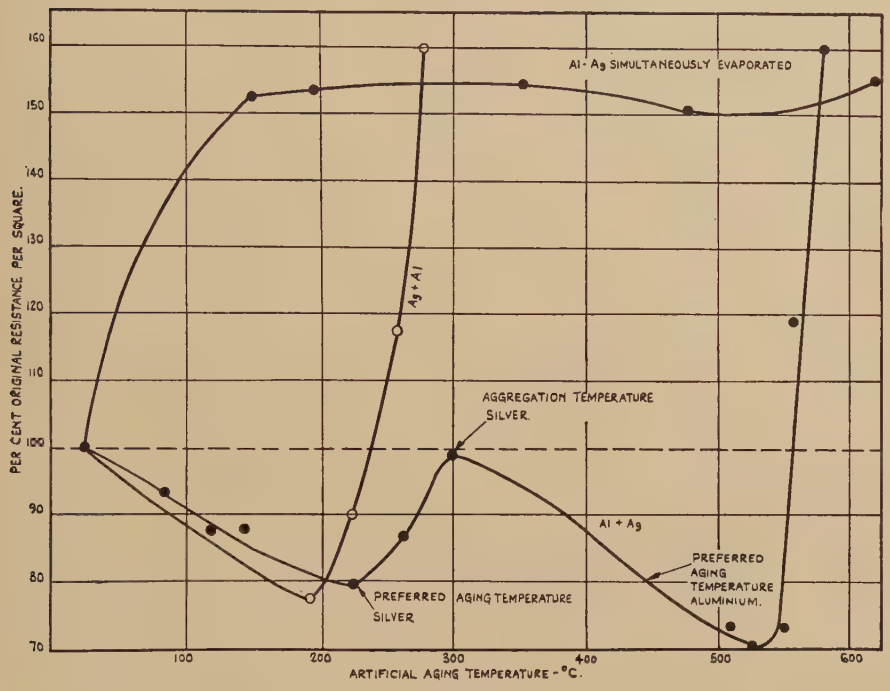


Resistance versus temperature characteristics of a film composed of successively deposited layers of sputtered platinum and sputtered gold. Note that alloying increased the film resistivity and decreased the temperature coefficient of resistance (after Belser).

Specimens were prepared firstly by evaporating silver before aluminium, then aluminium before silver and, finally, the two metals simultaneously. The results obtained during the first ageing cycle in each case are shown in fig. 14. When silver was deposited first, the double-layer film showed a sharp increase in resistance at a temperature of about 200°c. This

rise was ascribed to alloying of the two metals and the formation of an intermediate compound was shown by x-ray diffraction. When the aluminium was deposited first, a completely different behaviour was recorded. This was finally explained by assuming the formation of an oxide film on the aluminium before the silver was deposited. The silver would see this as a non-metallic substrate and the first part of the ageing

Fig. 14



Ageing of evaporated bimetallic films of evaporated aluminium and silver (after Belser).

cycle would then correspond to normal ageing of the silver on a single metal film even to the aggregation at 300°c. Above this temperature, the aluminium went through its normal ageing cycle as a single film. As the aluminium approached its aggregation temperature, the stresses caused cracking of the aluminium film and subsequent alloying with a resultant increase in resistance. This explanation was confirmed, not only by direct examination which showed aggregation of the silver on top of the aluminium, but also by showing that aluminium paired with other metals produced corresponding differences in alloying temperatures according to the order of deposition. The results indicated that an oxide film was formed readily on an evaporated aluminium surface even under vaccum (10^{-5} mm Hg). Belser 1959, private communication, later pointed out that the effects of the oxide layer disappeared if the time interval between

depositions was reduced to below one minute which indicates that a continuous oxide film took only a minute or two to form.

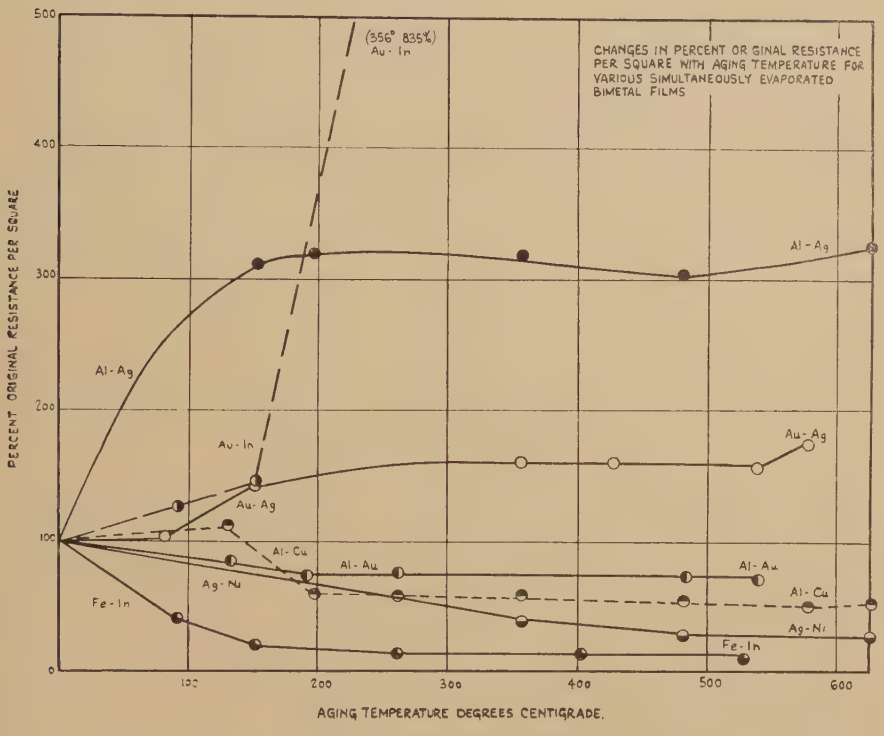
When aluminium and silver were deposited simultaneously, the resistance of the resultant film started to rise immediately and reached its full value at 150°C, remaining fairly constant thereafter. This suggests that alloying started during deposition and continued even at room temperature. It is significant that simultaneous deposition did not immediately produce a stable alloy film but that alloy formation apparently continued after deposition. From this it would appear that a film formed by simultaneous deposition is not necessarily homogeneous but may contain small clusters of like atoms. Homogeneity would, however, be attained fairly readily since atoms would only need to diffuse short distances to give a completely homogeneous structure and this appears to have happened in the present case. The temperature of 150°C at which alloying appeared to be complete agrees with the results of Boettcher who observed a marked increase of resistivity around 150°C. The fact that Belser observed alloy formation at lower temperatures would probably be due to the more intimate mingling of the components by simultaneous evaporation, which would make the formation of a new phase easier. When the components were completely separated by successive evaporation the resistance rise was delayed and occurred around 200°C. The differences could be due to a lag of the alloying effects behind the steadily rising temperature during the thermal cycle. The lag would naturally increase with the degree of component separation.

Changes in film resistance on ageing were observed for other films prepared by simultaneous evaporation and some of the results are shown in fig. 15. Belser suggested that a lack of miscibility or failure to alloy produced a high resistance film with a resistance drop on ageing whereas a strong alloying tendency was often reflected in a resistance increase during ageing. However, a definite pattern of behaviour does not appear to have been established.

These resistance studies were combined with other methods of observing structural changes. When gold or copper was paired with another metal, the temperature at which alloying occurred could readily be detected by visual observation of colour changes in the films. This method was also extended to Al–Pd which forms a pink alloy. The temperatures at which one metal disappeared into the other corresponded with the temperatures at which pronounced resistance changes occurred. Microscopic examination was used in other cases and the aluminium–silver combination was pursued by etching the films with hydrogen sulphide gas which blackened the silver, and thus showed its position. Using this method the aggregation of the silver on top of the aluminium at 350°C was readily detected. For metal pairs which alloyed readily, dendritic structures were frequently observed. The films used were generally too thick for examination by electron microscopy or electron diffraction, although these methods were used with the aluminium–copper films, but X-ray diffraction was used in a number of cases to show the presence of alloy phases. The

films were scraped off for this purpose, using the technique of Burr *et al.* (see § 5) and powder photographs were obtained. In general the results showed good correlation with the alloying predicted from resistance studies.

Fig. 15



Ageing of films deposited by simultaneous evaporation (after Belser). Resistances expressed as percentages of original resistance per square.

§ 7. Age-hardening in Thin Films

7.1. *Introduction*

It has recently been shown that information on alloying processes in thin films can be obtained from mechanical measurements of adhesion. Methods of measuring the adhesion of vacuum-deposited films have been reviewed by Weaver (1958) and a method used earlier by Heavens (1950) has been developed further. In this method a smoothly rounded chrome steel point was drawn across the film and the load pressing the point against the film was gradually increased until the film was removed by the point leaving a clear channel. The critical load at which this occurred was taken by Heavens as a measure of the adhesion of the film. The method has since been analysed both experimentally and theoretically (Benjamin and Weaver 1959) and it has been shown that for single-layer metallic films the shear strength of the adhesive bonding can be calculated

from the measured critical load. Attempts to use the same method for two-layer metallic films showed that new factors were introduced and the critical load was no longer purely a measure of adhesion. An investigation of the use of chromium as an underlayer to increase the durability of aluminium films (Weaver and Hill 1958) showed that the measured adhesion of a two-layer film was greater than the adhesion of either film as a single layer on glass. This was shown to be due to a hard intermediate layer formed by diffusion and intermetallic reaction, and curves obtained on ageing showed the formation and precipitation of this layer by typical age-hardening curves. Experiments on other metals confirmed this explanation and it was suggested that the discrepancies in adhesion measurements arose because the harder intermediate layer caused the load on the point to be distributed over a greater effective area. A greater critical load was then required to create the same basic shearing stress at the interface between film and substrate. The excess load thus formed a measure of the hardness or strength of the intermediate layer.

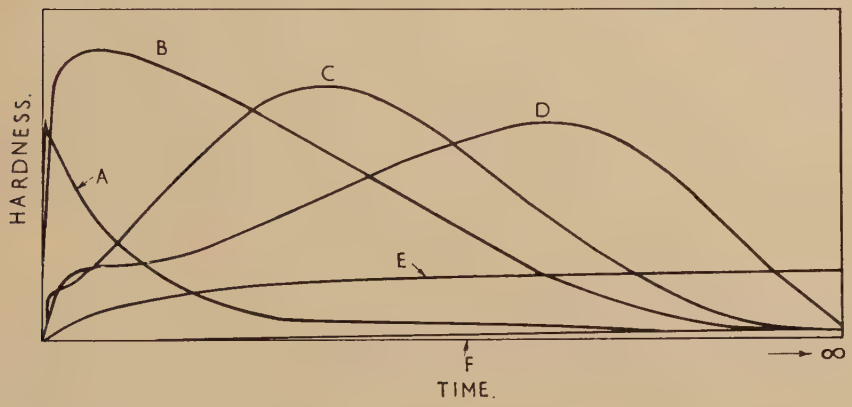
Thin film methods had been used earlier to investigate age-hardening (see § 4) but it had always been assumed that the structural changes observed in thin films were directly related to stages of the hardening process observed in bulk metal specimens. A direct correlation could not be established since it was virtually impossible to measure the hardness of metallic films by conventional methods. The film thickness was usually too small even for micro-indentation methods. The new methods not only introduce the possibility of obtaining the required correlation but also of following changes at the interface between any selected pair of metals.

7.2. *Theories of Age-hardening*

A number of theories of age-hardening have been formulated and discussed (Fink and Smith 1938, Mehl and Jetter 1939, Gayler 1947 a, b) and the entire field has been surveyed (Smith 1949). Present work indicates that the phenomena are generally due to coherent phase precipitation and the growth and release of the accompanying strains in the parent lattice structures. When a metallic solid solution is precipitated, it forms a separate phase which is generally of different composition from the original structure and it leaves a depleted matrix. Two types of precipitate are recognized, coherent and incoherent. The former are those which retain some degree of fit with the parent lattice and adopt a strained or metastable structure. The lattice of the precipitated particles is strained in such a way as to reduce the degree of mis-match with the parent lattice. The precipitation of these particles is followed by a gradual release of the coherency strains and possibly by the completion of the precipitation process to give the final structure. Incoherent precipitates, for which there is no continuity or matching of lattice structure are usually produced in these later stages. It has, however, been found that they tend to arrange their structural growth so as to reduce the discontinuity at the interface to a minimum.

The process of precipitation can only take place where there has been suitable nucleation. Incoherent precipitates require some degree of discontinuity of structure in order to form nuclei and the nuclei which are formed have to grow to a certain minimum size by random migration of suitable structural elements before they can influence the overall growth process (Fink and Smith 1940). From the nature of coherent precipitates it can be seen that less rigorous conditions govern nucleation and growth. As the precipitated particles increase in size and number, the depleted parent solution approaches the equilibrium concentration. However, due to the appreciable surface energy of the incoherent particles (Cottrell 1955) and to the strain energy of the coherent particles, a quasi-equilibrium is often established. When this occurs the earlier form of growth stops and it has been suggested that a new form of growth starts. This involves fresh nucleation and could account for the double and multiple ageing peaks which have been observed experimentally.

Fig. 16



Age-hardening curves (after Gayler). A, Upper rate limit of ageing ; B, second stage of ageing and slight indication of first stage ; C, D, first and second stages of ageing both apparent ; E, first stage of ageing with slight indication of second stage ; F, lower rate limit of ageing.

It is impossible to measure the velocities of these reactions since they are dependent on diffusion rates but it is obvious that a decrease in temperature will cause a large decrease in the reaction rate. The hardening processes therefore vary with temperature and fig. 16 gives a series of theoretical ageing curves calculated by Gayler (1937) for the same alloy at a series of temperatures. The theory outlined here does not agree completely with Gayler's original theory. At that period it was suggested that the diffusion process allowed 'molecules' of precipitate to form while still in solution in the original parent solid solution. As the 'molecules' grew the parent solid solution could no longer contain them and precipitation took place. The essential points about these phenomena were that the formation of 'molecules' was associated with an increase in hardness

while the precipitation was associated with a decrease. From the standpoint of the present theory it can be seen that the formation of dissolved 'molecules' corresponds to the present precipitation stage while Gayler's precipitation stage is now regarded as a release of coherency strains. The apparent change of scale which causes the same phenomenon to appear in two distinctly different stages can be attributed to the more advanced microscopical techniques which have become available and allowed precipitate formation to be detected at an earlier stage. The interpretation has changed somewhat but Gayler's theoretical graphs are still applicable and have been shown to be consistent with experimental results.

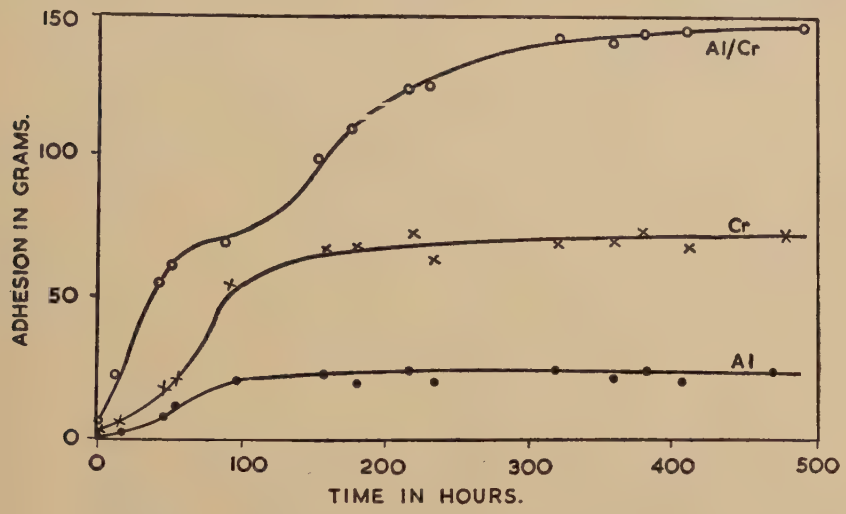
Gayler's curve E which was described by Gayler as being the result of the first stage of ageing is now seen to be caused by the simple precipitation process without release of the coherency strain. Curve F is the ageing curve for an alloy which does not precipitate, i.e. the components are perfectly miscible at all temperatures. The effect of the quasi-equilibrium and start of a new precipitation process can be seen in curve D. Curves C, B, A show progressively earlier release of the coherency strains as the precipitation and reprecipitation processes become more rapid. The curves represent the behaviour of one alloy at different temperatures but it is obvious that similar curves are to be expected at the same temperature for a series of alloys in which the rate of precipitate formation varies. Observation of a sufficiently wide range of metal pairs should give ageing curves of all types, more or less according to the nature of the phase diagrams.

7.3. *Experimental Results*

The work on aluminium–chromium has already been mentioned. Specimens were prepared on microscope slides by evaporating chromium and aluminium in succession and using masks to produce films which partially overlapped over the central section of the slide to give a two-layer film with chromium underneath. Figure 17 gives ageing curves which were obtained at room temperature with a typical specimen by measuring the adhesions of the films on the three sections of the substrate at appropriate intervals. The increased adhesion measurements obtained with the two-layer film could not be attributed to any changes at the glass-metal interface since the discrepancy arose long before any aluminium could diffuse through to this interface and action at a distance to produce an increase in adhesion is impossible, even though the upper film can produce a decrease in adhesion by stressing the underlayer to such an extent that it breaks up and loses its original adhesion. Examples where this occurs will be given but, in the absence of this effect, the basic adhesion of the two-layer film will generally be the same as the adhesion of the underlayer alone. The shape of the ageing curve for the two-layer film is the same as Gayler's theoretical curve D (fig. 16) and, as already explained the increased adhesion measurements can be attributed to the formation of a hard intermediate layer by diffusion and precipitation. In the case

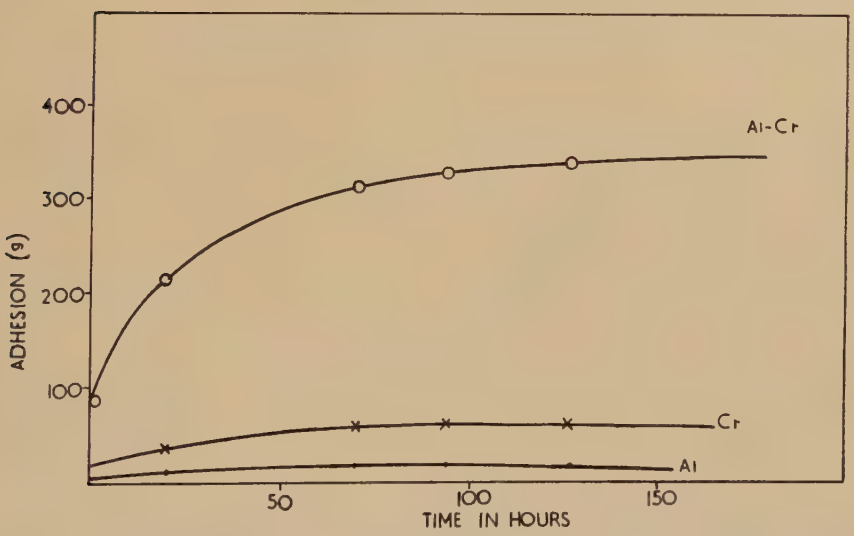
of aluminium–chromium, the existence of such a layer, differing in structure from both chromium and aluminium, has been demonstrated by electron diffraction (Weaver and Hill 1958). Ageing similar specimens at 120°c

Fig. 17



Ageing of aluminium film with chromium underlayer.
Adhesion/time at room temperature.

Fig. 18

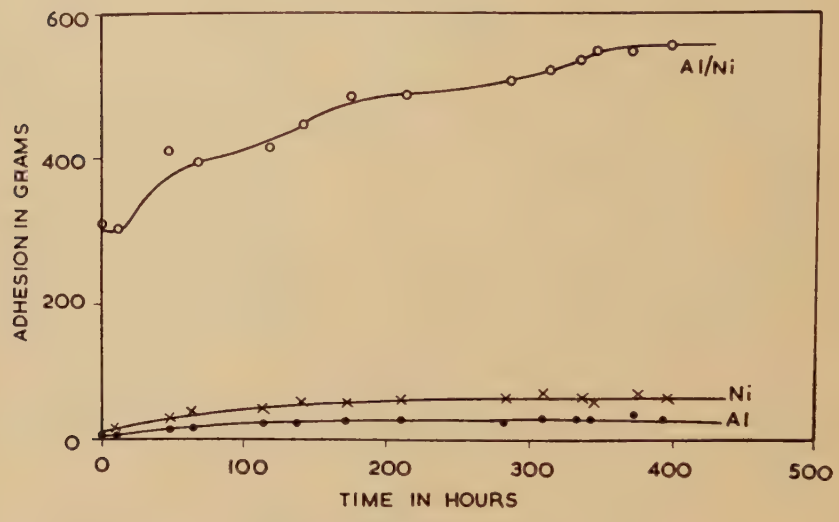


Ageing of aluminium film with chromium underlayer. Adhesion/time at 120°c.

gave the results shown in fig. 18. The increased temperature caused the two stages of ageing to overlap and give a curve similar to Gayler's curves B or C but without any final release of strain occurring.

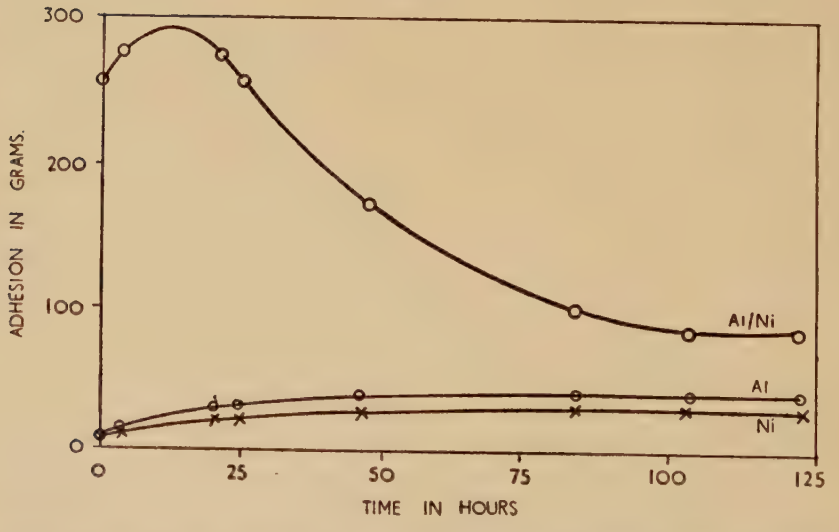
Later results obtained for aluminium films with underlayers of nickel and cobalt (Weaver and Hill 1959a, b) gave the ageing curves shown in figs. 19, 20, 21, 22. The curves for aluminium–nickel showed the temperature effects predicted by Gayler, the low-temperature curve corresponding more or less to Gayler's curve D while the high-temperature curve was the same as Gayler's curve B. The curves obtained using a

Fig. 19



Ageing of aluminium film with nickel underlayer. Adhesion/time at room temperature.

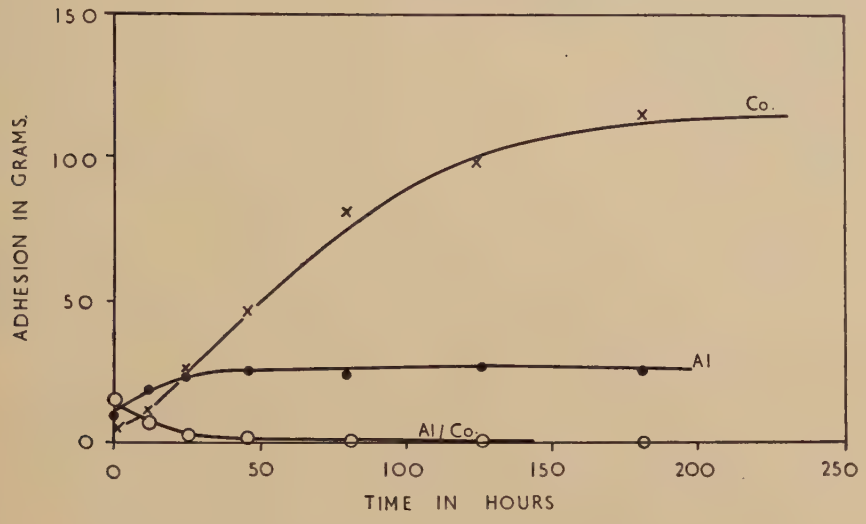
Fig. 20



Ageing of aluminium film with nickel underlayer. Adhesion/time at 120°c.

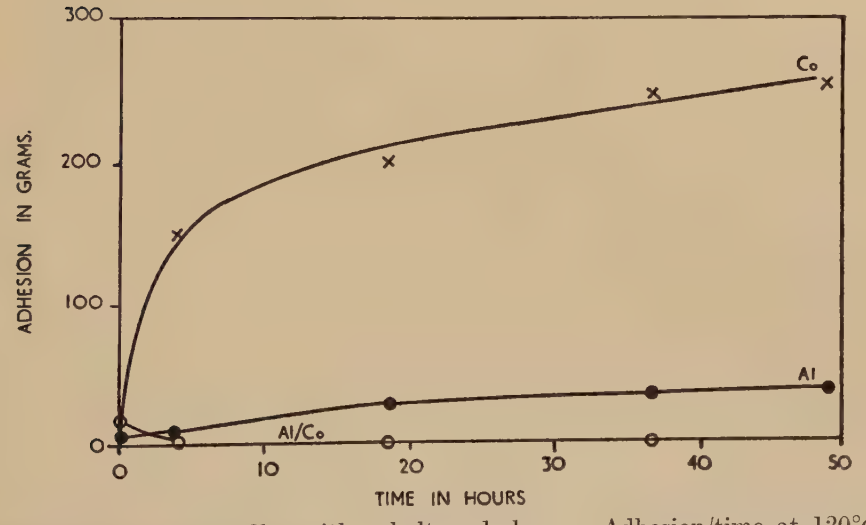
cobalt underlayer failed to show the initial hardening which apparently occurred before measurements could be made, in the short interval after deposition, while the specimens were being removed from the vacuum chamber. The curves corresponded to Gayler's curve A, showing a marked release of strain. The adhesion of the double layer even dropped below the basic adhesion of the cobalt alone as compound formation caused

Fig. 21



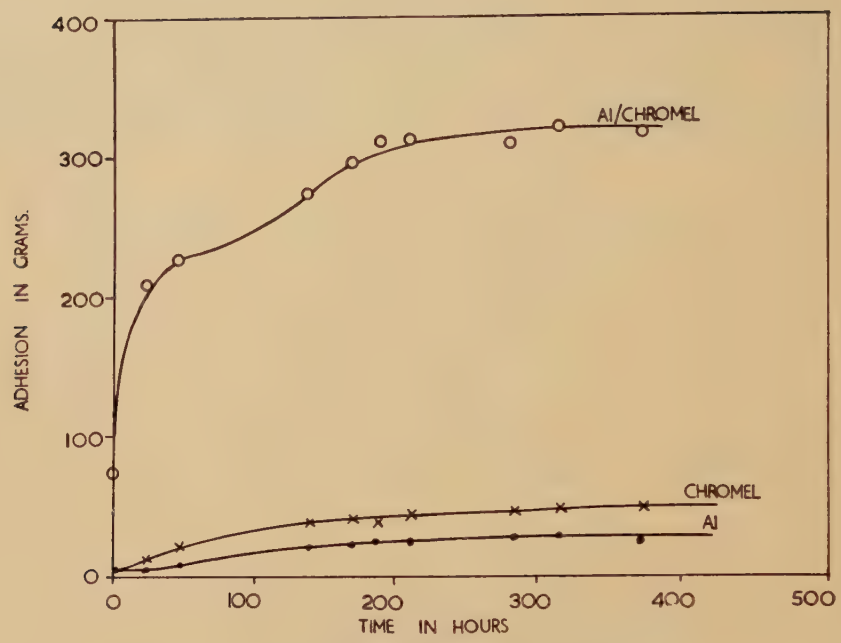
Ageing of aluminium film with cobalt underlayer.
Adhesion/time at room temperature.

Fig. 22



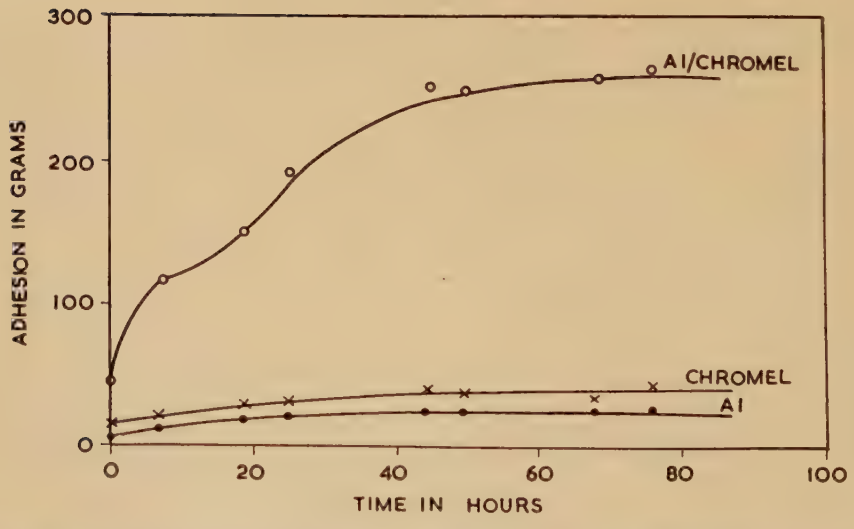
Ageing of aluminium film with cobalt underlayer. Adhesion/time at 120°c.

Fig. 23



Ageing of aluminium film with chromel underlayer.
Adhesion/time at room temperature.

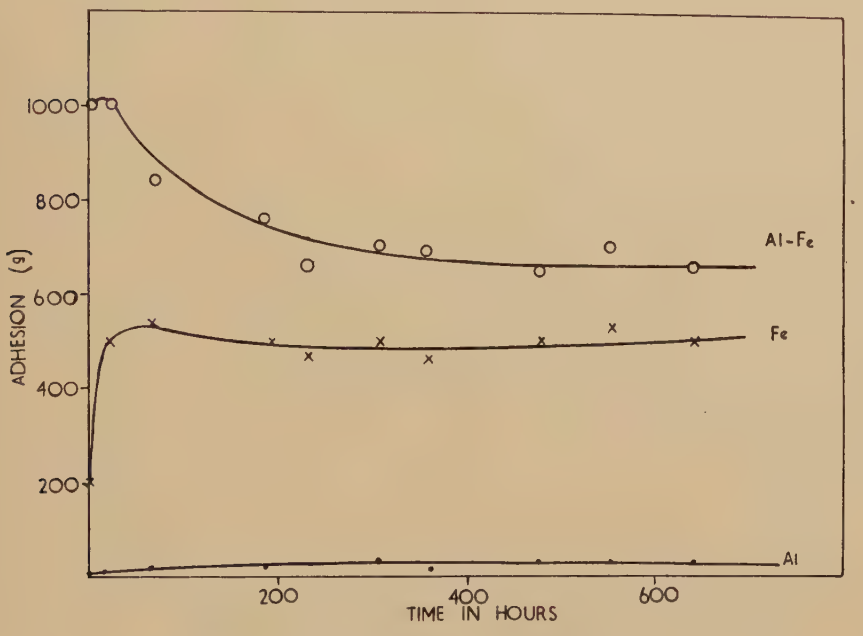
Fig. 24



Ageing of aluminium film with chromel underlayer. Adhesion/time at 120°c.

break-up and aggregation of the underlayer. Chromium, nickel and cobalt form a closely related group of metals and the age-hardening results given here show a progressive change in accordance with the differences in reactivity and tendency to compound formation. The nickel–chromium alloy chromel (80/20 Ni/Cr) was also used as an underlayer and gave the results shown in figs. 23, 24. The intimate mingling of the two components in the alloy apparently prevented the complete precipitation of large particles of AlNi compound and the softening effect which occurred at higher temperatures for nickel was never observed with the alloy. The final release of strain did not occur.

Fig. 25



Ageing of aluminium film with iron underlayer.
Adhesion/time at room temperature.

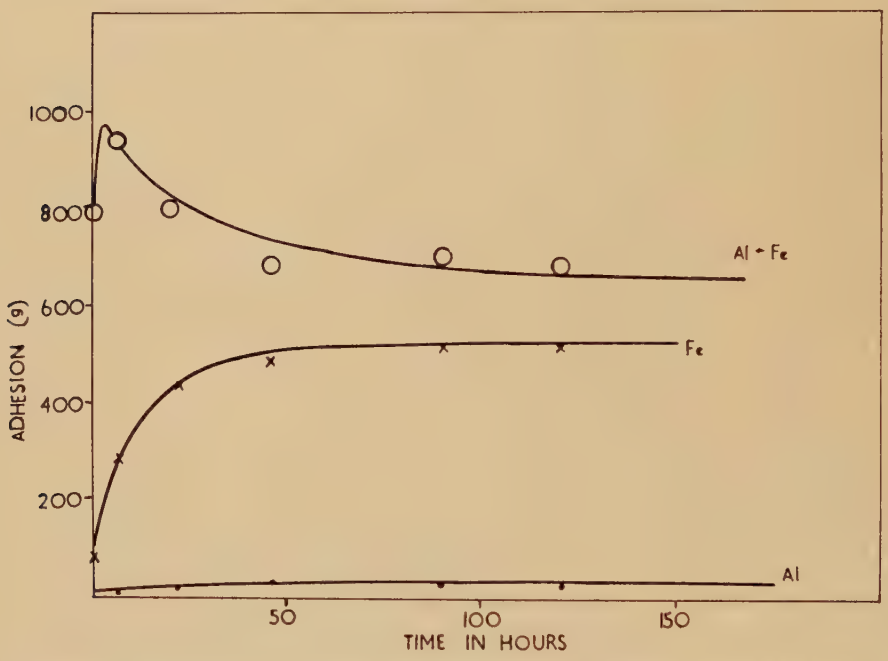
Results obtained for aluminium films with iron as an underlayer are given in figs. 25, 26. The behaviour of iron as an underlayer would place it between nickel and cobalt. The ageing curves are of Gayler's type A but compound formation does not reach the stage of film break-up which was observed with cobalt. On the other hand, nickel only reached Gayler's stage B even at the higher ageing temperature, although presumably still higher temperatures would give stage A. The phase diagram for aluminium-iron shows strong compound formation analogous to aluminium–nickel and aluminium–cobalt.

The phase diagram for aluminium–manganese (Hansen 1958) also shows strong compound formation although most of these are formed by

peritectic reactions but the behaviour of aluminium films with manganese as an underlayer is slightly peculiar. Ageing curves are shown in figs. 27, 28 and it can be seen that the double-layer films tend to follow Gayler's type A. The results are complicated by the fact that the manganese underlayer shows age-hardening effects on its own. These may be attributed to phase transitions which occur on cooling but a complete explanation cannot yet be given.

The results so far show the effects of increasingly strong compound formation but at the other end of the scale the results for silver–lead, aluminium–lead and silver–chromium which are given in figs. 29, 30, 31 show the effects of an almost complete lack of miscibility in the solid state

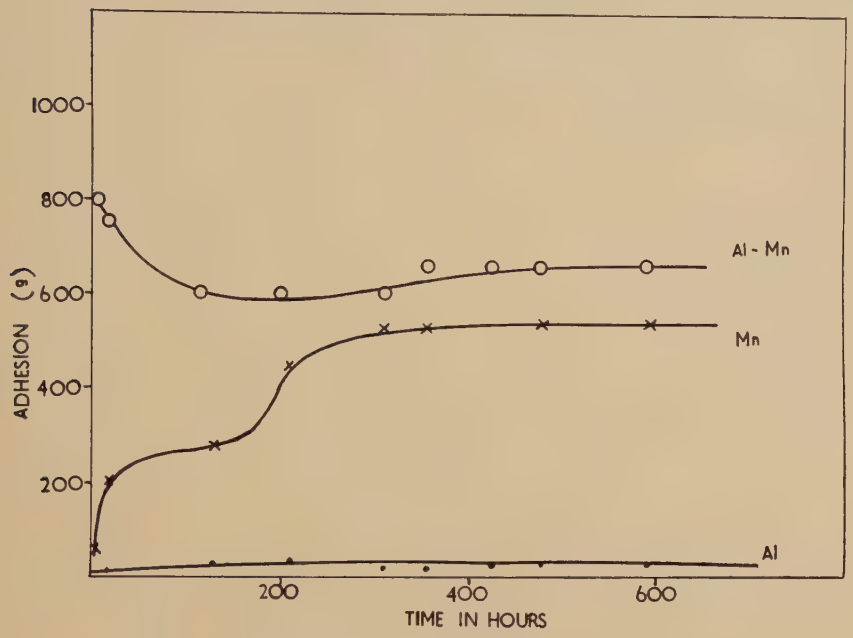
Fig. 26



Ageing of aluminium film with iron underlayer. Adhesion/time at 120°c.

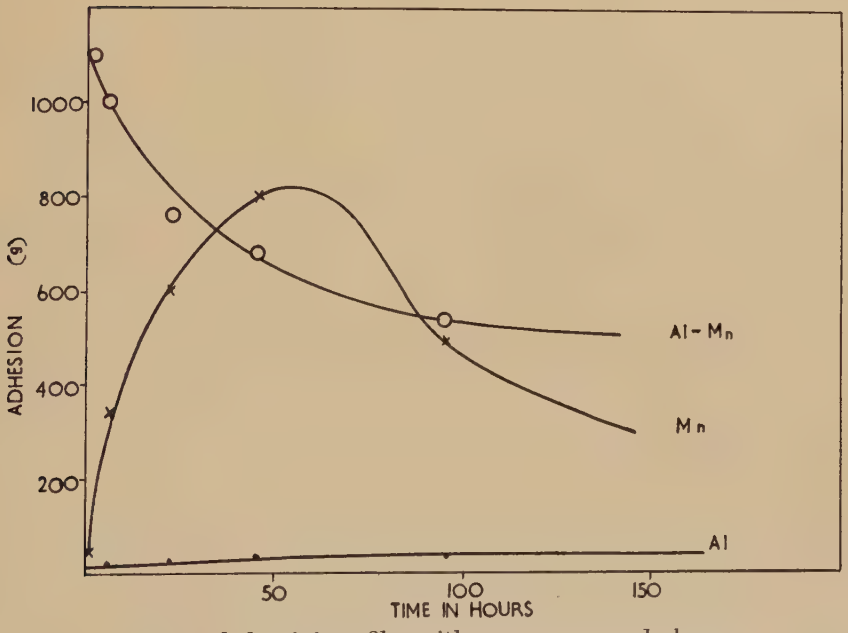
at room temperature. In each case the second metal named forms the underlayer and the adhesion figures obtained for the two-layer films are only slightly greater than for the underlayer alone. Diffusion is almost completely suppressed and any precipitation which may occur is very slight, in accordance with the severely limited solid solubilities. It is expected that complete miscibility would give similar effects since diffusion would occur readily but no precipitation could take place. The results shown in fig. 32 which are for an aluminium–lead specimen aged at a higher temperature appear anomalous. However, work on the basic adhesion of aluminium films to glass (Benjamin and Weaver 1959) makes it obvious

Fig. 27



Ageing of aluminium film with manganese underlayer.
Adhesion/time at room temperature.

Fig. 28

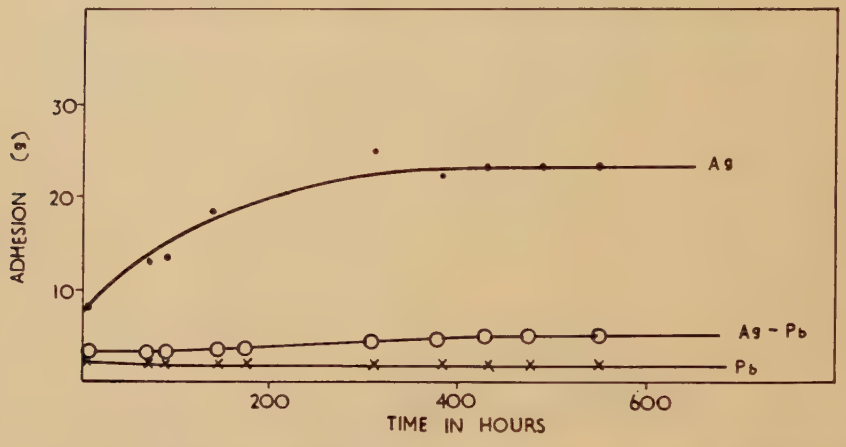


Ageing of aluminium film with manganese underlayer.
Adhesion/time at 120°c.

that the aluminium diffused right through the lead to the glass substrate and the marked increase in the adhesion of the double layer is really due to an increasing adhesion of the aluminium, aided by atmospheric oxidation.

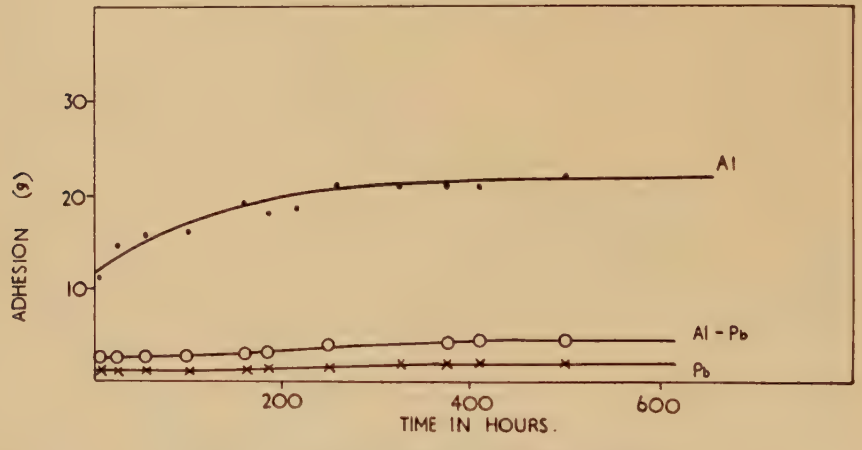
Further results for copper–chromium and gold–chromium are given in figs. 33, 34 and show the effects of increased solubility resulting in

Fig. 29



Ageing of silver film with lead underlayer. Adhesion time at room temperature.

Fig. 30

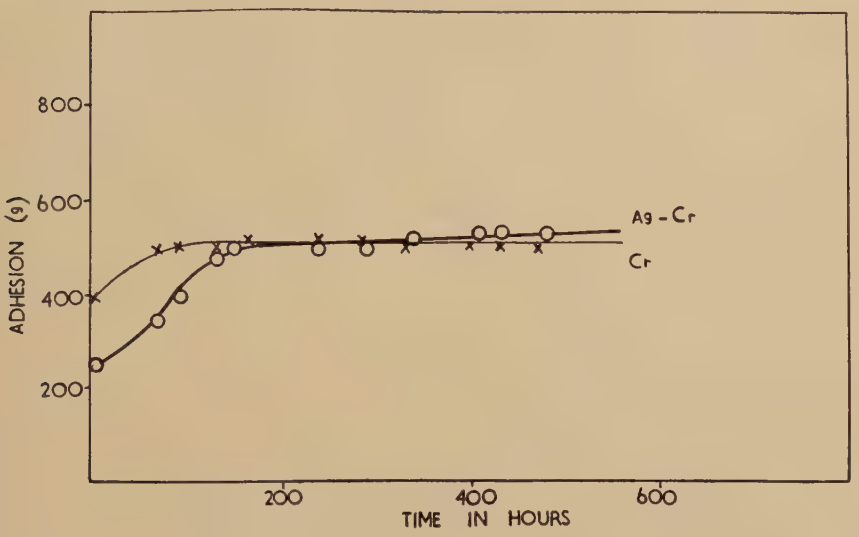


Ageing of aluminium film with lead underlayer.
Adhesion/time at room temperature.

terminal solid solutions without intermediate miscibility. A limited amount of precipitation can occur but the strains are easily relieved and the age-hardening curves therefore show in each case a small initial peak analogous to Gayler's type B but the effects are much less pronounced than when compound formation occurs.

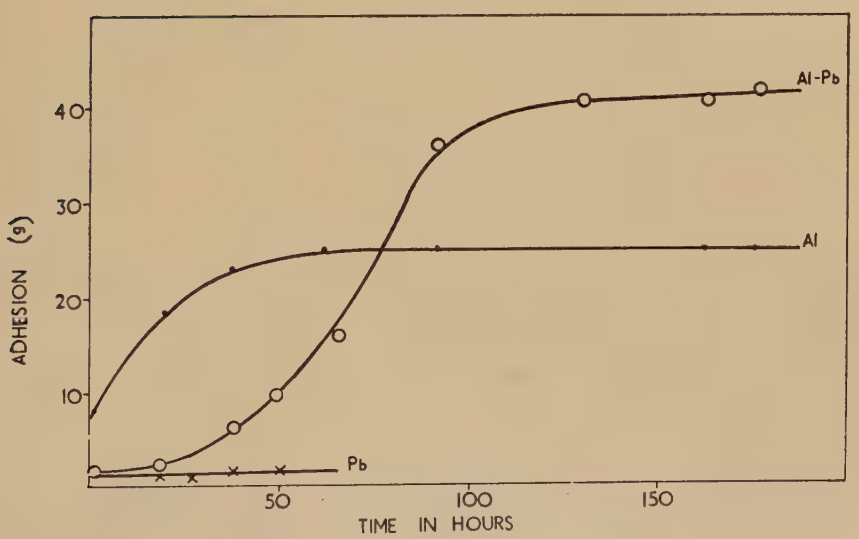
When chromium was used as an underlayer the behaviour of a two-layer film showed a marked dependence upon the thickness of the chromium. Such thickness effects have already been discussed in detail (Weaver and Hill 1959 b) and it has been shown that all the effects observed can be explained in terms of the structure of chromium films as deduced from

Fig. 31



Ageing of silver film with chromium underlayer.
Adhesion/time at room temperature.

Fig. 32

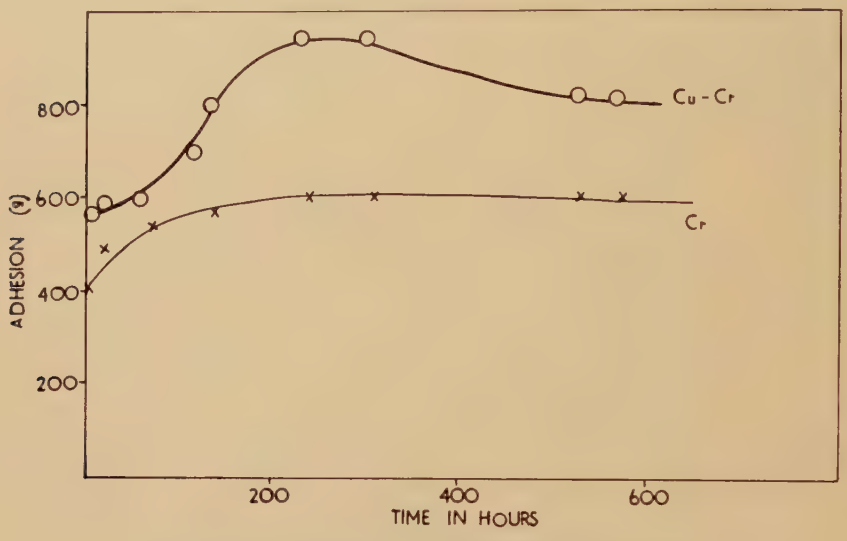


Ageing of aluminium film with lead underlayer. Adhesion/time at 120°C.

optical measurements (Hill and Weaver 1958a, b). However, all the results given here are for thicker films where such structural factors are unimportant so that direct comparisons can be made with the other results.

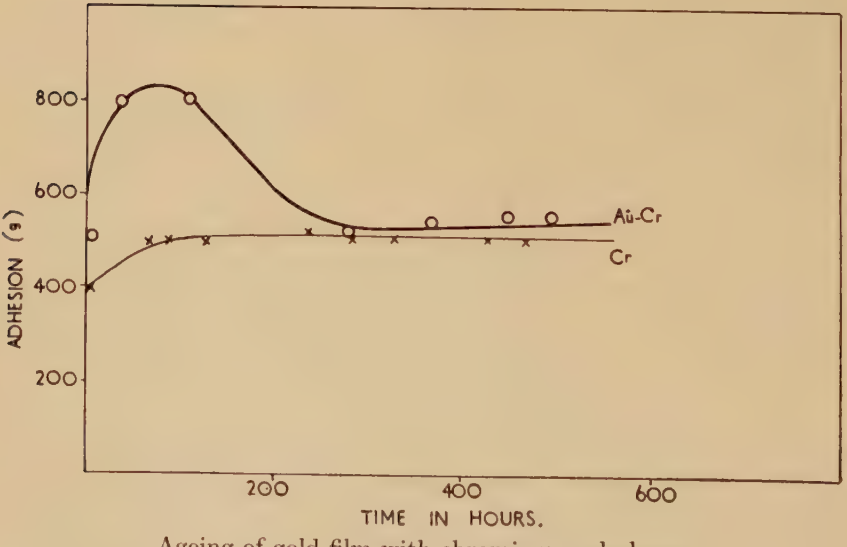
Further investigation is obviously necessary but the results obtained so far indicate a certain degree of correlation between the general nature of

Fig. 33



Ageing of copper film with chromium underlayer.
Adhesion/time at room temperature.

Fig. 34



Ageing of gold film with chromium underlayer.
Adhesion/time at room temperature.

the phase diagram and the ageing curves obtained. The intermediate layers formed between aluminium and chromium and between aluminium and nickel were so thin that some difficulty was experienced in obtaining confirmation by electron diffraction. Success was obtained in the first case by reducing the thicknesses of the individual aluminium and chromium films so as to reduce the intensities of the pure metal patterns relative to the pattern given by the intermediate layer and in the second case by using alternate layers in a multi-layer stack to increase the effective sensitivity of the electron diffraction technique. Electron diffraction methods were not used in the other cases. In the cases of copper–chromium and gold–chromium the intermediate layers must have been considerably thinner and therefore presumably more difficult to detect by electron diffraction. The fact that hardening effects were still detected in the ageing curves gives an indication of the sensitivity of this method for investigating inter-diffusion effects.

§ 8. Diffusion Measurements

8.1. *General*

Measurement of diffusion coefficients involves location of the diffusing atoms or particles, whereas practically all the methods which have been described so far only give information on structural changes and do not even give reliable indications of the thicknesses of any intermediate layers which may be formed. The methods which are used with bulk metal diffusion couples are generally inapplicable to vacuum-deposited films since any method of sectioning is virtually impossible and the quantity of material available is inadequate for normal chemical analysis. The use of radioactive tracer methods is precluded since the absorption of the films is negligible even for particles of low energy such as weak β rays. Consequently, no changes in emission would be observed as radioactive particles diffused through the films. Apart from DuMond and Youtz (1940) who used x-rays in an indirect manner (see § 5) the only measurements of diffusion in thin films have used optical techniques.

8.2. *Diffusion Through Films*

The diffusion of copper in thin films of zinc was investigated by Coleman and Yeagley (1943) using two-layer films deposited on microscope slides with the copper against the glass. Films of about 2000 Å thickness were used and after deposition the specimens were removed and placed in a reflectometer so that changes in the reflectivity of the upper zinc surface could be measured. An electric iron was used as a thermostatically controlled heater against the back surface of the specimen to maintain the temperature constant to $\pm 1\,^{\circ}$C during diffusion, and the output current of a photocell was recorded continuously and taken as a measure of reflectivity, R.

Assuming the diffusion equation

$$D = D_0 \exp(-Q/RT)$$

as giving the variation of the diffusion coefficient D with temperature, the value of Q, the activation energy can be obtained by plotting $\log D$ against $1/T$. To obtain Q without repeated calculations of D or D_0 a quantity t_∞ was defined as the time at which $dR/dt = a$. The value of the constant 'a' was taken as 0·00291 since this would specify a point at which the alloy was almost homogeneous (the slope of the reaction rate curve being then 10′). t_∞ must be proportional to the thickness x of the zinc and to the quantity m of metal which has to diffuse across the interface to produce homogeneity,

$$\text{i.e.} \quad t_\infty \propto xm \quad \text{or} \quad t_\infty = (1/K)xm$$

where K is a constant, depending on temperature in the same manner as D. Coleman and Yeagley therefore obtained values of Q by plotting the logarithm of $K = xm/t_\infty$ as a function of $1/T$.

They gave only one curve for the diffusion of copper into zinc and no values of D or Q were given but results were given for similar experiments with gold and lead where diffusion of the gold into the upper layer of lead was measured and a value of $Q = 13\,700$ cal/mole was obtained. This is in good agreement with the values of 14 kcal/mole (Seith and Etzold 1935) and 13·6 kcal/mole (Mehl 1936) obtained for bulk material.

It was later stated (Coleman and Yeagley 1944) that the values of diffusion coefficients for copper–zinc were several orders of magnitude higher than for earlier determinations on bulk metal and this was attributed to anisotropy of diffusion and the existence of a preferred orientation in the deposited films (Burr *et al.* 1944).

The interdiffusion of gold and lead was also considered by Schopper (1955) who used thin film methods to measure the diffusion rates for lead into gold. Double-layer films were produced by evaporation, the gold being deposited first. Reflectivity measurements were again used to trace the diffusing atoms but measurements were made at the metal glass interface rather than at the free surface. This eliminated any possibility of surface contamination or reflectivity changes due to causes other than diffusion. The free side of the films was used to measure the absolute change of phase on reflection by the three-slit method (Fleischmann and Schopper 1951) and hence to obtain the film thicknesses. Determination of D from the reflectivity measurements was discussed at length and preliminary experiments were carried out to determine the relationship between reflectivity and alloy concentration. It was found that consistent results were obtained only when $d_{\mathrm{Pb}} \geq 2d_{\mathrm{Au}}$ and this condition was maintained throughout the experiments. The results obtained over a temperature range from 18°C to 100°C were consistent and gave values of $D_0 = 0{\cdot}016$ cm^2/sec and an activation energy $E = 17$ kcal/mole for the diffusion of lead through gold. This activation energy is somewhat greater than the values of 13·6–14·0 kcal/mole obtained for the diffusion of gold

in lead but this is reasonable since lattice changes in gold require greater energies than in lead. This is obvious from the great differences in melting-point. The same reasons might be advanced to account for the lower value of D_0 as compared with $D_0 = 0{\cdot}35\,\text{cm}^2/\text{sec}$ for diffusion of gold into bulk lead (Jost 1952).

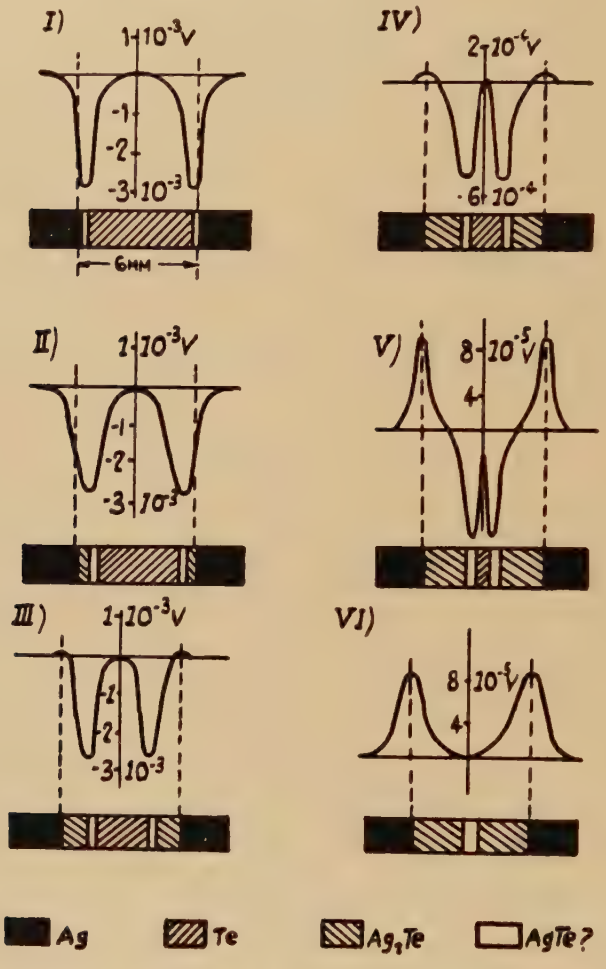
Previous work on bulk metal (Seith and Keil 1933, Seith and Etzhold 1934, 1935) had indicated that lead could accept up to 0·08 at% gold in interstitial positions in the lead lattice but Schopper's results suggested the formation of intermetallic compounds and indeed $AuPb_2$ was identified by x-ray diffraction. It was argued that grain boundary diffusion was impossible since there were no appreciable volume changes during diffusion (thickness measurements showed no change to ± 50 Å). This led to the suggestion that a sharply defined layer of compound might be formed between the gold and the lead, but this hypothesis did not agree with the experimental observations. The conclusion finally reached was that diffusion must occur by a diffusion of lead atoms into vacant sites in the gold lattice and that this might be assisted by the migration of gold atoms into interstitial positions in the lead. No sharply bounded intermediate layer was formed but instead a continuous concentration gradient was established.

8.3. *Diffusion Along Films*

The possibility of investigating diffusion along a film parallel to the surface has been demonstrated by Monch and his colleagues (1954). The work apparently started with attempts to produce radiation detectors (Monch 1952, 1953, Mohr 1953). A film of tellurium was evaporated so as to form a bridge between two thick silver electrodes which had themselves been deposited on a collodion film by evaporation. Two thermojunctions were thus produced at opposite ends of the bridge. On ageing, a diffusion of silver into the tellurium could be observed. The pure tellurium appeared greyish-brown while the diffusion zone could be observed as a yellowish-brown band of Ag_2Te, spreading outwards from the silver. At the same time there was a displacement of the thermojunctions which followed the advancing front of the diffusion zone while new thermojunctions producing voltages in the opposite sense started to develop in the original positions at the edge of the silver electrodes. When the diffusing junctions met in the centre of the tellurium bridge they disappeared, leaving a film of Ag_2Te bridging the silver electrodes and two thermojunctions in the opposite sense to the original junctions. This development is shown diagrammatically in fig. 35. The ageing could be eliminated or at least minimized by evaporating on to the tellurium a further layer of silver, sufficient to saturate and transform it to the compound. Mohr (1952, 1954 a, b) tried to measure the coefficient of diffusion of the silver by determining the width of the diffusion zone as a function of time. A variation with the thickness of tellurium was shown to be due to a folding or crinkling of thicker films which became partially

detached from the underlying glass surface. This folding was further shown to be due to a volumetric expansion of the tellurium lattice as the silver diffused in, resulting in a purely lateral expansion for thin films and a combined lateral and longitudinal expansion for thick films. Taking these volume changes into account, consistent results were obtained.

Fig. 35



Successive stages in the ageing of a thermo-element formed of a tellurium film bridging two silver electrodes. The movements of both the diffusion front and the e.m.f. at the thermojunctions are shown (after Monch).

Measurements over a range of temperatures gave $D = D_0 \exp(-B/T)$ $D_0 = 5 \times 10^7\,\mathrm{cm^2/day}$ and $B = 6910\,\mathrm{deg^{-1}}$.

Films were also examined by electron diffraction (Zorll 1954) and the formation of Ag_2Te in the diffusion zone was confirmed. The pure tellurium usually produced the rings of the hexagonal modification although an

amorphous modification was observed in some cases. A diffraction ring pattern obtained very close to the edge of the silver suggested another compound richer in silver but this could not be identified, and there was no indication of such a compound in the phase diagram.

Similar experiments were carried out using selenium instead of tellurium (Kienel 1955, Zorll 1955a) but the films were deposited on substrates at liquid air temperature because of the relative volatility of the selenium. Measurements of diffusion rate were again made by measuring the width of the diffusion zone but only approximate results were obtained since volume changes were not fully investigated. Neglecting the crinkling of the film, a slow decrease of the diffusion constant with time was observed which was attributed to a variation of diffusion rate with thickness. The results were in general agreement with the earlier results for silver and tellurium. Electron diffraction showed the presence in the diffusion zone of a low symmetry pseudo-cubic structure, closely related to a b.c.c. high temperature modification. In some cases this changed after a time to a rhombic form with the (001) axis normal to the substrate but only where evaporated silver had lain previously. Gold–tellurium and gold–selenium were also investigated by electron diffraction only (Zorll 1955b) but no compound formation occurred and no diffusion measurements were made.

A similar method has been used to study the ionic conductivities of thin evaporated films of lead chloride (Perrot and Sator 1952). The films formed a bridge between two metallic electrodes between which a high potential was applied. One electrode was attacked by chlorine as it was released while metal was deposited at the other and boundary movements were observed.

In the case of diffusion through films the method is restricted to metal pairs where there is a marked difference in reflectivity but this can often be achieved by choosing light of a suitable wavelength. Measurements of diffusion along films appear to be restricted at present to cases where a coloured intermetallic compound is formed since the moving boundary is otherwise difficult to identify. The method is also easier to use where the rate of diffusion is relatively high but under these conditions it is doubtful whether it really has any advantage over the use of conventional diffusion couples made from bulk metal. If the distance of diffusion is great enough to be readily visible then ordinary sectioning methods can be used.

§ 9. Conclusions

It is obvious from this survey of the applications of thin film methods to metallurgy that investigations of reactions in thin metallic films have been scattered over a wide field and in very few cases has a complete investigation of a given alloy been attempted. Electron diffraction has been used as the main or sole technique in many instances and this is very natural since the uses of vacuum-deposited films have developed concurrently with electron diffraction technique. The x-ray investigations

which have been described (§ 5) show that, except for the novel method of DuMond and Youtz (1940) x-ray technique has been stretched to the limit even with films which are some thousands of angstroms thick and thinner films are completely beyond its scope. Electron diffraction is therefore the obvious method of obtaining evidence on the crystalline structure of material in the form of thin films.

Much work has been done on age-hardening of the Al–Cu and Ag–Al alloys and there is no doubt that useful results have been obtained by thin film methods. The reactions in thin films do not, however, proceed at the same rate or necessarily in the same manner as in bulk material. Attention was drawn to this point by Winkelmann (1956 b, c) and for these well-known alloys a direct correlation between hardness measurements on thin films and the observed structural changes has not yet been established. It would be interesting to see whether the structural changes observed in thin films by electron diffraction can be directly related to observable stages of hardening.

The observation of ageing effects as resistivity changes or age-hardening or otherwise appears to offer most scope for future development. Ageing occurs even in alloy films prepared by simultaneous evaporation (Belser 1954, Michel 1956) although interpretation, or application of the theory of diffusion, is possibly easier for films prepared by successive evaporation. These methods of attacking alloying problems seem more sensitive to changes at the interface than electron diffraction but should be supplemented by structural information wherever possible. The multi-layer technique can be used to increase the effective sensitivity of electron diffraction for this purpose although for extremely thin layers there is a tendency to obtain amorphous patterns rather than well-defined rings. In the investigation of ageing effects, these later methods have developed independently but it is to be expected that in future work they will be used in conjunction and that attempts will be made to establish relationships between the results.

Considerable progress has already been made in interpreting resistivity changes but the results so far obtained are still not sufficiently comprehensive to alloy general conclusions to be drawn. This can be seen even in the curves of fig. 15 for simultaneously evaporated films. Establishing a consistent pattern of resistive behaviour for alloy films would be a major advance. More information on the electrical resistivities of intermetallic compounds would be valuable for this purpose. In this context it is worth considering whether thermal cycles represent the best method of approach. In a case such as this where time and temperature form two independent variables, can the sharp resistance increases observed by both Boettcher and Belser be regarded as purely thermal effects or are they are result of the films trying to attain an equlibrium state? In other words, are these temperatures critical or would the same changes occur at lower temperatures if sufficient time were allowed? The possibility of a time lag between the film reaching a critical temperature, and the corresponding

transformation being completed and producing a resistivity change, has already been mentioned as a possible explanation of differences between the results of the two workers. Under these circumstances it would appear advisable to observe ageing effects at a series of temperatures, keeping the temperature constant during ageing, in an attempt to separate the effects of the two variables.

The use of adhesion measurements to obtain information on hardening effects in thin films was an unexpected development which opened up a new field. The results obtained so far have shown some general trends and there are indications of some relationships between the shapes of the ageing curves and the nature of the phase diagram or the type of alloy, but more results are still required. No work has yet been done on metals which are perfectly miscible although some degree of solution hardening (Parker and Hazlett 1954) is to be expected. Since this is not a direct method of measuring hardness and the measurements can be affected by other factors, considerable care is necessary in interpreting results. In all cases measurements have been made on metal films which partially overlapped so that results could be obtained for each of the pure metal films as well as the two layer film and comparisons could be made. The results obtained when using chromium as an underlayer have been discussed elsewhere and show that structural factors must be taken into account when present. This often means using other methods such as electron microscopy or optical methods to investigate the structures of the films used.

A tendency towards work of a more quantitative nature is shown by the attempts to measure diffusion coefficients in thin films. Existing knowledge of the structure of thin films indicates that metal films are usually microcrystalline and that the crystallites are generally randomly oriented. This in turn implies a high concentration of grain boundaries and for diffusion at relatively low temperatures grain boundary diffusion should have a pronounced effect. It is unfortunate that a comparison can be made between thin film results and bulk metal results only for the gold-lead system and the results obtained here allow no definite conclusions to be drawn as to the existence or otherwise of grain boundary diffusion. The results obtained by Monch and his colleagues are interesting but no other figures appear to be available for comparison.

§ 10. Summary

10.1. *Binary Systems*

Ag–Al. Electron diffraction investigations of this alloy system are discussed in § 4.4. It has also been the subject of resistance measurements by Boettcher and Belser (§ 6).

Ag–Au. These metals have been investigated by Belser by resistance methods using films of gold on copper, copper on gold and films prepared by simultaneous evaporation. X-ray diffraction and metallographic examination were also used. No compounds were identified.

Ag–Cr. The only investigation by Belser used a film of chromium on top of silver. Adhesion measurements showed no compound formation (Weaver and Hill 1959 b).

Ag–Cu. Films of silver were evaporated on to polished and etched copper surfaces by Finch *et al.* (1934) and Cramer (1939). The former observed a slow diffusion into the polished surface which was not confirmed by the latter. No changes occurred on etched surfaces.

Ag–Hg. Pinsker and Tatarinova (1941) showed amalgamation effects in silver films due to mercury vapour from the diffusion pumps. Tetragonal f.c. structure shown, in agreement with Aylmer *et al.* (1936).

Ag–Mg. Michel (1956) showed that simultaneous evaporation gave all alloy phases except γ, but no compounds were found by successive evaporation. See Goldsztaub and Michel (1951).

Ag–Ni. Belser (1954) measured resistances of films prepared by successive deposition in both orders and also by simultaneous evaporation. No alloying was observed.

Ag–Rh. Resistances of films prepared by electroplating rhodium on top of sputtered silver were measured by Belser (1954).

Ag–Se. Diffusion has been investigated (§ 8).

Ag–Su. Michel (1956) showed alloy formation in films prepared by both successive and simultaneous evaporation.

Ag–Te. Diffusion in this system is discussed in § 8.

Ag–Zn. Films have been prepared by successive evaporation and by simultaneous evaporation (Michel 1956). Intermediate phases formed in both cases.

Al–Au. Belser (1954) prepared films by evaporation in the order Al–Au, Au–Al and simultaneously. Effect of aluminium oxide was shown as for Ag–Al. Observation of colour changes gave alloying temperatures of 480–505°c and 190°c for Al–Au and Au–Al respectively. Results of electron microscopy and electron diffraction were given. Three intermediate phases were observed but only one was definitely identified as β' phase Au_4Al.

Al–Co. Age-hardening results (Weaver and Hill 1959 a). See also § 7.

Al–Cr. Original example of age-hardening effects (Weaver and Hill 1958). See also § 7.

Al–Cu. This system is fully discussed in § 4.3. Belser (1954) studied resistance changes. Observation of colour changes gave alloying temperatures of 495°c and 260–335°c for the orders Al–Cu and Cu–Al respectively, due to oxide formation on the aluminium. γ' phase formation was shown by x-rays (Belser 1954). Practical information on evaporation of Al–Cu alloys is given by Holland (1956).

Al–Fe. See § 7.

Al–In. Belser (1954) measured resistances of films prepared in the order Al–In and In–A X-ray diffraction showed presence of In_2O_3.

Al–Mg. Investigated by Boettcher (1950). See § 6.

Al–Mn. See § 7.

Al–Ni. Age-hardening results (Weaver and Hill 1959a). See also § 7.

Al–Pb. See § 7.

Al–Pd. These metals were studied by Belser. Resistance measurements were made for films in the order Al–Pd and Pd–Al. Visual observation of a film of aluminium on palladium showed alloying as the formation of a pink film at 260°C. X-rays showed formation of AlPd and Al_3Pd_2.

Al–Zn. Belser examined films deposited in order Al–Zn and Zn–Al but zinc sublimed at the temperatures obtained in the infra-red oven.

Al–Zr. Specimens were prepared by successive evaporation, examined metallographically, and resistance measurements were made by Belser (1954).

As–Sb. Richter (1943) showed by electron diffraction that complete evaporation of an alloy containing equal proportions gave sharp rings of an alloy with lattice parameter between the parameters of the pure components. Successive evaporation showed no alloying but only superposition of the pure metal patterns.

Au–Cd. Harris and Siegel (1948) showed that an alloy 50/50 at % could vaporize unchanged using their 'flash' technique. The structure of the deposited film was not checked.

Au–Cu. Examinations of this system by electron diffraction are discussed in § 4.2. Films of gold were evaporated on to polished and etched copper surfaces by Cramer (1939). No alloy formation was detected by electron diffraction even on heating to temperatures between 150°C and 500°C.

Au–In. Belser (1954) examined gold on indium and films evaporated simultaneously. Alloying occurred at room temperature, as shown by colour change. Simultaneously evaporated films showed a marked dendritic structure on heating and the resistance rose sharply (fig. 15). $AuIn_2$ was identified by x-rays in both types of film.

Au–Ni. Belser (1954) prepared films by evaporating nickel on to an evaporated gold film and also by electroplating nickel on to both evaporated and sputtered gold films. Alloying started at about 150°C. There was a marked resistance rise at about 350°C, and alloying appeared to be complete at 510°C, as judged by observation of colour changes but another resistance rise occurred at 600°C. However, no compound formation was traced by x-ray diffraction.

Au–Pb. Diffusion measurements are covered in § 8. Finch *et al.* (1934) evaporated lead films onto polished and etched gold surface and showed by electron diffraction that diffusion seemed to occur rapidly into the Beilby layer but not into the etched surface.

Au–Pd. Using electron diffraction Lafourcade (1954) showed a separation of components with the alloys used for shadow-casting in electron microscopy. Gold vaporized preferentially, producing films with a concentration gradient. Mixed crystals were formed in all proportions.

Au–Pt. Gold was sputtered on to a sputtered platinum film (Belser

1957) and the resistance changes during temperature cycles are shown in fig. 13.

Au–Rh. Rhodium was electroplated on to a sputtered gold film (Belser 1954) but resistance measurements showed no alloying up to 600°C.

Au–Se. Zorll (1955 a, b) used films prepared by successive evaporation. No alloying could be detected by electron diffraction.

Au–Sn. Films of tin were evaporated on to polished and etched gold surfaces (Finch *et al.* 1934). The electron diffraction pattern of the tin vanished after half-an-hour on the polished surface but remained unchanged after 12 hours on the etched surface.

Au–Te. Films were prepared by successive evaporation (Zorll 1955 a, b). No alloying could be detected by electron diffraction. Rings of HgTe were observed due to back diffusion from the mercury pump used.

Au–Zn. Zinc films were evaporated on to polished and etched gold surfaces (Finch *et al.* 1934). Electron diffraction pattern of film on polished surface disappeared within 2 hours whereas film on etched surface showed no change after 15 hours.

Be–Cu. An alloy containing 58% Be was completely evaporated but the electron diffraction pattern showed an alloy containing less beryllium. Structural changes and precipitation occurred on heating and the original alloy was reformed (Vizwanathan 1956).

Bi–Pb. The eutectic alloy 56/44 at % Bi/Pb was evaporated onto collodion and examined by electron diffraction. Melting the film at 125°C. and then cooling produced a mixture of lead crystals containing bismuth and almost pure bismuth (Richter 1943).

Bi–Sb. Resistance measurements were made using films of bismuth upon antimony (Belser 1954). No further details are available. Metals are completely miscible (Hansen 1958).

Bi–Sn. Evaporation of the eutectic alloy on to a rock-salt face (Richter 1943) produced films which gave electron diffraction patterns only of the pure metals. Amorphous rings were produced on melting the films at 139°C.

Cr–Cu. Films of copper evaporated on chromium films showed some age-hardening effects (Weaver and Hill 1959 b). See § 7.

Cr–Ni. Evaporation of various alloys is discussed by Holland (1956). Films of nickel were evaporated on to chromium surface by Cramer (1939). Considerable oxidation was observed.

Cu–Ni. Nickel films were deposited on top of evaporated copper films by evaporation and by electroplating (Belser 1954). Alloying was observed in the range 475–555°C.

Cu–Pb. Lead films were evaporated on to polished copper surfaces (Finch *et al.* 1934). A faint pattern was obtained by electron diffraction but faded rapidly.

Cu–Sb. Boettcher and Thun (1954) showed structural changes occurring in a film obtained by evaporation of a 65/35 Cu/Sb alloy. Electron diffraction patterns were recorded continuously. See § 4.1.

Cu–Sn. Alloy films were produced by successive and by simultaneous evaporation (Efendiev 1948). Vaporization of various alloy compositions is discussed by Holland (1956). Tin films were evaporated onto polished and etched copper surfaces and examined continuously by electron diffraction (Finch *et al.* 1934). On polished copper the first layer of tin disappeared within five minutes and a second layer gave a sharp pattern which faded but still remained after half-an-hour. On etched copper the tin pattern remained unchanged after 12 hours.

Cu–Zn. Diffusion measurements were made by Coleman and Yeagley (1943), see § 8, and x-ray studies by Burr *et al.* (1944), see § 5. Harris and Siegel (1948) evaporated alloys unchanged by using a 'flash' technique. Cramer (1939) evaporated zinc on to polished and etched copper surfaces. The electron diffraction patterns obtained showed considerable oxidation at 300°C and a marked diffusion of copper into the zinc oxide lattice, transforming it to Cu_2O. The transformation was almost complete at 450°C.

Fe–In. Films were prepared by Belser (1954) evaporating simultaneously as well as in normal and inverse orders. Indium on iron showed strong aggregation at 175°C. This could be due to the presence of an oxide film on the iron or to a lack of any alloying tendency. A marked increase of resistance was observed for the double layers at the aggregation point, but the simultaneously evaporated films showed only an annealing effect. No suggestion of alloy formation was observed at any stage, and x-ray diffraction showed only the pure components.

Fe–Ni. Nickel films were evaporated on to iron surfaces by Cramer (1939) and oxidation was observed.

Fe–Sn. Tin films were evaporated on to polished mild steel surfaces and observed by electron diffraction (Finch *et al.* 1934). The pattern of the tin faded over a period of 25 min to a weaker but permanent pattern.

Fe–Zn. Zinc films were evaporated on to both polished and etched mild steel surfaces by Finch *et al.* (1934). On the polished surfaces the pattern of the first layer of zinc disappeared within three minutes and a second layer gave a pattern which weakened considerably within five minutes but still remained after $1\frac{1}{4}$ hours. Zinc on etched steel gave a pattern which remained unchanged after 2 hours.

Ga–In. Films were prepared by complete evaporation of a 67/33 at % Ga/In alloy and by simultaneous evaporation of the pure components (Richter 1943). A continuous variation of lattice constants with composition was observed by electron diffraction and the metals appeared to be miscible in all proportions without any compound formation.

Ga–Sb. Films prepared by successive evaporation of antimony after gallium gave the electron diffraction patterns of the pure components even after long annealing at 150°C but at 200°C sharp rings of GaSb compound appeared (Richter 1943). Gallium evaporated after antimony or simultaneous evaporation produced the compound GaSb immediately.

In–Sb. The work on this system is reviewed in § 4.5.

Ir–Pt. Iridium was sputtered on top of sputtered platinum by Belser (1957). The results of thermal cycles are shown in fig. 12.

Ni–Pt. Films were prepared by Belser (1957) by successive deposition.

Ni–Sn. Alloys of composition 35/65 Ni/Sn have been evaporated by 'flash' technique (Holland 1956).

Pb–Sn. The eutectic alloy (26/74 at % Pb/Sn) was vaporized and condensed on collodion and rock-salt surfaces (Richter 1943). Cooling below the melting point of 183°C gave the patterns of almost pure tin and tin-rich lead crystals. Films of tin were evaporated on to a polished lead surface (Finch *et al.* 1934) but no ring pattern of tin could be obtained by electron diffraction although seven successive layers were deposited. This suggests extremely rapid diffusion of the tin into the polish layer of the lead surface.

Pb–Zn. Zinc was deposited on a polished lead surface and examined continuously by electron diffraction (Finch *et al.* 1934). The pattern of the zinc disappeared in $2\frac{1}{2}$ min.

Sn–Zn. A film of tin was deposited on polished zinc and examined continuously by electron diffraction (Finch *et al.* 1934). The pattern had not changed after 1 hour. This could be due to an oxide film on the zinc.

10.2. *Other Systems*

The evaporation of various commercial alloys (Al–Fe–Cu, Al–Cu–Mg, Cr–Fe–Ni) has been discussed by Holland 1956. Rose-metal (Sn–Bi–Pb) alloy was vaporized by Richter (1943) to produce films of slightly different composition having a crystalline or microcrystalline structure and a slightly higher melting-point than the original alloy. Lipowitz-metal (Sn–Bi–Pb–Cd) was also vaporized by Richter (1943). The original alloy melted at 60°C, indicating a marked change of composition.

Acknowledgments

One of us (R.M.H.) wishes to thank the Caird Trust for a grant to permit some of the investigations described here and Dr. C. F. Bruce (C.S.I.R.O.) for the interest which he has shown.

References

Appleyard, E. T. S., 1937, *Proc. phys. Soc. Lond.*, **49**, 118.

Aylmer, A. E., Finch, G. I., and Fordham, S., 1936, *Trans. Faraday Soc.*, **32**, 864.

Barrer, R. M., 1951, *Diffusion in and through Solids* (Cambridge : University Press), p. 340.

Bauer, G., 1934, *Ann. Phys., Lpz.*, **19**, 434.

Belbeoch, B., and Guinier, A., 1954, *Comptes Rendus*, **238**, 1003.

Belser, R. B., 1954, Report No. 7. Project No. 163–176. U.S. Army Signal Corps. Contract DA–36–039–SC–42453 ; 1957, *J. appl. Phys.*, **28**, 109.

Belser, R. B., and Hicklin, W. H., 1957, Wright Air Development Centre Technical Report 57–660, Nov. 1957.

Benjamin, P., and Weaver, C., 1959, *Proc. roy. Soc.* (in the press).
Bethe, H. A., 1935, *Proc. roy. Soc.* A, **150,** 552.
Blanc-Lapierre, A., and Perrot, M., 1954, *Memorials des Sciences Physiques* (Paris : Gauthier-Villars), p. 57.
Boettcher, A., 1950, *Z. angew. Phys.*, **2,** 193, 249, 340 ; 1953, *Aus. Forschung und Produktion*, p. 16.
Boettcher, A., and Hass, G., 1950, *Optik*, **6,** 299.
Boettcher, A., and Thun, R., 1952, *Phys. Vorhand*, **3,** 115 ; 1954, *Optik*, **11,** 22.
Bragg, W. L., and Williams, E. G., 1934, *Proc. roy. Soc.* A, **145,** 699.
Broniewski, W., 1912, *Ann. Chim.* (*Phys.*), **25,** 80.
Bulnow, N., and Komar, A. J., 1939, *J. exp. theor. Phys. SSSR*, **9,** 1135.
Bungardt, W., 1937, *Luft-Forschung*, **14,** 208.
Burch, C. R., 1928, *Nature, Lond.*, **122,** 729.
Burr, A. A., Coleman, H. S., and Davey, W. P., 1944, *Trans. Amer. Soc. Metals*, **33,** 73.
Coleman, H. S., and Yeagley, H. L., 1943, *Trans. Amer. Soc. Metals*, **31,** 105 ; 1944 *Phys. Rev.*, **65,** 56.
Cottrell, A. H., 1955, *Theoretical Structural Metallurgy* (London : Arnold).
Cowley, J. M., 1950, *Phys. Rev.*, **77,** 669.
Cramer, H., 1939, *Ann. Phys., Lpz.*, **34,** 237.
DuMond, J., and Youtz, J. P., 1940, *J. appl. Phys.*, **11,** 357.
Dushman, S., 1949, *Scientific Foundations of Vacuum Technique* (New York : Wiley).
Efendiev, G. A., 1948, *J. tech. Phys., Moscow*, **18,** 1159.
Eisenhutt, O., and Kaupp, E., 1931, *Z. Elektrochem.*, **37,** 466.
Finch, G. L., Quarrel, A. G., and Roebuck, J. S., 1934, *Proc. roy. Soc.* A, **145,** 676.
Fink, W. L., and Smith, D. W., 1938, *Trans. Amer. Inst. min.* (*metall.*) *Engrs*, **128,** 223 ; 1940, *Ibid.*, **137,** 95.
Fleischmann, and Schopper, H., 1951, *Z. Phys.*, **130,** 304.
Gayler, M. L. V., 1937, *J. Inst. Met.*, **60,** 249 ; 1947 a, *Ibid.*, **73,** 581 ; 1947 b, *Symposium on Internal Stresses in Metals and Alloys* (Inst. of Metals), p. 255.
Germer, L. H., Haworth, F. E., and Lander, J. J., 1942, *Phys. Rev.*, **61,** 614.
Goldsztaub, S., and Michel, P., 1951, *Comptes Rendus*, **232,** 1843.
Göttsche, H., 1953, *Z. Phys.*, **134,** 504.
Götzberger, A., 1955, *Z. Phys.*, **142,** 739.
Hansen, M., 1928, *Naturwissenschaften*, **16,** 417 ; 1958, *Constitution of Binary Alloys* (New York : McGraw-Hill).
Harding, S. W., Smith, F. R., and Davey, W. P., 1942, *Phys. Rev.*, **62,** 296.
Harris, L., and Siegel, B. M., 1948, *J. appl. Phys.*, **19,** 739.
Heavens, O. S., 1950, *J. Phys. Radium*, **11,** 355.
Hill, R. M., and Weaver, C., 1958 a, *Trans. Faraday Soc.*, **54,** 1140 ; 1958 b, *Ibid.*, **54,** 1464.
Hirabayashi, 1951, *J. phys. Soc., Japan*, **6,** 129.
Hirano, K., 1953, *J. phys. Soc., Japan*, **8,** 603.
Hirano, K. *et al.*, 1955 a, *J. phys. Soc., Japan*, **10,** 23 ; 1955 b, *Ibid.*, **10,** 454.
Hoffman, R. W., and Storey, H. S., 1956, *J. appl. Phys.*, **19,** 739.
Holland, L., 1956, *Vacuum Deposition of Thin Films* (London : Chapman & Hall).
Jones, E. W., and Sykes, C., 1938, *Proc. roy. Soc.* A, **166,** 376.
Jost, W., 1932, *Z. phys. Chem.* B, **16,** 123 ; 1933, *Ibid.*, B, **21,** 158 ; 1952, *Diffusion* (New York : Academic Press), p. 70.
Kawakami, M., 1933, *Kinzoku no kenkyu*, **10,** 532.

Kienel, G., 1955, *Ann. Phys., Lpz.*, **6**, 1.
Kirkwood, I. G., 1938, *J. chem. Phys.*, **6**, 70.
Konozenko, I. D., and Mikhnovsky, S. D., 1956, *Ukrayin. fiz. J.*, p. 151.
Kurov, G. A., and Pinsker, Z. G., 1958, *J. tech. Phys., Moscow*, **28**, 29.
Lafourcade, L., 1954, Theses, University of Toulouse.
Levinstein, H., 1949, *J. appl. Phys.*, **20**, 306.
McLauchlan, T. A., Sennett, R. S., and Scott, G. D., 1950, *Canad. J. Res.* A, **28**, 530.
Mehl, R. F., 1936, *Trans. Amer. Inst. min. (metall.) Engrs*, **122**, 11.
Mehl, R. F., and Jetter, L. K., 1939, *Age-hardening of Metals* (Symposium of Amer. Soc. Metals), p. 342.
Michel, P., 1952, *Comptes Rendus*, **235**, 377 ; 1956, *Theses*, University of Strasbourg.
Mohr, T., 1952, *Wiss. Z.*, Martin-Luther Univ., Halle-Wittenberg, **2**, 601; 1953, *Ann. Phys., Lpz.*, **12**, 175; 1954 a, *Ibid.*, **14**, 367; 1954 b, *Ibid.*, **14**, 377.
Monch, G. C., 1952, *Wiss. Z.*, Martin-Luther Univ., Halle-Wittenberg, **2**, 599 ; 1953, *Ann. Phys. Lpz.*, **12**, 161 ; 1954, *Ibid.*, **14**, 363.
Mostovetch, N., and Vodar, B., 1951, *Semiconducting Materials* (London : Butterworths Scientific Pubs.), p. 260.
Ogawa, S. S., and Watanabe, D., 1952, *J. phys. Soc., Japan*, **7**, 36.
Parker, E. R., and Hazlett, T. H., 1954, *Relation of Properties to Microstructures* (Cleveland, Ohio : Amer. Soc. Metals), p. 30.
Peierls, R., 1936, *Proc. roy. Soc.* A, **154**, 207.
Perrot, M., and Sator, A., 1952, *Comptes Rendus*, **234**, 1883.
Pickard, R. G., and Duffendack, O. S., 1943, *J. appl. Phys.*, **14**, 291.
Pinsker, Z., and Tatarinova, L., 1941, *Acta phys. chim., URSS.*, **14**, 193.
Presnov, V. A., and Synorov., V. F., 1957, *Soviet Physics—Technical Physics*, **2**, 104 (Trans. from *J. tech. Phys., Moscow*, **27**, 123, 1957).
Pringsheim, P., and Pohl, R., 1912, *Ver. dtsch. phys. Ges.*, **15**, 506.
Raether, H., 1950, *Comptes Rendus*, **231**, 653 ; 1951, *Acta Cryst.*, **4**, 70.
Richter, H., 1943, *Phys. Z.*, **44**, 406.
Schopper, H., 1955, *Z. Phys.*, **143**, 93.
Seith, W., and Etzhold, H., 1934, *Z. Elektrochem.*, **40**, 829 ; 1935, *Ibid.*, **41**, 122.
Seith, W., and Keil, W., 1933, *Z. phys. Chem.* B, **22**, 350.
Semiltov, S. A., Rozseval, 1957, *Kristallografiya*, **2**, 287.
Smith, G. C., 1949, *Progress in Metal Physics* (London : Butterworths Scientific Pubs.), **1**, p. 163.
Smithells, C. J., 1949, *Metals Reference Book* (London: Butterworths Scientific Pubs.).
Strong, J., 1935, *Rev. sci. Instrum.*, **6**, 97 ; 1936, *J. opt. Soc. Amer.*, **26**, 73.
Sykes, C., and Evans, H., 1936, *J. Inst. Met.*, **58**, 255.
Sykes, C., and Jones, E. W., 1936, *Proc. roy. Soc.* A, **157**, 213.
Takahashi, N., and Fert, C., 1953, *Comptes Rendus*, **237**, 1664.
Thomas, G., and Nutting, J., 1956, *Symposium on the Mechanism of Phase transformations in Metals* (London : Inst. Metals), p. 57.
Thomas, G., and Whelan, M. J., 1958, *Precipitation in an Al–4% Cu alloy.* Conf. on Interfacial Phenomena, Cavendish Laboratory, Cambridge.
Tolansky, S., 1955, *An introduction to Interferometry* (London : Longmans, Green), p. 169.
Trillat, J. J., 1954, *Cah. Phys.*, **49**, 44.
Trillat, J. J., and Takahashi, N., 1952, *Comptes Rendus*, **235**, 1306 ; 1953, *Ibid.*, **236**, 790.
Trillat, J. J., Terao, N., Tertian, L., and Gervais, H., 1956, *J. phys. Soc., Japan*, **11**, 406.
Viswanathan, A., 1956, *Comptes Rendus*, **242**, 1586.

Walker, C. B., and Guinier, A., 1953, *Acta Met.*, **1,** 568.
Watanabe, D., 1956, *Comptes Rendus*, **242,** 1586.
Weaver, C., 1958, *Proc. 1st Int. Conf. on Vacuum Techniques, Namur* (London : Pergamon Press).
Weaver, C., and Hill, R. M., 1958, *Phil. Mag.*, **3,** 1402 ; 1959 a, *Ibid.*, **4,** 253 ; 1959 b, *Ibid.* (in the press).
Winkelmann, A., and Raether, H., 1953, *Naturwissenschaften*, **20,** 526.
Winkelmann, A., 1955 a, *Z. angew. Phys.*, **7,** 7 ; 1955 b, *Ibid.*, **7,** 296 ; 1956 a, *Ibid.*, **8,** 218 ; 1956 b, *Z. Metallk.*, **47,** 621 ; 1956 c, *Ibid.*, **47,** 627.
Yamaguchi, S., 1956, *Z. angew. Phys.*, **8,** 221.
Zorll, U., 1954, *Ann. Phys., Lpz.*, **14,** 385 ; 1955 a, *Ibid.*, **16,** 7 ; 1955 b, *Wiss. Z.*, Martin-Luther Univ., Halle-Wittenberg, **4,** 823.

FILED IN STACKS
28Mar